Theses and Dissertations

2016

A Foundation for Analysis of Spherical System Linkages Inspired by Origami and Kinematic Paper Art

Marc R. Wiener
Lehigh University

A Foundation for Analysis of Spherical System Linkages

Inspired by Origami and Kinematic Paper Art

by

Marc R. Wiener

A Thesis

Presented to the Graduate and Research Committee

of Lehigh University

in Candidacy for the Degree of

Master of Science

in

Mechanical Engineering

Lehigh University

May 23, 2016

This thesis is accepted and approved in partial fulfillment of the requirements for the Master of Science.

_____

Date

_____

Meng-Sang Chew

Thesis Advisor

_____

D. Gary Harlow

Chairperson of Department

ACKNOWLEDGEMENTS

TABLE OF CONTENTS

LIST OF FIGURES

LIST OF TABLES

LIST OF EQUATIONS

LIST OF ELEMENTS

ABSTRACT

Origami and its related fields of paper art are known to map to mechanisms, permitting kinematic analysis. Many origami folds have been studied in the context of engineering applications, but a sufficient foundation of principles of the underlying class of mechanism has not been developed. In this work, the mechanisms underlying paper art are identified as "spherical system linkages" and are studied in the context of generic mobility analysis with the goal of establishing a foundation upon which future work can develop.

Spherical systems consist of coupled spherical and planar loops, and they motivate a reclassification of mechanisms based on the Chebyshev-Grübler-Kutzbach framework. Spherical systems are capable of complex, closed-loop motion in 3D space despite the mobility calculation treating the links as constrained to a single 2D surface. This property permits generalization of some multi-loop planar mechanisms, such as the Watt mechanism, to a generalized 3D form with equal mobility. A minimal connectivity graph representation of spherical systems is developed, and generic mobility equations are identified.

Spherical system linkages are generalized further into spherical/spatial hybrid mechanisms which may have any combination of spherical, planar, and spatial loops. These are represented and analyzed with a polyhedron model. The connectivity graph is modified for this case and appropriate generic mobility equations are identified and adapted.

The generic analyses developed for spherical system linkages are sufficient to inform an exhaustive type synthesis process. Generation of all configurations of a paper art inspired mechanism subject to constraints is discussed, and a case study generates all configurations of a spatial chain using specified link types. This design process is enabled by the developed notation and analyses, which are used to identify, depict, and classify kinematic paper art inspired mechanisms.

1 INTRODUCTION

1.1 CONTEXT AND MOTIVATION

1.1.1 Perspective on Origami and Paper Art

Origami is the art of sculpting paper into a spatial geometry using folding and creases. The roots of the Japanese word are *ori* ("fold") and *kami* ("paper"). Generally, an origami piece is developed from a square piece of paper and does not allow cutting or fastening (e.g. gluing, taping) [1]. Rigid origami is a subset of origami in which the only deformations of the paper are the creases such that the panels remain perfectly rigid and flat [2], whereas compliant origami relies on deformation or curvature of panels in addition to the creases. Kinematic origami is a subset of origami in which the final form promotes some motion rather than remaining a static structure [3]. Origami and its variants have existed for centuries, and its cultural prevalence and geometric complexity has motivated extensive mathematical and engineering analysis [4]. Figure 1 depicts origami cranes, a well-known introductory origami fold. One crane has compliant features due to a crushing construction step, whereas the other has all rigid panels.

Figure 1. Origami cranes with compliant features (left) and rigid features (right)

Figure 2. A pop-up book (top, left), a decorative, kirigami-inspired carton (top, right), and a paper model (bottom)

Paper art is an umbrella term which encapsulates all products whose creation utilizes the foldability of paper, paperboard, cardboard, and other comparable materials. These products share the fundamental characteristic of being a spatial form sculpted from flat material stock. Non-origami examples which are constructed by cutting, folding, and sometimes fastening are as follows: kirigami is a variation of paper folding art which involves cutting the paper (*kiru* means "cut") [2], pop-ups are three-dimensional paper features in books and cards which reveal upon opening and flatten upon closing [5], cartons are boxes and containers of varying geometry which are generally manufactured from a single, flat piece of cardboard [6], paper models are generally decorative sculptures which are assembled from flat templates [7]. Examples of each are depicted in Figure 2. There is intersection between most subfields of paper art [5], so these classifications are used very loosely to illustrate practical applications. Origami is often used as the quintessential example of paper art, and the characteristics of rigid origami and kinematic origami can both be generalized to all paper art. Rigid kinematic paper art is a term which describes most examples in this paper.

The purpose of paper art varies. Origami, kirigami, pop-ups, and paper models are generally decorative and fun, whereas cartons often serve a utilitarian purpose for transportation or storage. As a result, development in the first group is traditionally done by artists, whereas development in cartons is often done by engineers [8]. The union of the subfields into the broad classification of "paper art" allows research in each subfield to be combined, bringing together perspectives of origamists (origami artists), kinematicians (mechanism engineers), mathematicians, and packaging industry engineers in the study of paper art.

1.1.2   Deconstructing Creativity

1.1.2.1   Mapping Domains

Artmimetics is the utilization of art as inspiration for a solution in the context of conceptual design [9]; orimimetics is the subset of artmimetics in which the art source is origami [2]. It has been determined in the academic literature that there is a mapping between rigid paper art and mechanisms based on the equivalence between an ideal crease and a revolute joint and between an ideal rigid panel and a rigid link [10] as depicted in Figure 3. Consequently, recognition that development in origami is traditionally isolated from development in mechanism design suggests that paper art-mimetics is a fertile area for new mechanism design techniques. The motivation of the research in this paper is to explore ways in which origami and paper art can inform mechanism analysis and design.

Origamists, a subset of artists, are experimentally creative within their domain (i.e. the paper art domain). Origami's existence over centuries has allowed the art to develop incrementally as each artist inherits the status quo and then experiments, tweaks, and adds to the existing body of knowledge. Furthermore, the strict limitations imposed on origami (i.e. the use of a single square piece of paper with no folding or fastening) provides constraints which test origamists' creative capacity even further. The resulting trial-and-error development is inherent to origami, and it is akin to a genetic optimization algorithm involving random "mutations" over many iterations.

Kinematicians, a subset of engineers, are typically methodical within their domain (i.e. the mechanism domain). Modern mechanism synthesis is not the result of experimentation or serendipity but rather methodical, exhaustive techniques such as type synthesis methods which generate all combinations of link-joint connectivities and dimension synthesis methods which use closed form equations or optimization algorithms to

trace a desired path or function [11]. Ideal implementation of these methodologies remove the need for human creativity or trial-and-error techniques and often generate a quantifiably optimal solution.

The contrasting methodologies of origami and mechanism design parallel the open-ended, artistic nature of origami vs. the utilitarian, product design-driven nature of mechanisms. Due to the mapping between the domains, these differences can be leveraged such that an origamist's approach could be utilized to develop mechanisms and vice versa [5]. This mentality anticipates radical new mechanism design techniques inspired by kinematic paper art which can flourish once a proper foundation of rules is established.
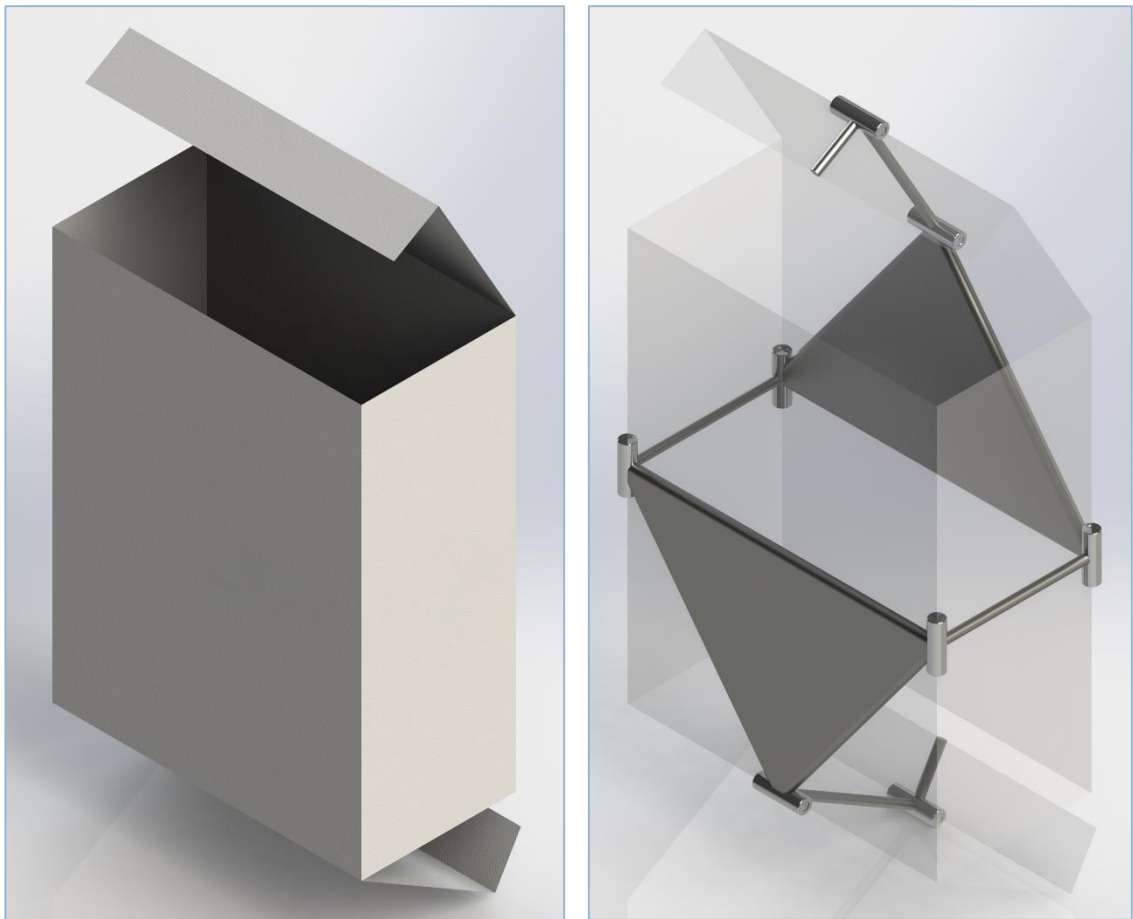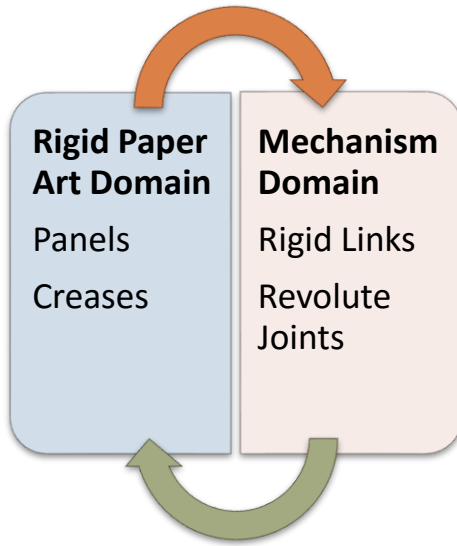
Figure 3. Process of mapping a mechanism between domains (top) with an example of a partially assembled carton in the paper art domain (bottom, left) and mechanism domain (bottom, right)

1.1.2.2 Developing a Foundation

Upon review of the academic literature in the subfields of paper art, it was determined that publications on the mapping between the paper art and mechanism domains generally consist of two major areas of development. The first area establishes the low-level, basic rules about the correspondence of panels and creases to links and joints, respectively. The second area consists of specific examples of individual mechanisms and their analyses. What is lacking in the literature is a complete foundation of fundamental principles which eliminates the reliance on experimentation but instead fuels a methodical approach in design. In other words, a foundation of general rules developed from artmimetic studies would allow kinematicians to bypass the need to mimic specific examples.

Due to the artmimetics field's reliance on mimicking individual examples of paper art, kinematicians tend to map the specific geometric features of single cases rather than generalizing to a broader class of cases. Characteristics inherent to many examples of paper art include special geometric features such as symmetry, right angles, supplementary angles, regular polygons, and link planarity. These features are prevalent in paper art for a variety of aesthetic and practical reasons, but their characteristics often fail to provide insight into a generalized class of mechanism. Developing a broad foundation of analysis principles would require generalizing mappings such that there is no reliance on special dimensional properties.
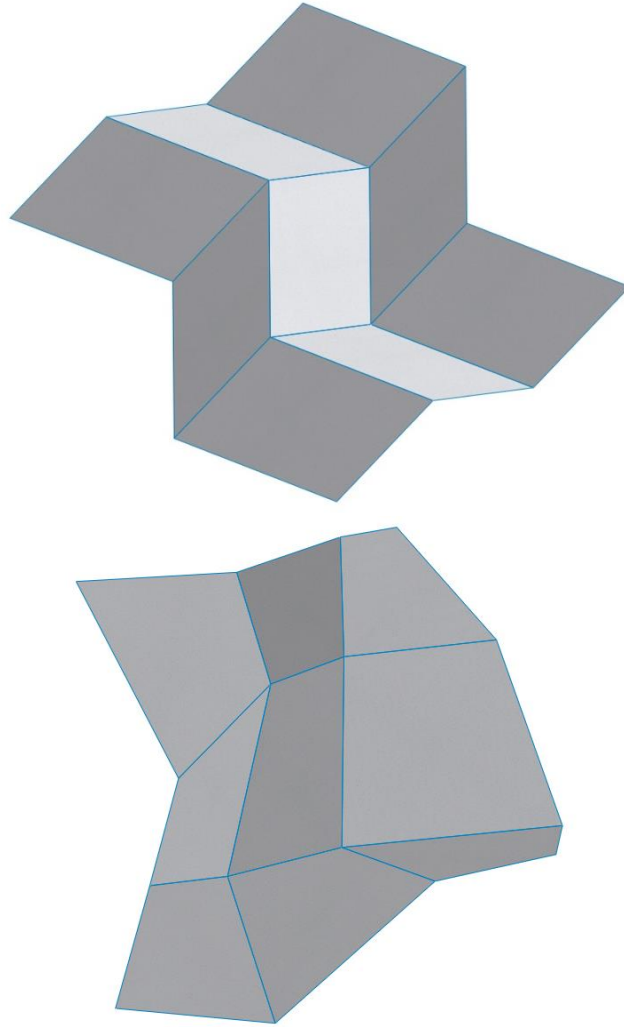
Figure 4. A highly symmetric fold (top) and its generalized analogue (bottom)
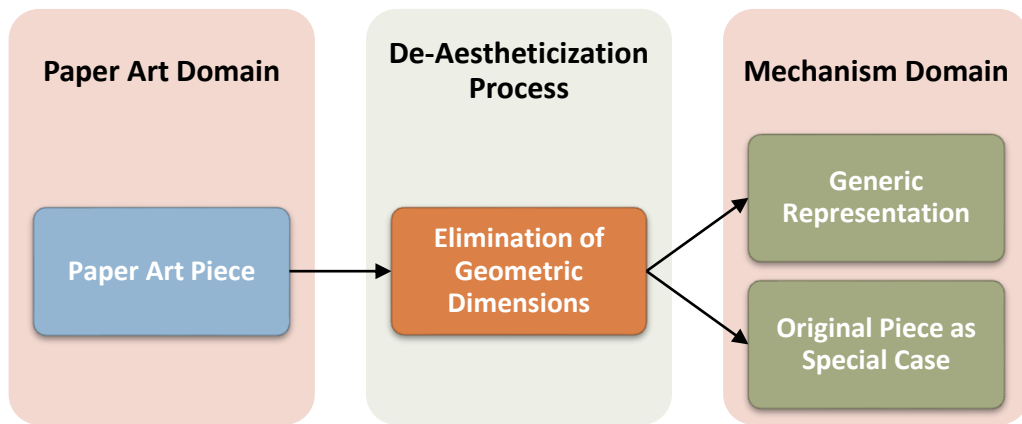
Figure 5. Process to determine the generic mechanism from a specific paper art piece

Generalization of dimensions with the goal of eliminating special geometric dimensions in effect removes the proportions of lengths and angles which typically gives a piece of art its aesthetic appeal. Symmetric pieces become asymmetric, and planar, polygonal panels become distorted in an effectively random way as demonstrated in the generalization of the highly symmetric fold in Figure 4. This deconstruction of art into a generic, representative form is called de-aestheticization. In the case of paper art, de-aestheticization removes all dimensional relations but maintains the salient features of the piece, which are the connectivity of panels by creases and the intersection of creases at vertices. In the mechanism domain, this corresponds to the link-joint connectivity and joint axes' intersections. The minimal representation of just these salient features is this class of mechanism's generic representation, which is defined exclusively by the mechanism connectivity without regard for geometric dimensions.

It is important to establish fundamental principles using the generic representations of paper art and their equivalent mechanisms because mapping the cases with special geometries may exhibit kinematic properties which are caused by the dimensional relations rather than the connectivity relations. As a result, the special cases would be a specific case of the generalized mappings as depicted in Figure 5. To establish a proper foundation for paper art-mimetic techniques, one must first establish a representation of the salient features of a generalized piece, then proceed to develop analyses of the generic representation, and then incorporate special cases. From that broad foundation, further in-depth analyses and methodical design techniques can be developed.

1.2 LITERATURE REVIEW

1.2.1 Paper Art Literature

1.2.1.1 *Identification and Representation of Paper Art as Mechanisms*

The literature which identifies paper art as mechanisms generally provide a foundation for the mapping between domains and begin preliminary analysis of the graphs developed. Dai and Jones map cartons to mechanisms treating creases as ideal revolute joints and panels as rigid links and use graphs to represent these mechanisms [10]. Winder et al. examine pop-up mechanisms, identify planar and spherical mechanisms, use PRBM to represent paper's compliance with modified rigid links, and map common features and equivalent joints in the two domains including designing a RSSR pop-up mechanism [5]. Greenberg et al. provide a review of the mapping between kinetic origami and mechanisms, use link-joint graphs as a tool to map domains, and perform basic analysis using the graphs [2]. Bowen et al. identify kinematic origami as a system of spherical mechanisms and present a vertex-edge graph which is used to classify various origami folds [3]. Much of this literature lacks a comprehensive graph scheme for depiction of all salient features of paper art mechanisms and as a result fails to generalize the representation of its paper art subfield to a broader class of mechanisms.

1.2.1.2 *Analysis of Generic Mobility in Paper Art*

The literature which analyzes the generic mobility of mechanisms in the paper art domain generally utilize a non-traditional mobility analysis approach in the context of the analysis of a specific fold. Dai and Jones develop an adapted Kutzbach criterion for cartons using screw theory as a foundation [6]. Beatini and Korkmaz extrapolate Grübler's equation to develop a "two-strip" condition for mechanism addenda and develop a term for overconstraint in the study of Miura-ori meshes [12]. Yellowhorse and Howell employ a

polyhedron model [13] to discuss the changes in mobility of paper art introduced by various modifications [14]. Each of these works employ generic mobility techniques which are valuable in the context of their domain of paper art, but few attempt to generalize a generic mobility formulation technique over a broader class of non-paper art mechanisms.

1.2.1.3   *Analysis of Specific Mobility in Paper Art (Closure Equations, Screw Theory)*

Much of the literature in the field of paper art applies closure equation analysis to a specific mechanism taken from the paper art domain. Balkcom et al. analyze the paper shopping bag using its graph and dihedral angle analysis [15]. Tachi develops a program which simulates rigid origami using Jacobian matrices at instantaneous positions to calculate loop closures [16]. Wei and Dai examine a specific novel eight-bar mechanism developed from a carton using screw theory and comment on the use of an adapted Kutzbach criterion to calculate its mobility [9] and later evolve it into a different novel mechanism which is again analyzed with screw theory [17]. Bowen et al. extend the earlier identification of origami as systems of spherical mechanisms and proceed to perform position calculation of specific, simple folds representing coupled spherical mechanisms using spherical trigonometry and symmetry [18]. The literature which analyzes individual mechanisms in the domain of paper art provide examples of appropriate analysis techniques for those pieces, but the closure equations used only apply to the specific mechanism rather than presenting a generalized analysis which may apply to a broader class of mechanisms and be used in the conceptual design stage.

1.2.1.4   *Analysis of Mobile Overconstrained Patterns*

This section of the literature examines well-known mobile overconstrained origami folds whose special geometric conditions such as symmetry, angular relations, and

tessellation permit mobility despite a predicted generic mobility of zero. Tachi presents numerous papers on the topic. Tachi presents rigid cylinders developed from the overconstrained Miura-ori fold, generalizes the design process to a broader class of cross sectional shape, and analyzes the use of thick panels in its construction [19]. Next, Tachi analyzes geometric conditions for rigid mobility in meshes using dihedral angle and polyhedron analysis to present a generalization of overconstrained patterns which can be designed using optimization processes [20]. Tachi and Miura expand the application of the Miura-ori cell in cylinders and meshes to 3D cellular structures based on their symmetry properties [21]. Evans et al. provide a review of tessellating meshes and the generalizations of the properties which permit mobile overconstraint [22]. This area of the literature is a very specific subfield of paper art, and it has been generalized fairly well within its domain.

1.2.1.5 Paper Art Reference

This area of literature provides basic background information related to the domain of paper art. Demaine and O'Rourke review classical and modern problems and algorithms which involve folding, overlapping with the fields of linkages, origami, and polyhedra [4]. Dureisseix introduces origami background, basic properties, and observations on overconstrained mechanisms [1]. Massarwi et al. discusses the definition and develops a design algorithm for papercraft models [7].

1.2.2 Non-Paper Art Systems of Spherical Linkages

This area of literature explores systems of spherical linkages in the kinematic domain without direct inspiration or application to paper art. Makhsudyan et al. identify a novel linkage described as serially connected spherical mechanisms and perform position analysis [23]. Dzhavakhyan et al. perform analysis which demonstrates the favorability of spherical

linkage pressure angles to planar linkage pressure angles [24]. Wilding et al. explore spherical lamina emergent mechanisms and include examples of serially connected spherical mechanisms [25]. This section of the literature is fairly sparse, which suggests that paper art provides a significant inspiration for the design of systems of spherical mechanisms.

1.2.3   Generic Mobility Formulation

Literature on the mobility calculation of mechanisms is incredibly extensive, but literature on the generic mobility calculation of systems of spherical mechanisms is fairly sparse. Gogu provides a review of numerous generic mobility calculation techniques including recognition of conditions in which generic mobility may be calculated for common cases of systems of spherical mechanisms [26]. Wampler et al. provides a fresh perspective on mobility using salient features of a mechanism expressed as vertices and edges of a polyhedron to calculate the generic mobility of spherical/spatial hybrid mechanisms [13]. Shai and Müller modify the connectivity graph representation of a mechanism and provide a robust generic mobility calculation through the pebble game algorithm [27]. This section of the literature provides sufficient evidence to develop multiple generic mobility formulae appropriate to systems of spherical mechanisms and spherical/spatial hybrid mechanisms. The analysis developed by Wampler et al. is the most robust of these in the context of paper art.

1.2.4   Reference

This area of the literature provides fundamental, traditional background on kinematics. Sandor and Erdman establish traditional mechanism analysis including generic mobility and degree of freedom definitions [28]. Erdman presents a review of traditional,

computational kinematics development techniques [11]. Norton provides an alternative mobility formulation and definitions of kinematics terms [29].

1.3 TERMINOLOGY, NOTATION, AND ASSUMPTIONS

1.3.1 Mechanism Domain Assumptions and Terminology

The terms "linkage" and "mechanism" interchangeably refer to a combination of links and joints. The terms "link" and "body" interchangeably refers to an entity in the mechanism whose position and mobility can be defined in space relative to an absolute reference point. Mechanisms are assumed to have all rigid links unless otherwise specified. The term "joint" refers to an entity in the mechanism which connects links and provides some specific degree(s) of freedom between the connected links. Revolute, prismatic, universal, and spherical joints can be abbreviated as R, P, U, and S joints, respectively. The term "spherical center" refers to the exact point of intersection of all revolute joint axes in a spherical loop within a mechanism. Mechanisms are assumed to have unspecified, generic dimensions unless otherwise specified. Mechanisms with specified dimensions are assumed to have mathematically perfect dimensions, angles, axes, and intersections. Mobility refers to the capability of motion within a finite range of angles about the current position. The range of angles in neither infinitesimal nor global due to mechanisms generally reaching some singular positions and/or self-intersecting.

1.3.2 Paper Art Domain Assumptions and Terminology

The terms "piece" and "fold" interchangeably refer to paper art entities in the context of their physical implementations. The terms "linkage" and "mechanism" interchangeably refer to paper art entities in the context of their kinematic representation. The terms "panel" and "link" interchangeably refer to a paper face. Panels are assumed to be perfect, ideal, rigid

15

planes in the kinematic representation unless otherwise specified. The terms "crease," "edge," and "joint" refer to the intersections of paper faces in the context of a physical paper art piece. Creases are assumed to be perfect, ideal, one-dimensional revolute joints in the kinematic representation. The only creases considered in a piece are those which mate panels, not those used in the construction of the piece which have been flattened. The term "vertex" refers to the intersection of edges into a point in the context of a physical paper art piece. Vertices are assumed to be perfect, ideal, zero-dimensional points and can serve as spherical centers of a loop.

2 IDENTIFICATION OF SPHERICAL SYSTEM LINKAGES

2.1 PROPERTIES OF TRADITIONAL LINKAGES

2.1.1 Degrees of Freedom and Classification

In mechanism analysis, a fundamental property is a mechanism's mobility, or its degrees of freedom (DOF). This quantity represents the number of inputs required to completely define the positioning of all links in the system based on the dependencies established by the link-joint connectivity. The calculation of mobility of a linkage depends on the degrees of freedom available in the constraint space of the mechanism, which is defined by how each body, or link, is constrained to move. Typical constraint spaces which are well-studied are planar, spherical, and spatial spaces, which each correspond to those classes of mechanism [28].

Planar mechanisms typically consist of rigid links whose translations are constrained to a plane with two degrees of translational freedom $\{x, y\}$ and one degree of rotational freedom normal to the plane of constraint $\{\theta_z\}$ for a total of three degrees of freedom $\{x, y, \theta_z\}$ as depicted in Figure 6, top. Spherical mechanisms typically consist of rigid links constrained to a sphere with a specified center and of fixed radius with two degrees of freedom of rotation about the spherical center analogous to translation over the sphere surface $\{\theta_x, \theta_y\}$ and one degree of rotational freedom normal to the sphere of constraint $\{\theta_z\}$ for a total of three degrees of freedom $\{\theta_x, \theta_y, \theta_z\}$ as depicted in Figure 6, bottom. It can be shown that as the radius of curvature of the sphere approaches infinity, the spherical mechanism can be represented as a planar mechanism, i.e. a planar mechanism is a special case of a spherical mechanism with the spherical center located an infinite distance away [13]. Spatial mechanisms consist of rigid links with three degrees of translational freedom $\{x, y, z\}$ and

with three degrees of rotational freedom $\{\theta_x, \theta_y, \theta_z\}$ for a total of six degrees of freedom $\{x, y, z, \theta_x, \theta_y, \theta_z\}$ as depicted in Figure 7.

To constrain link motion relative to each other, joints are used to connect links. Common joints are revolute and prismatic joints, which permit one degree of relative freedom between two bodies by rotation or translation, respectively. The relative degree of freedom between two links permitted by a revolute joint is depicted in Figure 8. Spatial mechanisms also often include joints that permit higher mobility including cylindrical, spherical, and planar joints which permit two, three, and three degrees of relative freedom, respectively. The number of degrees of relative freedom of each joint is a crucial parameter for determining the overall mobility of a mechanism [28].
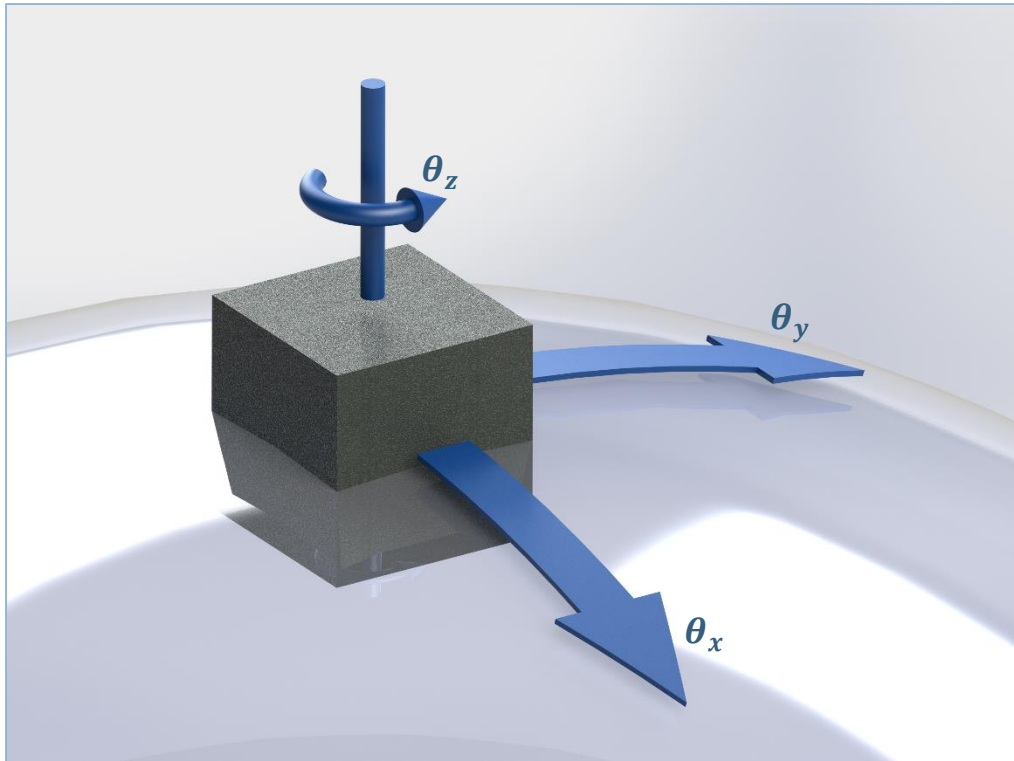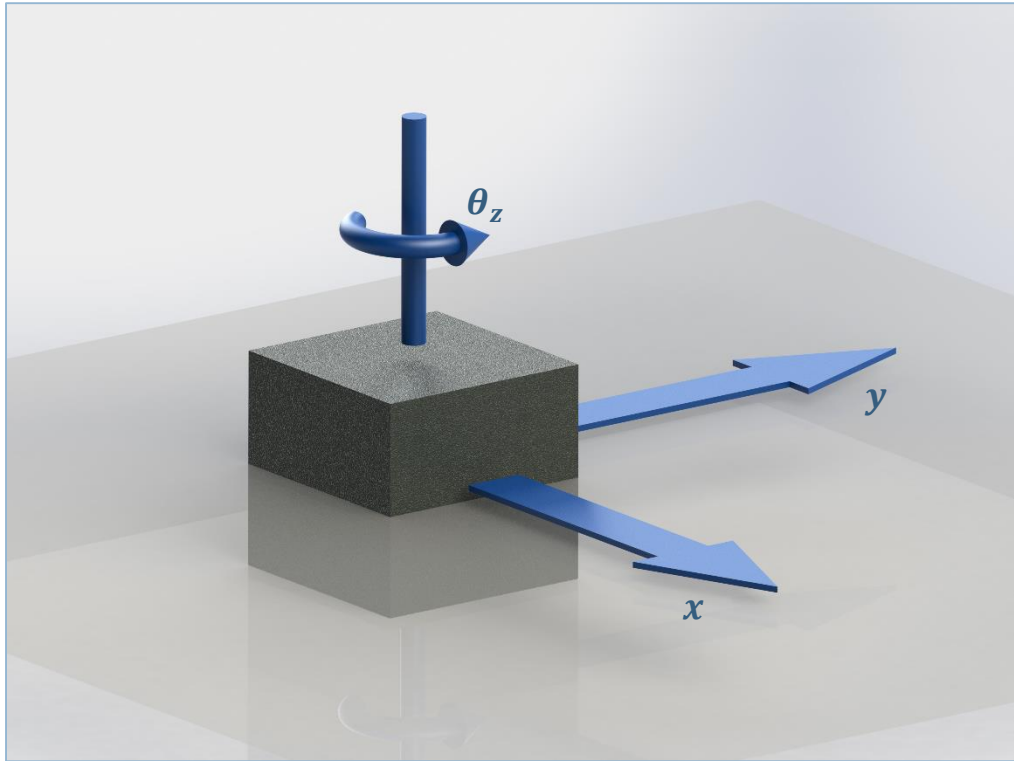
Figure 6. Diagram of planar (top) and spherical (bottom) degrees of freedom
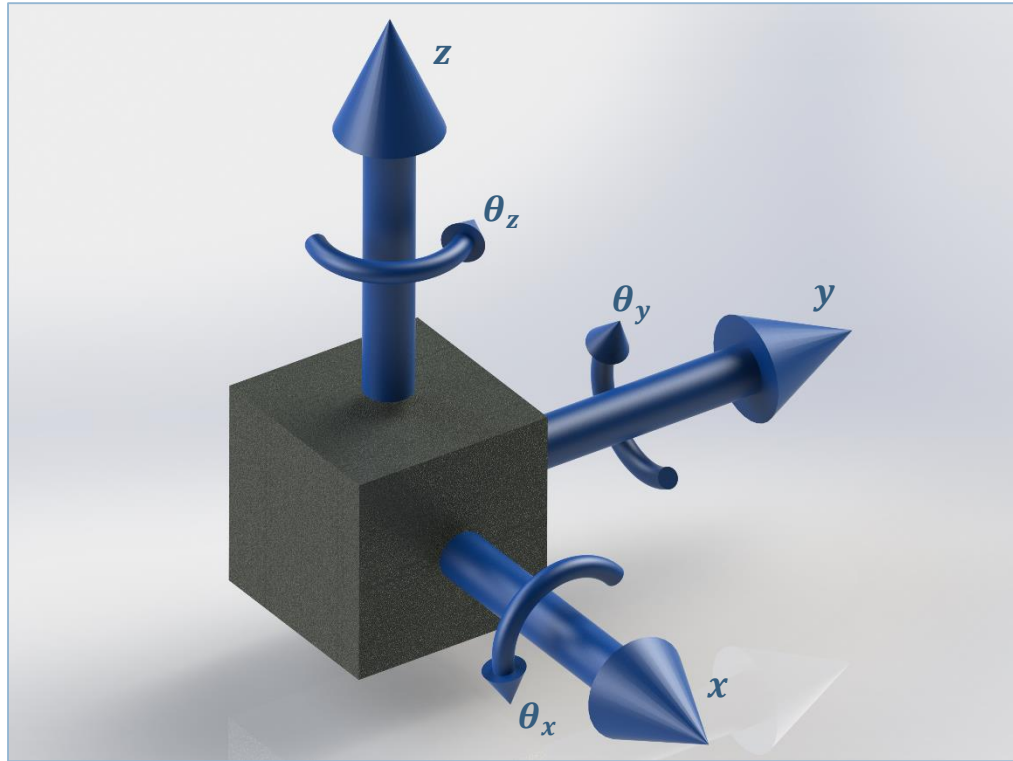
Figure 7. Diagram of spatial degrees of freedom

Figure 8. Diagram of the degree of freedom between two bodies permitted by a revolute joint

2.1.2 Traditional Chebyshev-Grübler-Kutzbach Equation

The traditional Chebyshev-Grübler-Kutzbach (C-G-K) equation (Eqn. 1) provides a formulation to predict the number of degrees of freedom of the generic representation of a planar, spherical, or spatial mechanism (i.e. traditional mechanisms) when one link is taken to be grounded, or fixed in space [28]. The generic representation of a mechanism only considers the connectivity of links and joints without regard for geometric dimensions. This formula is a simple function of the number of rigid links, the number of joints, and the degrees of freedom provided by each joint. An extra parameter in this equation considers the degrees of freedom of the constraint space of the mechanism, which is equal to 3 DOF for planar and spherical mechanisms and 6 DOF for spatial mechanisms. The C-G-K equation does not depend on the arrangement of link-joint connectivity or geometric dimensions, so the output is called the generic mobility for a mechanism of arbitrary connectivity and dimension. There are often cases in which a special combination of dimensions and connectivity will produce a mechanism with a higher number of degrees of freedom than predicted by the C-G-K equation, which is called a mobile overconstrained mechanism. There are techniques to predict the existence and mobility of these overconstrained mechanisms, but in general the generic mobility is sufficient as it covers nearly every geometric configuration.

$$M = \lambda \, (N - J - 1) + \sum f_i \qquad \text{(Eqn. 1)}$$

$M = generic\ mobility\ of\ mechanism$
$N = number\ of\ links;\quad J = number\ of\ joints$
$f_i = degrees\ of\ freedom\ of\ i^{th} joint\ for\ i = 1, 2, \dots, J$
$\lambda = constraint\ space\ parameter$
      $\lambda = 6$ for spatial constraint space
      $\lambda = 3$ for planar/spherical constraint space

An example of the C-G-K equation's use is depicted in Table 1 where it is used to calculate the mobility of three mechanisms composed of six rigid links and six revolute joints forming a loop ($N = 6$, $J = 6$, $f_i = 1$). In each case, the orientation of the joints decide the

constraint space parameter λ, and the mobility M is calculated using C-G-K. The planar mechanism is identified by recognizing that all of its joints are parallel; the spherical mechanism is identified by recognizing that all of its joints intersect in a common point (depicted explicitly in the diagram); the spatial mechanism is identified by recognizing that it is neither planar nor spherical due to skew axes. Both the planar and spatial mechanism have 3 DOF, meaning three relational inputs must be established to fully define the position of the linkage. The spatial mechanism has 0 DOF, meaning its position is already fully defined and it cannot move.
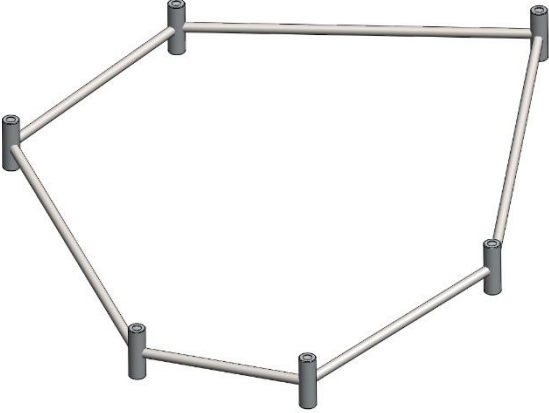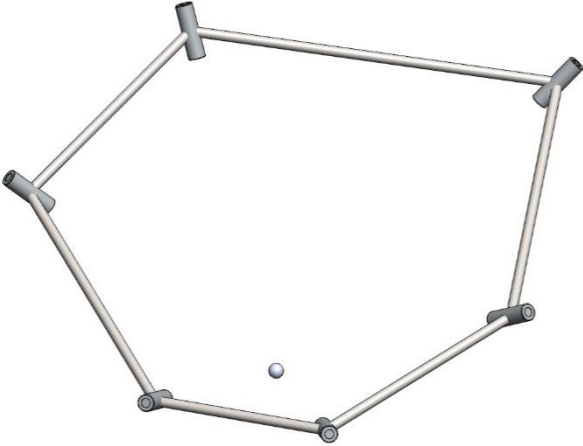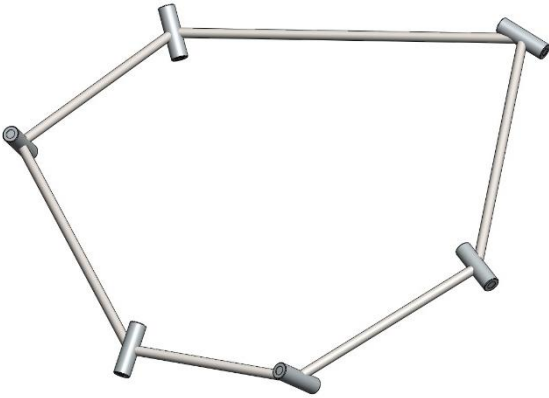
Class	Diagram	λ	M
Planar		3	3
Spherical		3	3
Spatial		6	0

Table 1. Calculation of mobility of six-bar loops

2.2 PROPERTIES OF SPHERICAL SYSTEM LINKAGES

2.2.1 Identification of Spherical System Linkages

While the C-G-K equation generally correctly predicts the generic mobility of planar/spherical and spatial mechanisms, it is also applicable to another class of mechanisms. This class is composed of linkages that are systems of coupled spherical mechanisms that consist of all revolute joints. Spherical system linkages (spherical systems) are characterized by having all of the revolute joint axes of each loop closure meet at a spherical center, and all of the loop closures may have non-coincident spherical centers. This class of linkages describes the underlying mechanism of most kinematic paper art [3]. This contrasts with strict spherical mechanisms in which the joint axes of all loop closures meet at a single spherical center. An example spherical system is shown in   Figure 9 which has two loops with two unique spherical centers. Upon attempting traditional C-G-K analysis, one determines that spherical systems don't meet the definition of a spherical or planar mechanism, and as a result one would attempt use the spatial mechanism constraint space parameter (6 DOF) in the C-G-K equation; however, using this parameter fails to properly predict the generic mobility of spherical systems. This problem is rectified in the literature by recognition of a little-used property of the C-G-K equation for multi-loop systems, permitting modification of the C-G-K equation.
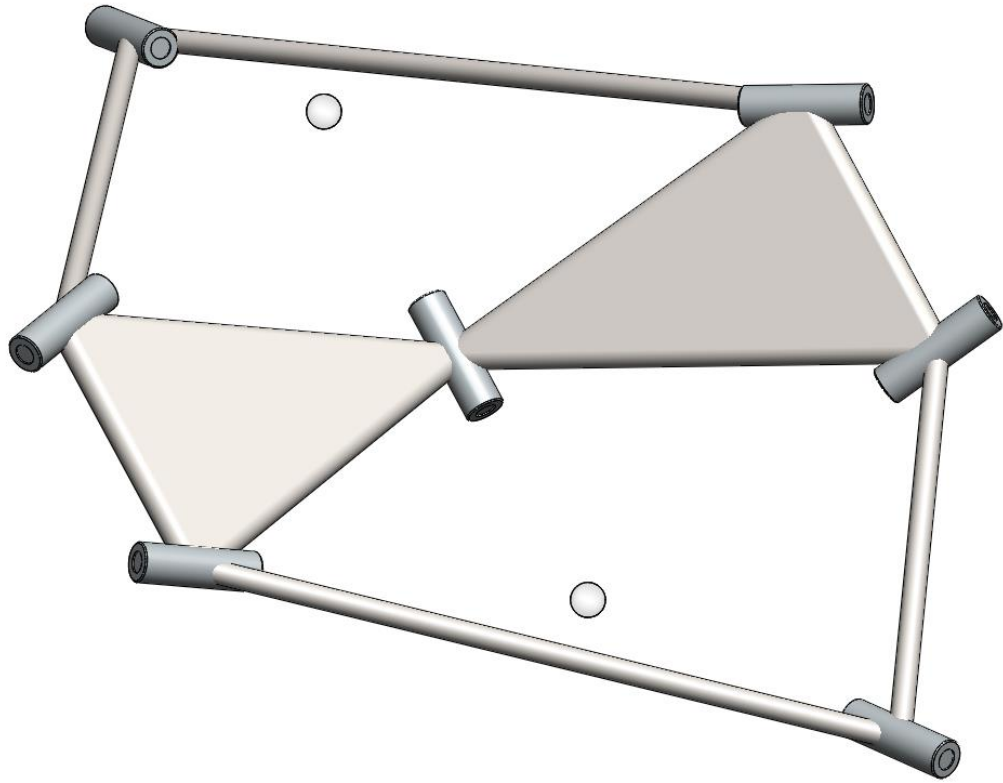
Figure 9. Diagram of a two-loop spherical system linkage

2.2.2 Modified Chebyshev-Grübler-Kutzbach Equation

In the literature, evidence for the validity of the C-G-K equation for spherical systems is sparse but extant. Gogu states Hochman's recognition that the generic mobility formulation applies to any mechanism with the same constraint space parameter in each independent loop, and the equation will properly predict the overall mechanism's generic mobility using that parameter [26]. Wampler et al. conjecture that the C-G-K equation with a spherical constraint space parameter accounts for the generic mobility of spherical systems with only revolute joints [13]. Lastly, Wei and Dai use screw theory to analyze a specific carton-derived spherical system mechanism, but they also recognize that the constraint space parameter of each loop is the same, and therefore it can be used in the overall mechanism C-G-K equation, which is used to corroborate their screw equation results [9]. Each of these cases agrees that the C-G-K equation can be modified for use in the case of a mechanism with all revolute joints in which each mechanism loop has an identical constraint space parameter.

In the case of revolute-only spherical systems, each loop has a spherical constraint space, and therefore the spherical constraint space parameter is appropriate for the modified C-G-K equation for spherical system linkages. Therefore, revolute-only spherical systems is recognized as a class of mechanisms properly described by the C-G-K equation, and the C-G-K constraint space parameter list can be modified to account for spherical systems (Eqn. 2). This is notable because spherical system mechanism links may have complex motion in three-dimensional space, but the constraint space parameter is only 3 DOF. Traditionally, the 3 DOF constraint is associated with all mechanism links constrained to a two-dimensional surface (i.e. a plane or sphere). It should be noted that spherical mechanisms themselves are a special subset of spherical system mechanisms in which each loop closure's spherical center is coincident, and furthermore planar mechanisms are a doubly special subset of spherical

systems in which each loop closure's spherical center is coincident and is located an infinite distance away [13]. From this, the traditional classes of planar and spherical mechanisms can be generalized into the single class of spherical system mechanisms with the defining characteristic of a 3 DOF constraint space. This unifies the classification of all 3 DOF constraint space mechanisms in contrast to spatial, 6 DOF constraint space mechanisms, and the modified C-G-K constraint space parameter definition is generalized to reflect this.

$$M = \lambda (N - J - 1) + \sum f_i$$

<div align="right">(Eqn. 2)</div>

$M = generic\ mobility\ of\ mechanism$
$N = number\ of\ links;\quad J = number\ of\ joints$
$f_i = degrees\ of\ freedom\ of\ i^{th} joint\ for\ i = 1, 2, ..., J$
$\lambda = constraint\ space\ parameter$
$\quad\quad \lambda = 6 \quad\quad$ for spatial constraint space
$\quad\quad \lambda = 3 \quad\quad$ for spherical system constraint space

2.2.3   Reclassification of Mechanisms

The hierarchy depicted in Figure 10 visualizes the relationship of each class of mechanism based on recognition of the generalized spherical system class. The hierarchy first differentiates spatial mechanisms and spherical systems by their constraint space parameter. It then acknowledges single-centered spherical mechanisms as a special case of spherical systems in contrast to general, multiple-centered spherical systems. Within the spherical mechanism category it then acknowledges planar mechanisms as a special case of spherical mechanisms in contrast to general finite-centered spherical mechanisms. Finally, the general spherical system branch notes that most kinematic paper art is contained in this category and that it is a relatively unexplored class of mechanism compared to the planar/spherical subsets.
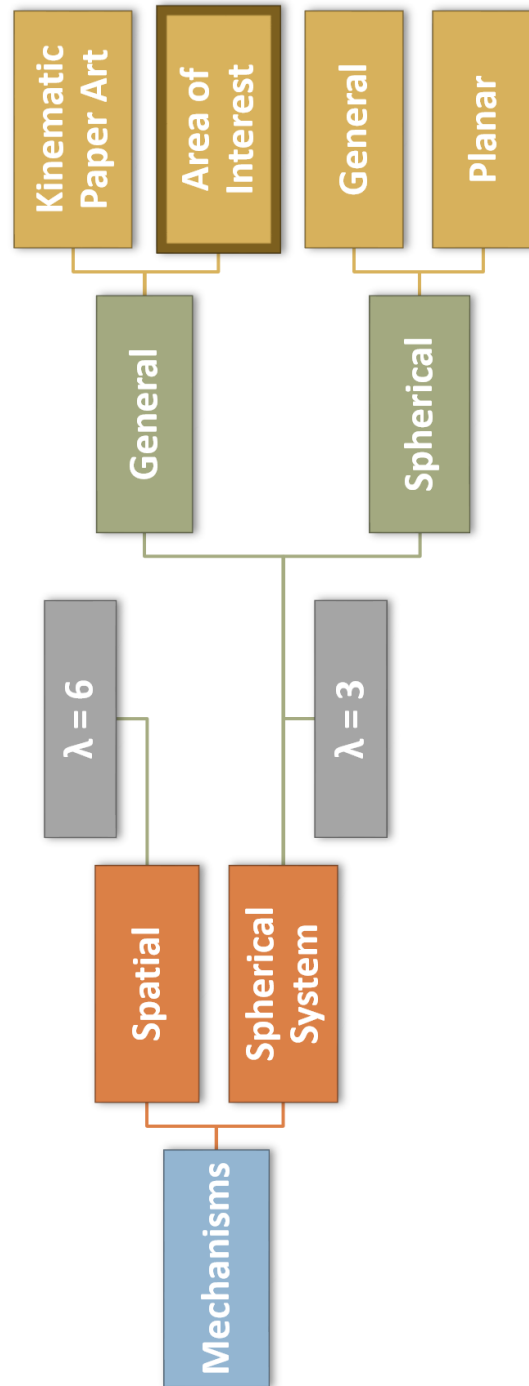
Figure 10. Classification of mechanisms by constraint space (landscape)

This modified version of the C-G-K equation and reconstructed mechanism classification scheme motivates development of generalized notation which encodes the salient features of spherical system linkages. The traditional notation is limited to the specific cases of planar/spherical and spatial mechanisms which do not require indication of multiple non-coincident spherical centers in a single mechanism as is required by spherical systems. Spherical system mechanism notation and depiction requires placing emphasis on the quantity and relations of spherical centers in each loop to allow classification and analysis.

2.3 ANALOGOUS PHYSICAL REPRESENTATIONS OF SPHERICAL SYSTEMS

The mapping between the paper art and mechanism domains relies on the equivalence of kinematic features of the underlying spherical system linkages [3]. The representations of these features in each domain vary in geometry and appearance, and therefore a specific mechanism can be depicted in multiple equivalent ways; an example of this is the eight-bar spherical system mechanism depicted in Figure 11, Figure 12, and Figure 13. These different geometries motivate different dimensional generalizations and inform different mobility analyses, so interchanging between the models is a necessary tool. These interchangeable representations are valid for spherical system mechanisms with all revolute joints [13].

2.3.1 Rigid Linkage Model

The rigid linkage model is the typical kinematic representation of a mechanism. An example is depicted in Figure 11. Rigid links are represented by bars or polygons whose dimensions are stated for a specific geometry or are left arbitrary for the generic case. These links are connected by revolute joints with a specified orientation such that the intersection of joint axes (i.e. spherical centers) of a loop are known and should be depicted explicitly with

dots or spheres. This information is required for determining the constraint space of each loop. Loops with all intersecting joint axes are spherical loops, loops with all parallel joint axes are planar loops, and loops with skew joint axes are spatial loops. In the most generic representation of a mechanism, the joint intersections (or parallelism) must be known to assess the mechanism class, but the specific dimensional features such as axis angles and spherical center locations do not need to be known specifically.

2.3.2 Rigid Panel Model

The rigid panel model is the typical paper art representation of a mechanism. An example is depicted in Figure 12. Rigid panels are represented by infinitely thin polygons [2] whose dimensions are stated for a specific geometry or are left arbitrary for the generic case. These links are connected by creases represented by one-dimensional edges. Intersecting creases create a vertex, which is often represented explicitly in the geometry; however, any known crease axis intersections of a loop which are not explicitly represented by a vertex should be depicted explicitly by a spherical center as in the rigid linkage model. The sets of vertices and spherical centers internal to the loops need to be known to assess the mechanism class.
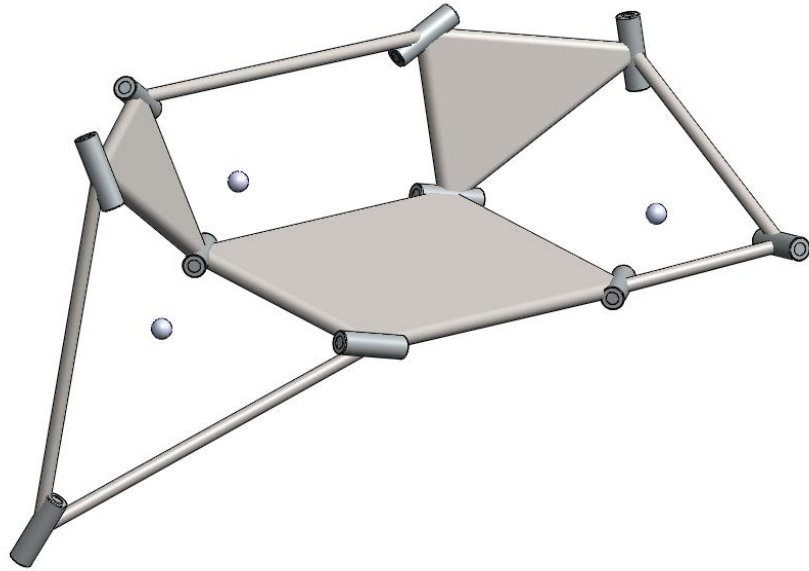
Figure 11. Rigid linkage representation of a three-loop eight-bar
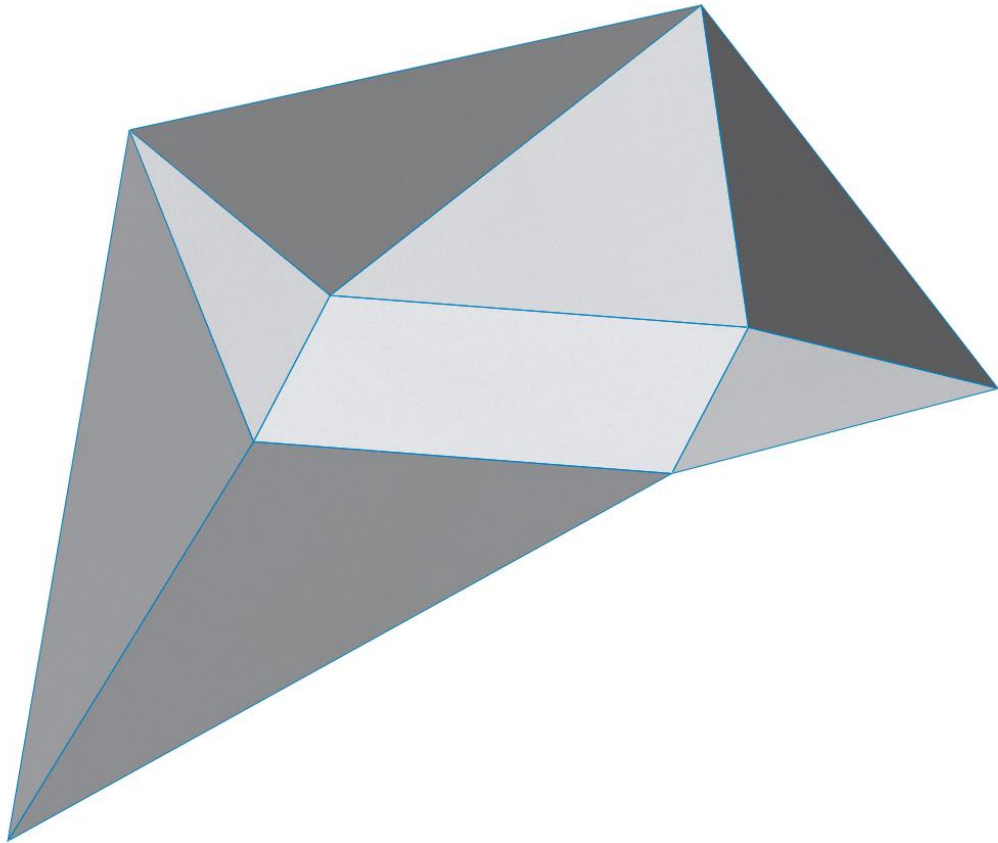
Figure 12. Rigid panel representation of a three-loop eight-bar

2.3.3   Polyhedron Model

The polyhedron model introduced by Wampler et al. takes a different kinematic approach to the representation of mechanisms [13]. An example is depicted in Figure 13. All vertices formed by joint intersections are represented explicitly by spherical joints, and they are connected by rigid rods which correspond to one-dimensional joint axes, or edges. Rigid link analogues are developed by vertex-edge (i.e. sphere-rod) combinations; the simplest rigid body is represented by a triangular truss of three edges and three vertices. Polygons with n sides are constructed by connecting a loop of n vertices with n external edges in a plane, then adding $2n - 6$ internal edges between non-adjacent vertices to ensure link rigidity [13]. Links are connected by sharing two vertices and one edge, where the shared edge serves a crease, or revolute joint axis. Rigid links in the polyhedron model resemble a skeleton of the panels in the rigid panel model with external edges corresponding to the rigid panel's perimeter. An example of a six-sided rigid link is depicted in Figure 14 with six external edges connecting six vertices as well as six internal edges to ensure link rigidity. In this model, link dimensions are stated for a specific geometry or are left arbitrary for the generic case, and any known edge axis intersections of a loop which are not explicitly represented by a vertex should be depicted explicitly by a spherical center. The sets of vertices and spherical centers internal to the loops need to be known to assess the mechanism class.
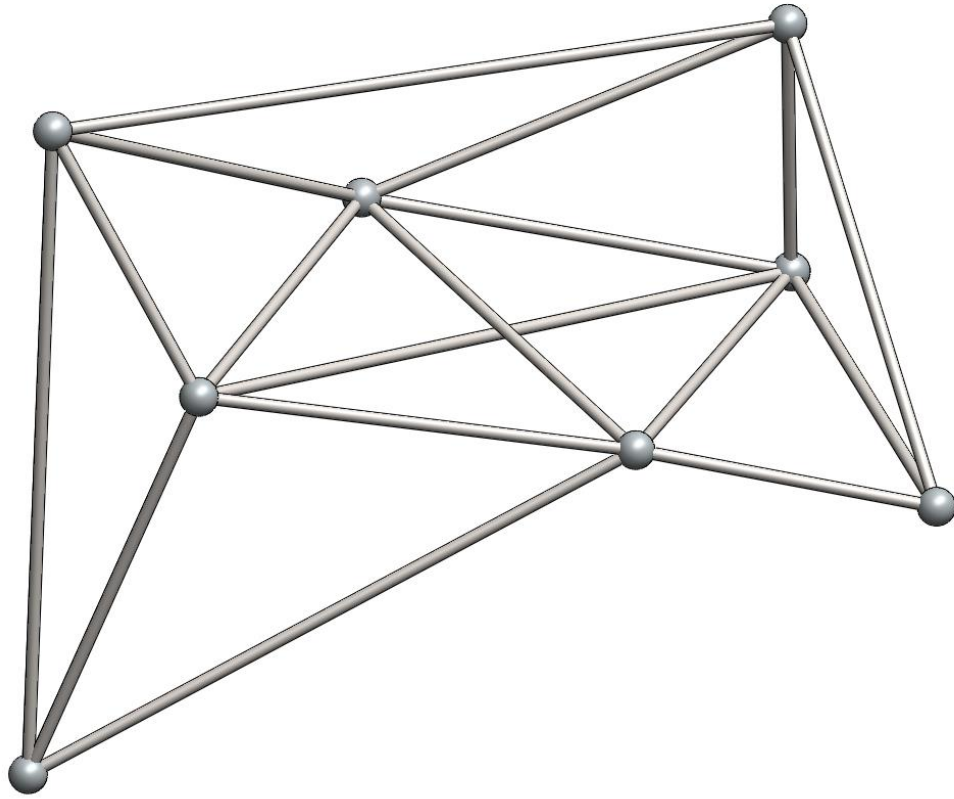
Figure 13. Polyhedron representation of a three-loop eight-bar
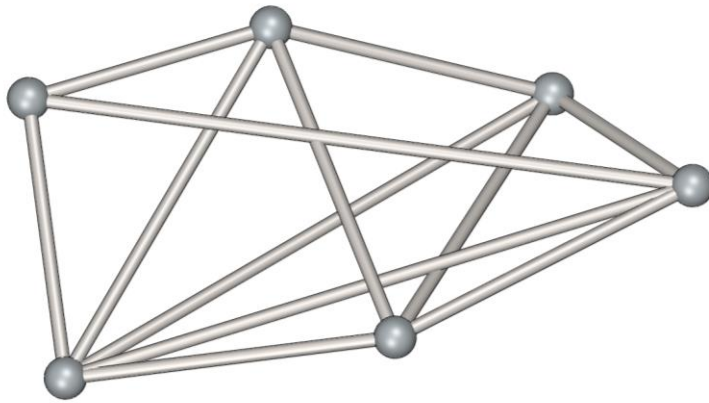
Figure 14. Rigid, six-sided polyhedron link

In the polyhedron model, the planarity of polygonal links is not maintained in the most generic representation of a mechanism; polygons can be generalized to non-planar, rigid polyhedral skeletons (polyhedra). The generalized polyhedron link maintains connectivity of the n vertices by a loop of n external edges, but it does not constrain the vertices to a plane as a polygon does. Thus, a planar polygon can be generalized in this model by randomly perturbing each vertex in three dimensions and re-dimensioning the edges appropriately; the $3n - 6$ total edges will maintain link rigidity. The most generic representation of a polyhedron will have no planarity, axis intersection, or parallel relations between non-adjacent external edges, and thus all non-adjacent edges are skew. An example of this is the generalization of the rigid, planar quadrilateral panel at the center of the mechanism in Figure 12 to the rigid, skew tetrahedron link at the center of the equivalent mechanism in Figure 13. A generalized rigid polyhedron's geometry is described by its number of external edges (or equivalently, by their number of vertices), e.g. the link depicted in Figure 14 is called a six-sided polyhedron.

The polyhedron model's capability of generalization expands beyond eliminating planarity from a polygonal panel; it can also remove special geometric features to ensure a linkage is represented in its most generic form. An example of a special geometric relation is the coincidence of the edge connecting link 2 and 3 with the plane of link 2 in the rigid panel linkage depicted in Figure 15. Generalization is accomplished by identifying vertices, developing a polyhedron link from them, and then perturbing the vertices to eliminate the special dimensions. To develop the polyhedron link, the number vertices must be accounted for by counting two vertices for each shared edge and adding any other vertices found in the geometry. For each link, the n vertices are connected by n external edges and $2n - 6$ internal edges. In the case of the linkage in Figure 15, three vertices are identified in link 1 (two on

34

the shared edge and one polygon vertex), five vertices are identified on link 2 (two for each shared edge and one polygon vertex), and three vertices are identified on link 3 (two on the shared edge and one polygon vertex). Thus, link 2 is generalized from a rigid, planar triangular panel to a polyhedron with five vertices, five external edges, and four internal edges to maintain rigidity. Perturbation of the vertices ensures all edges of link 2 are skew to develop its most generic form. Thus, the generalized polyhedron model linkage in Figure 15 maintains all of the salient vertices and connectivity of the original linkage while eliminating all special geometric features.
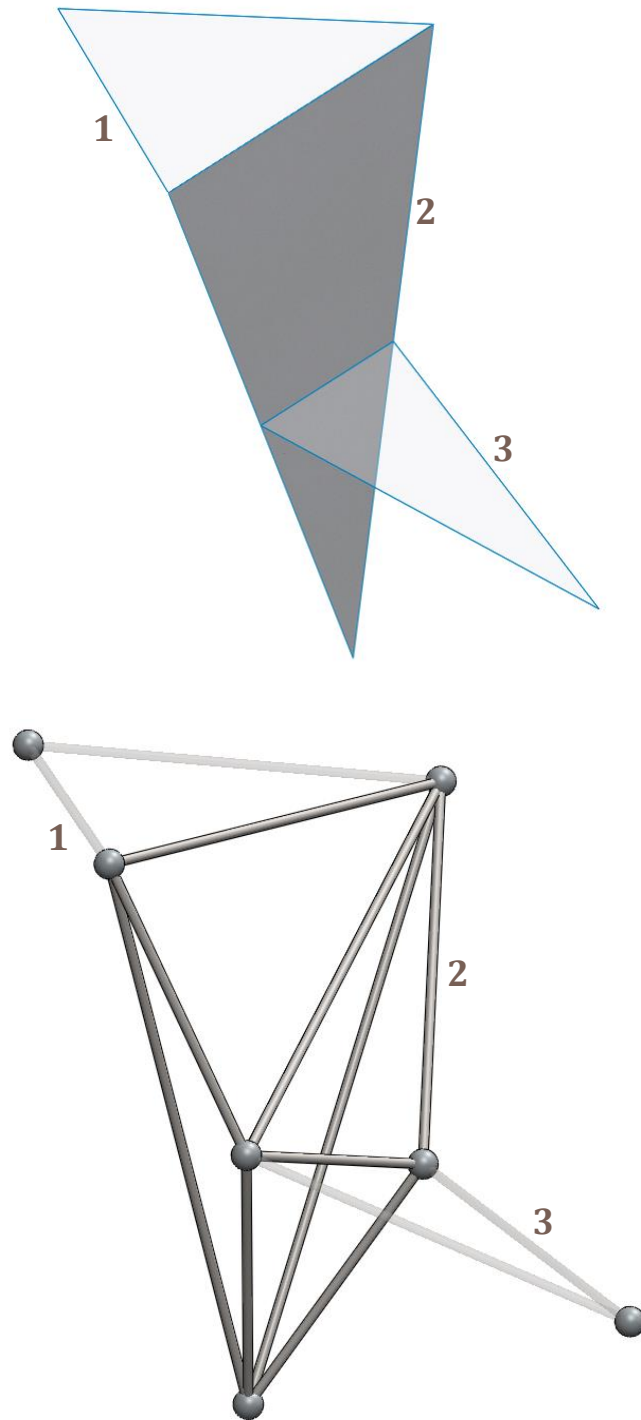
Figure 15. Rigid panel linkage with edge-plane coincidence (top) and its generic polyhedron form (bottom) with corresponding links numbered

2.3.4   Comparison of Representations

The three models each have merits and drawbacks in their use of depicting spherical system mechanisms. The rigid linkage model visualizes a kinematic representation of a mechanism in terms of links and joints, which may appeal to kinematicians. The rigid panel model visualizes the equivalent mechanism as though constructed from panels and creases as in paper art, which may appeal to non-kinematicians. On the other hand, the polyhedron model abstracts the geometry of an equivalent mechanism to vertices and edges and requires supplementary features such as internal edges to correctly depict a mechanism, which complicates its visualization. However, the generalized, richer vertex-edge connectivity information of the polyhedron model allows for a more robust mechanism analysis scheme, which will be explored later. Furthermore, whereas the rigid panel model represents kinematic paper art directly, the polyhedron model generalizes the planar links to polyhedra, which represents a broader class of spherical system mechanisms of which kinematic paper art is a subset. The properties of each model are compared for quick reference in Figure 16.

As a result of these properties, the rigid panel model is often used for visualization of a spherical system mechanism in this analysis. The rigid linkage model is used interchangeably in some cases for kinematic visualization. The rigid panel model is often converted to the polyhedron model for the purposes of analysis by converting each n-sided rigid polygon to a generalized n-sided polyhedron while maintaining link connectivity. The least obvious aspect of the conversion from panel to polyhedron is the introduction of $2n - 6$ internal edges to ensure link rigidity. The conversions between models are simplified by the introduction of connectivity graph schemes that are capable of encoding all salient information of each physical representation model.
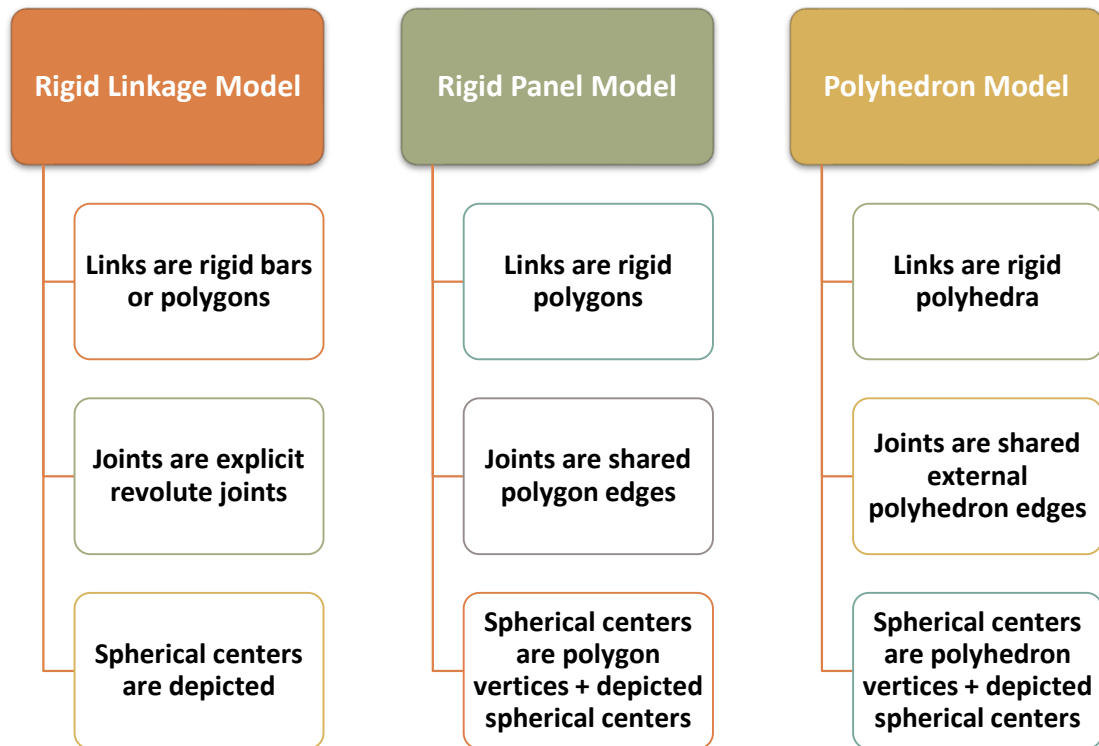
Figure 16. Comparison of physical model characteristics

3 Spherical System Connectivity Graphs

3.1 Link-Joint Connectivity Graphs for Traditional Mechanisms

Connectivity graphs have been used to represent generic planar mechanisms since the birth of computational mechanism synthesis [11]. These graphs simply use vertices to represent links and edges to represent joints. The edges connecting vertices on the graph correspond to the joints connecting the associated links in the mechanism as depicted in the planar mechanism and its link-joint graph in Figure 17. This connectivity graph scheme encodes sufficient information to encode link-joint connectivity as well as calculate generic mobility in a given constraint space using the traditional C-G-K equation. However, these graphs don't encode any spherical center information associated with loops as that data is not needed in the generic analysis of traditional mechanisms. The missing information prevents this connectivity graph scheme from effectively generalizing to spherical systems linkages which require spherical center data to identify and analyze. This shortcoming of traditional connectivity graphs motivates the development of a generalized graph representation of spherical systems.
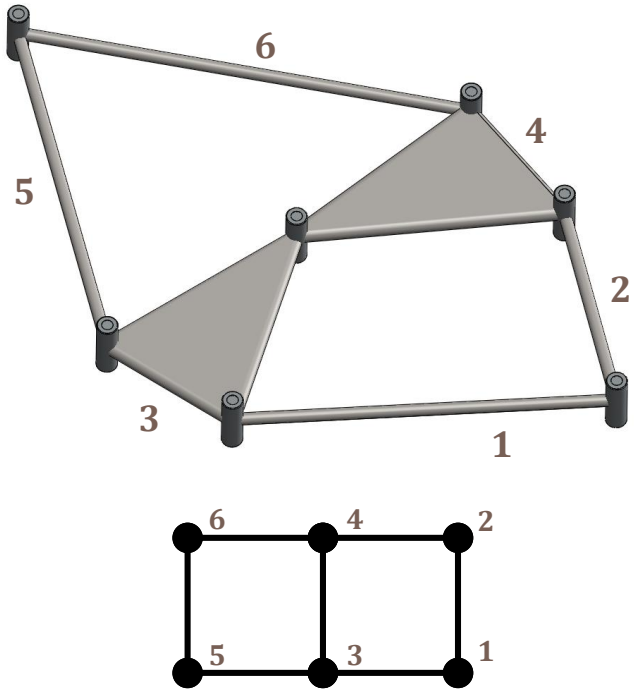
Figure 17. Planar six-bar (top) and its link-joint connectivity graph (bottom)
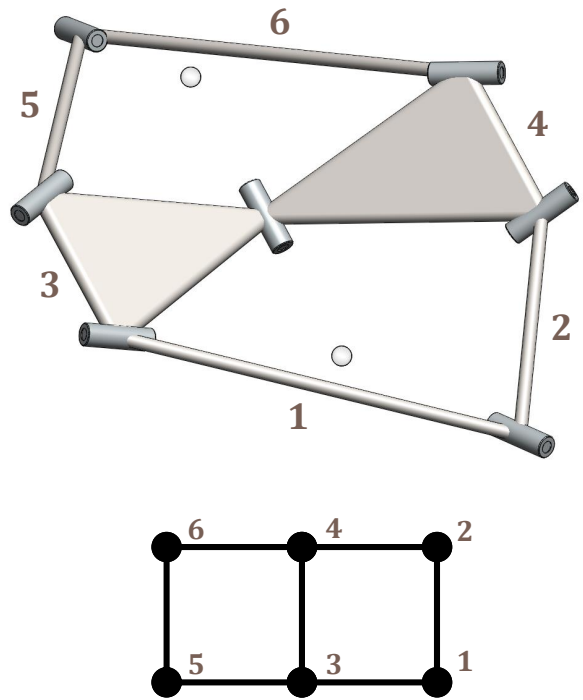
Figure 18. Spherical system six-bar (top) and its link-joint connectivity graph (bottom)

3.2 LINK-JOINT AND VERTEX-EDGE CONNECTIVITY GRAPHS FOR SPHERICAL SYSTEMS

It has been presented in the paper art literature that cartons and origami can be represented by traditional link-joint graphs based on the mechanisms' construction of rigid links connected by revolute joints [10] [2] as depicted in Figure 18. However, these simple connectivity graphs still do not encode the spherical center information associated with each loop which permits spherical system linkage identification and analysis, and the graphs are ambiguous about the joint orientation in the physical representation of the mechanism. On the other hand, Greenberg et al. note that in a simple rigid panel case with all explicit vertices, the connectivity graph is the dual of the crease graph of a mechanism [2], which implies that each loop of the link-joint graph surrounds an explicit vertex as depicted in Figure 19. This knowledge informs the necessary spherical center information in the simple, all-explicit vertex spherical system case, but this data is still not explicitly depicted in the graph.

Another graph scheme for spherical systems uses graph vertices to represent physical vertices, or spherical centers, and graph edges to represent physical creases, or joint axes. The scheme utilizes dashed edges to indicate joint axes shared between spherical centers [3] as depicted in Figure 19. This representation is a pared-down representation of the crease graph of the rigid panel model, and as a result it is essentially the dual of the link-joint connectivity graph. The vertices and edges in this graph scheme explicitly represent the spherical centers and creases, respectively, but as a result it leaves link information implicit as links are located between the open edges of the graph. The existence of important mechanism data left implicit in each of these graph schemes motivates the development of a new graph scheme to encode all salient spherical system information explicitly. It is apparent from the two insufficient graph schemes that information from both the link-joint graph and its dual vertex-edge graph is necessary to encode the salient spherical system linkage data.
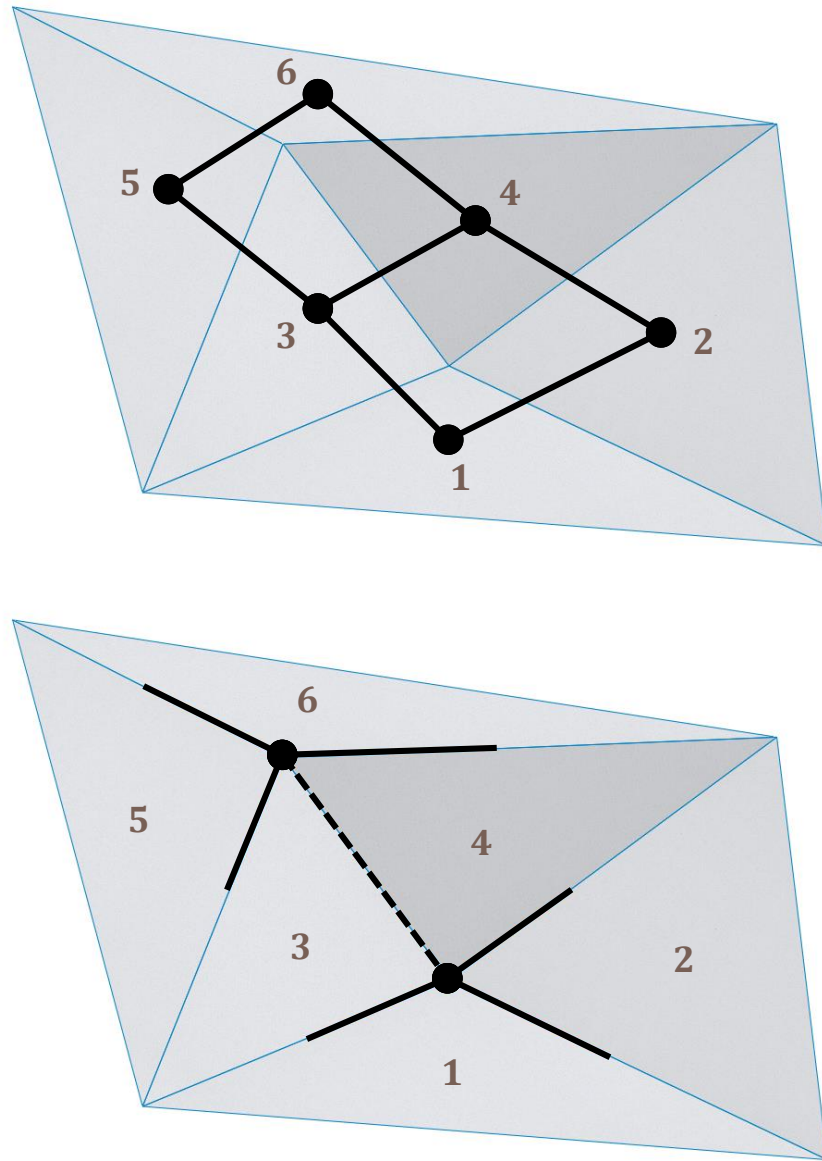
Figure 19. Spherical system six-bar with its link-joint (Greenberg et al.) connectivity graph overlaid (top) and with its vertex-edge (Bowen et al.) connectivity graph overlaid (bottom)

3.3 SPHERICAL CENTER (SC) CONNECTIVITY GRAPH

3.3.1 Definition

A new type of graph was developed to explicitly encode all salient information of the generic representation of a spherical system linkage. This data includes link-joint connectivity as well as any spherical centers shared by the joints in the loops. This graph format is valid for mechanisms with only revolute joints. The Spherical Center graph (SC graph) format uses vertices to represent links and edges to represent revolute joints as in the spherical system link-joint graph. To encode salient joint orientation information explicitly, if all joint axes of a loop are oriented to a single spherical center (or vertex), the loop formed by the associated edges in the graph will enclose an explicitly-represented spherical center symbol. The spherical center in the SC graph is represented with a circled dot (⊙), which represents any arbitrary spherical center in finite space as depicted by spherical centers a and b in Figure 20.

When the SC graph is overlaid on the corresponding rigid panel model as in Figure 21, the graph vertices lie on the physical panels they represent, and the graph edges intersect the physical creases they represent. The circled dot in each loop of the graph can be centered on the physical vertex or spherical center formed by the loop of intersecting crease axes that it represents. In interpreting the SC graph, it is known that all edges surrounding a circled dot in the graph represent physical joint axes oriented toward the corresponding spherical center in the mechanism. Any edge which is shared by two loops in the graph (such as the edge connecting the vertices 3 and 4 in the graphs of both Figure 20 and Figure 21) corresponds to a physical joint axis oriented toward the spherical centers of both loops, (i.e. spherical centers a and b). In a general spherical system mechanism, the spherical centers are not coincident, and the constraints on the physical joint axis shared between two loops fully

43

defines a line in space along which the joint axis must lie. In the case of Figure 20, the revolute joint axis connecting links 3 and 4 is aligned with the line through spherical centers a and b. In Figure 21, the joint axis connecting panels 3 and 4 is the crease connecting the physical vertices a and b. If the two spherical centers were coincident in space, which is a special case, the shared joint axis must simply pass through the single spherical center and may have any orientation.

In the special case of a mechanism loop with parallel joint axes (a planar loop), the spherical center is located an infinite distance away [13], so the spherical center can be represented on the SC graph by an infinity symbol (∞) rather than a circled dot, which explicitly indicates a spherical center at an infinite distance. A mechanism with both a finite spherical center and an infinite spherical center is depicted in Figure 22. In generic analysis, the infinite center is interchanged for an arbitrary finite center to eliminate the special parallel dimensional relation.
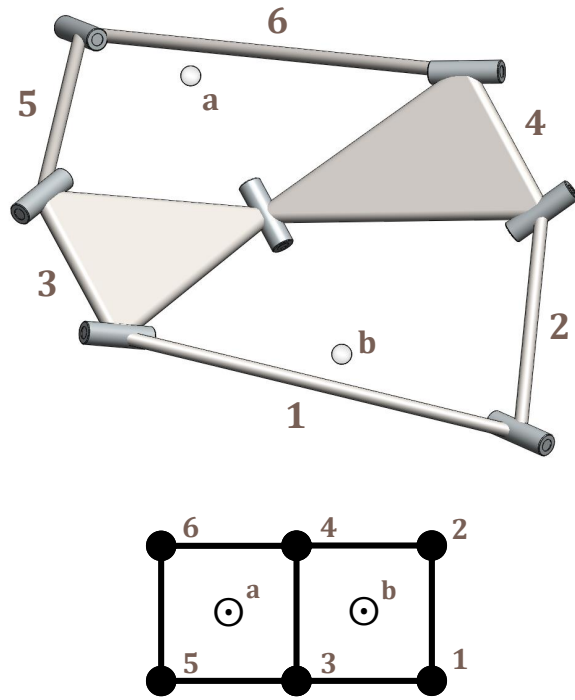
Figure 20. Spherical system six-bar (top) and its SC graph (bottom)
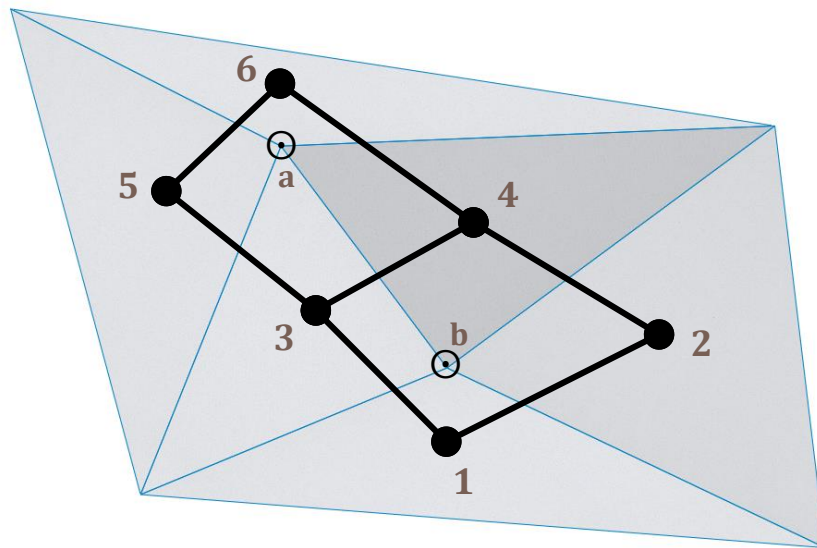
Figure 21. Spherical system six-bar with its SC graph overlaid
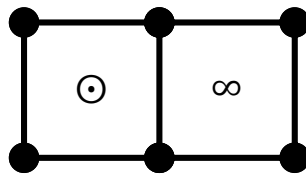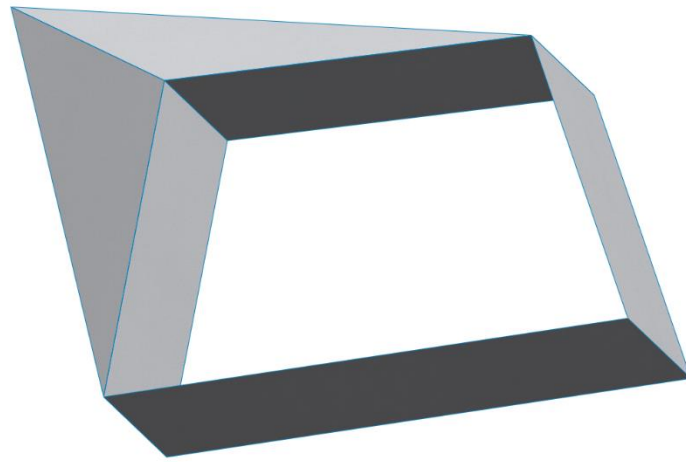
Figure 22. Spherical system six-bar with a planar loop (top) and its SC graph (bottom)

3.3.2   Application to Modified C-G-K for Spherical Systems

The data encoded in an SC graph contains sufficient information to apply the modified C-G-K equation for spherical system linkages. The graph encodes the number of links through its vertices, the number of joint through its edges, and the constraint space parameter by the existence of a spherical center in each loop. This contrasts with the traditional connectivity graph, which does not depict the spherical center data explicitly and fails to encode the constraint space parameter.

> **The accounting rules for determining the number of each feature in the modified C-G-K equation for spherical systems from the SC graph are as follows:**
>
> The number of links N is equal to the number of vertices in the SC graph
>
> The number of joints J is the number of edges in the SC graph
>
> The degree of freedom f_i of each joint is 1 DOF as all joints are assumed to be revolute
>
> The constraint space parameter λ is 3 DOF if all loops have a spherical center

3.3.3   Representation of Non-Spherical Systems

The SC graph scheme accomplishes the same encoding of information as a conventional link-joint graph, but the additional explicit spherical center information can be used to assert that each loop has a spherical center such that spherical system properties apply to the mechanism, including the validity of the modified C-G-K equation for spherical systems. If any loop does not have a single spherical center to which all loop joint axes are oriented, the linkage is not a spherical system. A spatial or spherical/spatial hybrid mechanism can still be depicted with an SC graph that lacks a spherical center in all or some loops, respectively. An example of a multi-loop hybrid mechanism with one non-spherical loop is depicted in Figure 23. If the SC graph indicates no loops have a spherical center, the mechanism is fully spatial, and the modified C-G-K equation for spatial mechanisms may be used.
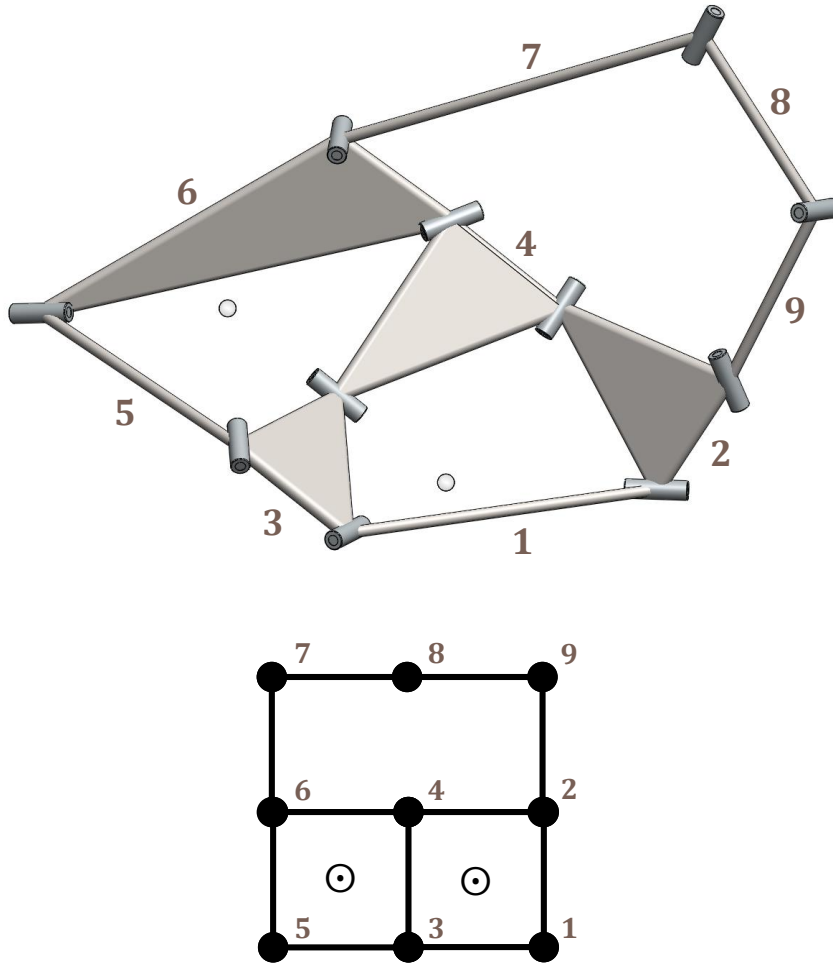
Figure 23. Spherical/spatial hybrid mechanism with two spherical loops and one spatial loop (top) and its SC graph (bottom)

3.3.4 Planar and Spherical System Analogues

Special cases occur when the spherical centers of all loops of a spherical system are coincident in space creating a spherical mechanism, and when the spherical centers are all coincident at an infinite distance away creating a planar mechanism. This distinction has no effect on the use of the modified C-G-K equation for spherical systems as the SC graph is identical (other than possibly substituting the spherical center symbols ∞ and $\odot$) and there is no change in the constraint space parameter. Because of this property, a general spherical system mechanism can be represented by its planar analogue, which is a planar mechanism with an equivalent SC graph and equal generic mobility created when the spherical centers of all loops of the SC graph are taken to be coincident at an infinite distance away. Furthermore, any planar or spherical mechanism can be represented by its spherical system analogue which represents its most generalized spherical system form with equal generic mobility created when each loop's spherical center is taken to be non-coincident and at a finite distance. An example of a spherical system mechanism, its planar analogue, and their common SC graph is depicted in Figure 24.
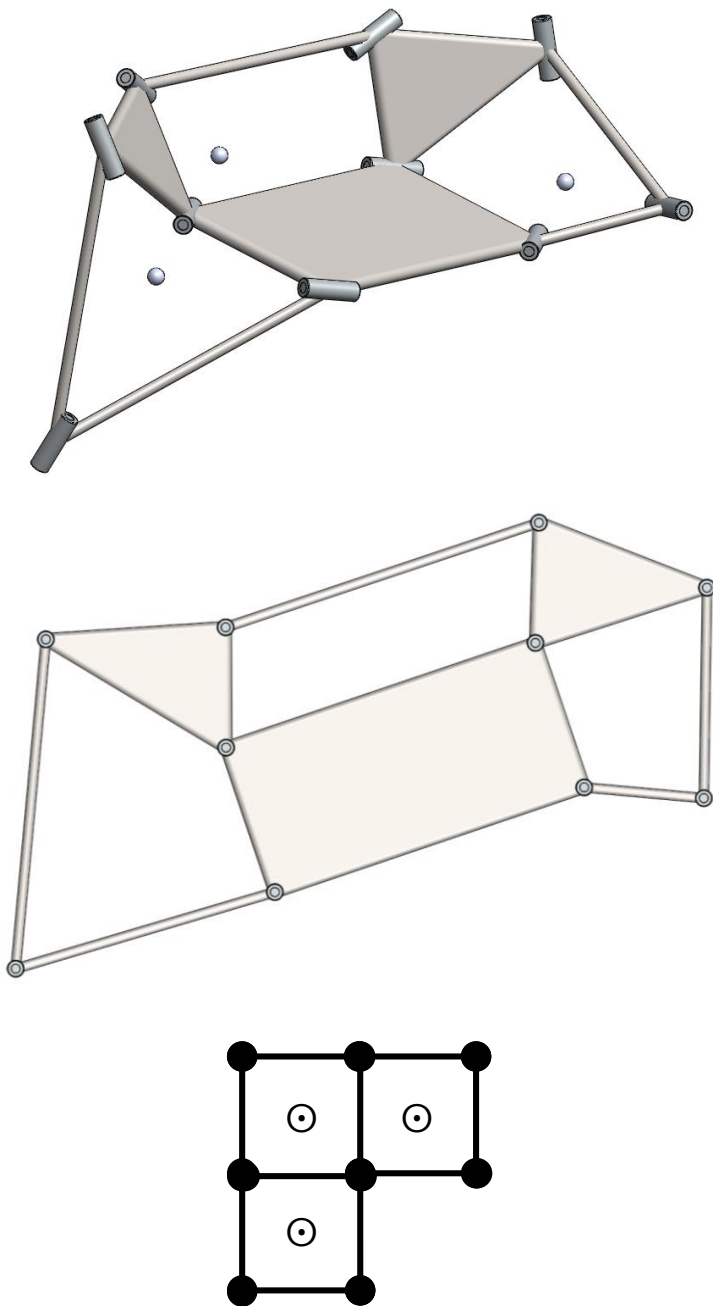
Figure 24. Spherical system eight-bar linkage (top), its planar analogue (center), and their common SC graph (bottom)

3.3.5   Case Study: Watt and Stephenson Mechanism Analogues

A benchmark example of a planar six-bar mechanism that can be generalized to a spherical system analogue with equivalent generic mobility is the planar Watt mechanism, which is depicted with its planar link-joint graph in Figure 17. A generalized Watt mechanism is developed by identifying the two loops in the graph and assigning them two arbitrary, non-coincident, finite-distanced spherical centers to form a spherical system analogue of the Watt mechanism as depicted in Figure 25. The rigid linkage and SC graph depict two distinct spherical centers in the two loops. This generalized Watt mechanism has the same generic mobility as the planar Watt mechanism as no C-G-K parameters have changed.

One can attempt to generalize the Stephenson mechanism, a similar benchmark planar six-bar mechanism, in the same way as the Watt mechanism. One first must identify the loops in the Stephenson graph, which is depicted as an SC graph in Figure 26. There are two loops in this graph so one would seek to assign two arbitrary, non-coincident, finite-distanced spherical centers. However, the two loops share two edges in the graph, which correspond to two distinct joints. Because these two non-coincident joint axes must be oriented toward both spherical centers, the only way this can be achieved if the two spherical centers are coincident in space. Thus the most generalized form of the Stephenson mechanism is a spherical mechanism because the spherical centers of the two loops are coincident in space. This generalized Stephenson mechanism has the same generic mobility as the planar Stephenson mechanism as no C-G-K parameters have changed.
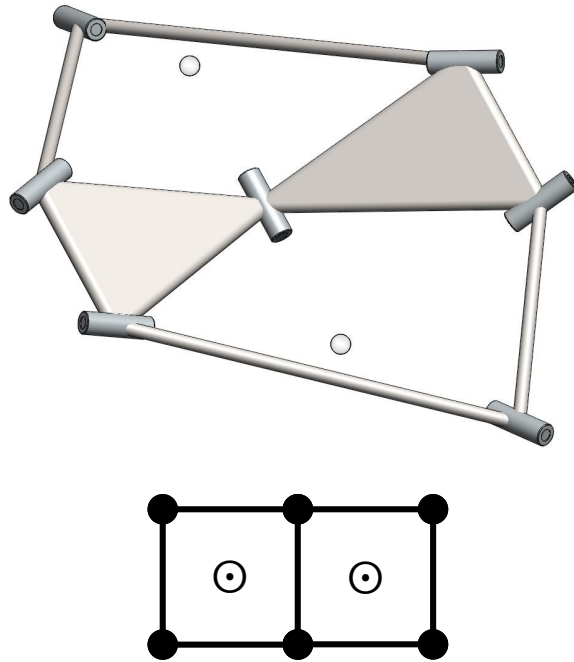
Figure 25. Spherical system analogue of a Watt mechanism (top) and its SC graph (bottom)
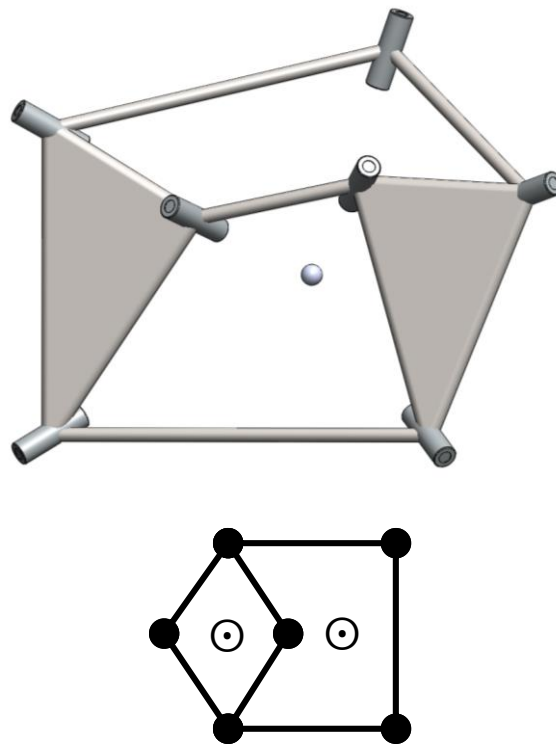
Figure 26. Spherical system analogue of a Stephenson mechanism (top) and its SC graph (bottom)

3.3.6 Exceptional Case: Concentric Loops

A very unique case occurs when two loops of an SC graph each having unique spherical centers have all graph vertices connected between loops. The resulting SC graph will appear as two interlocked, concentric loops as depicted in Figure 28, which has two interlocked, concentric eight-bar loops. The linkage depicted represents the upper section of the inflatable cube origami fold, depicted in Figure 27, which relies on the compliance of paper rather than rigid kinematics to be inflated to its open state. The inner loop of the SC graph represents the eight-bar loop of triangles (including link 1) forming the finite spherical center a, which is located at the intersection of the creases at the peak of the mechanism. The outer loop of the SC graph is the eight-bar loop of rectangles (including link 2) which have parallel axes creating a planar loop. This loop's planarity is indicated by the ∞_{outer} symbol on the SC graph, which represents the spherical center that the outer loop "encloses."

The concentricity of the graph introduces difficulty in depicting the spherical centers enclosed by the loops, and the outer loop's spherical center is thus depicted outside the loop rather than inside. Furthermore, the two eight-bar loops are connected link-to-link as in links 1 and 2, which forms eight loops with spherical centers between the outer and inner eight-bar loops. Application of the modified C-G-K equation for spherical systems fails in the presence of this type of concentricity, and the associated mechanism is observed to possess a high level of overconstraint. For these reason, concentric mechanisms will be considered an exceptional case of spherical systems which will not be pursued further in the analysis.
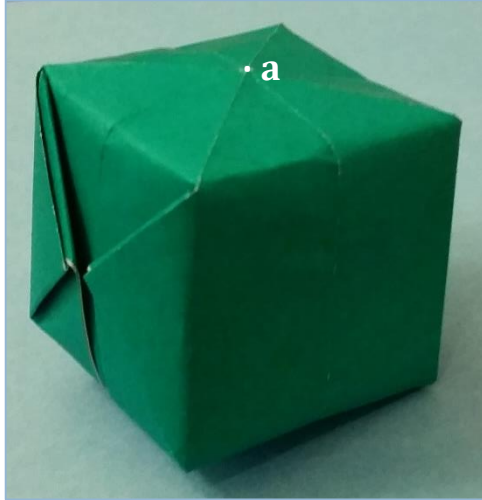
Figure 27. Inflatable cube fold with vertex highlighted
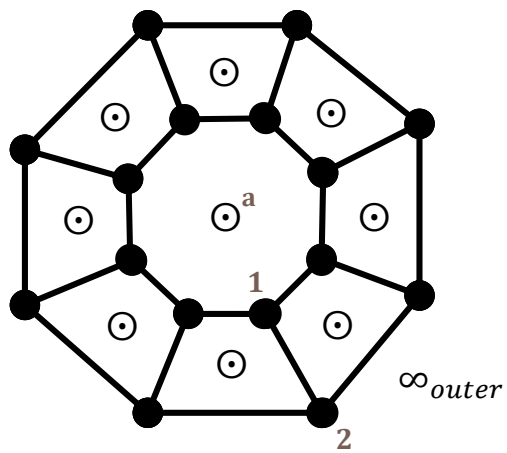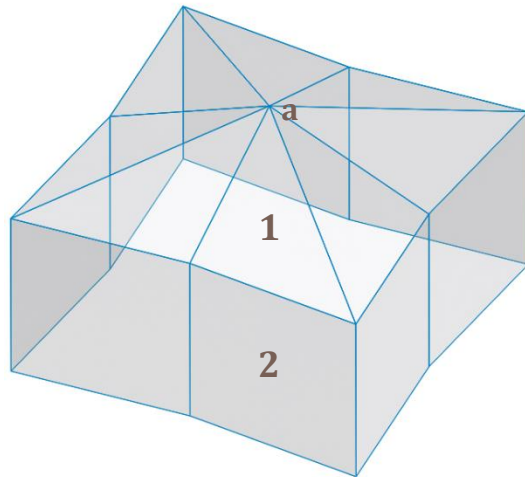
Figure 28. Rigid panel representation of upper section of inflatable cube fold (top) and its SC graph (bottom)

3.3.7 Shortcomings

The SC graph efficiently encodes the salient features of a spherical system linkage. However, the variety of geometries which may have equivalent SC graphs (evidenced in Table 2) illustrates that the SC graph fails to fully encode the geometry of the links making up the spherical system, and as a result there is ambiguity when attempting to reconstruct a physical representation of the spherical system linkage from the SC graph. Furthermore, the SC graph only encodes data for use in spherical system or fully spatial mobility calculation through the modified C-G-K equation, but it does not inform analysis of hybrid mechanisms with both spherical and spatial loops. These shortcomings motivate the development of a connectivity graph scheme that allows for the complete reconstruction of the polyhedron model of a spherical system linkage from the graph representation and inform analysis of a larger class of mechanisms.

3.4 SPHERICAL CENTER AND DEGREE (SCD) CONNECTIVITY GRAPH

3.4.1 Definition

An extension of the SC graph scheme was developed with the intention of explicitly describing the geometry of the links of which the mechanism is composed. Whereas the SC graph does not encode the link geometry, the Spherical Center and Degree graph (SCD graph) adds information about the generic polyhedron links to the SC graph through the explicit representation of vertex degree in the graph, which is the total number of edges attached to a vertex. This information can be used to reconstruct the polyhedron model of each link. All properties of the SC graph also apply to the SCD graph as the SC graph can be recovered from an SCD graph by the removal of the vertex degree information.
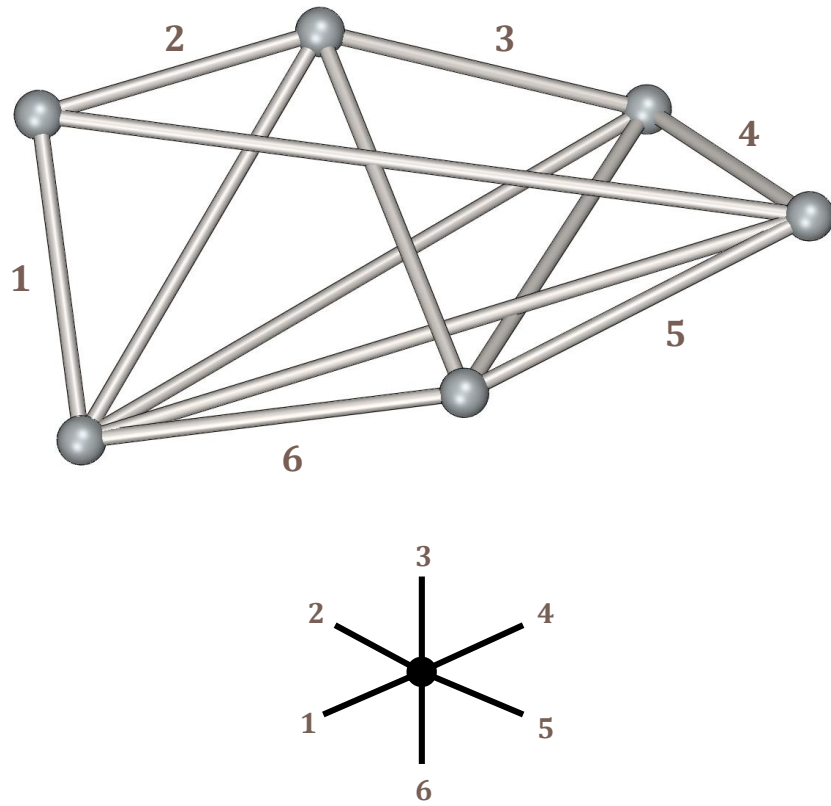
Figure 29. A six-sided rigid polyhedron link (top) and its SCD representation (bottom)

The SCD graph scheme is developed by modifying the definition of graph vertices representing links such that the edges emanating from a vertex in the graph correspond one-to-one with the external polyhedron edges connecting the vertices of the rigid polyhedron link. A rigid polyhedron with n external edges is represented in the SCD graph by a vertex with n edges emanating from it, and adjacent polygon edges are represented by radially adjacent edges about the graph vertex as depicted Figure 29. As in the SC graph, edges connecting vertices in the SCD graph correspond to joints connecting rigid links; however in the SCD graph the edge connecting the vertices must correspond to the specific, corresponding edge of the rigid polyhedron.

Open edges are unconnected edges emanating from a vertex in the SCD graph, and they represent external edges of a polyhedron which are not connected to another link. These open edges can be depicted external to a loop as in edges 1 and 2 in Figure 30 and edge 1 in Figure 31, representing exterior unconnected edges of the polyhedron facing away from a loop's vertex or spherical center. Alternatively, open edges can be depicted internal to a loop as in edge 2 in Figure 31, representing interior unconnected edges of the polyhedron facing toward an implicit spherical center.
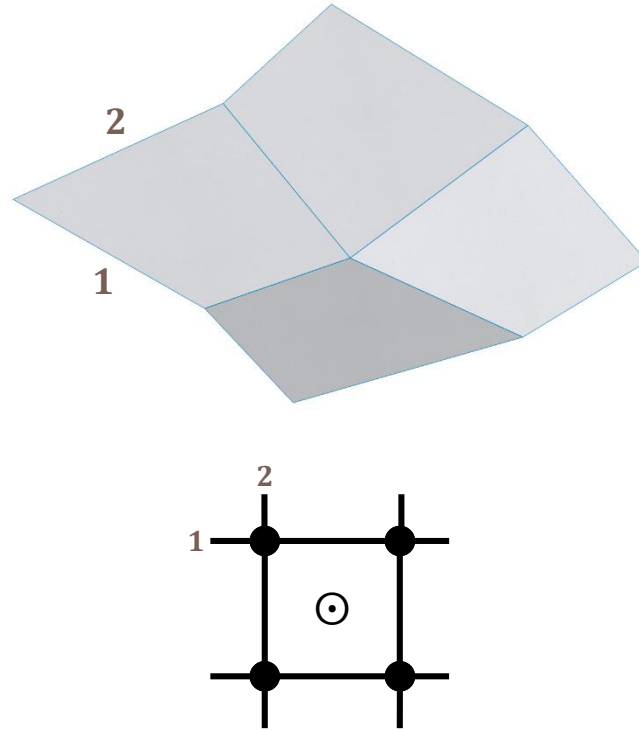
Figure 30. Spherical four-bar (top) with its SCD graph (bottom) indicating open edges external to the loop (1, 2)
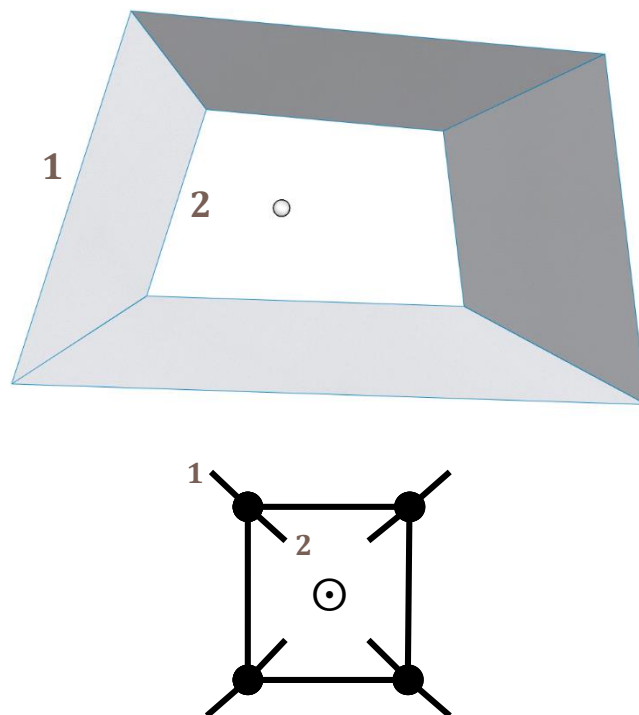
Figure 31. Spherical four-bar (top) with its SCD graph (bottom) indicating open edges external (1) and internal (2) to the loop

A rigid panel visualization of a multi-loop mechanism with its SCD graph overlaid as well as the same SCD graph redrawn with straight edges is depicted in Figure 32. This visualization reinforces that the SCD graph vertices correspond to panels, the connected edges intersect creases, and the circled dots correspond to vertices and implicit spherical centers as in the SC graph; the visualization also conveys that open edges on the SCD graph intersect unconnected panel edges. The vertex-edge portion of the SCD graph is essentially the dual of the graph formed by all creases and edges of the rigid panel model including the outer edges of the polygons.

Encoding the degree of the SCD graph vertices and the location of the open edges relative to the connected edges in the graph fully defines the generic geometry and link connectivity in the polyhedron model. Furthermore, mechanisms with different geometries which would have identical SC graphs are differentiated in their SCD graphs based on the vertex degree and edge adjacency data encoding each link's number of edges and edge connectivities. For example, removal of the open edges in the SCD graphs of the mechanisms in Figure 30 and Figure 31 demonstrates that their SC graphs are identical, whereas their differing SCD graphs encode each mechanism's unique connectivity.
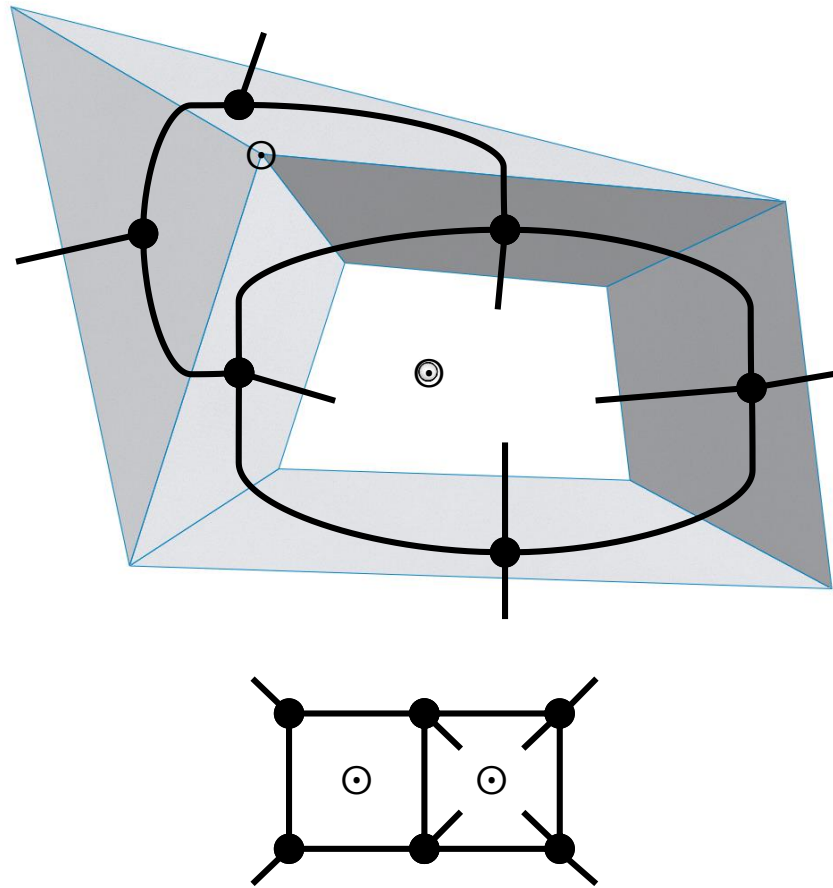
Figure 32. Multi-loop spherical system with its SCD graph overlaid (top) and its SCD graph redrawn (bottom)

3.4.2 Exceptional Case: Interior Sub-Loops

In the SCD graph of a mechanism with open edges interior to a loop, additional links may connect these open edges, forming a sub-loop inside the initial loop. It is important to note that the joint axes of the sub-loop are not necessarily oriented toward the initial loop's spherical center as the SCD graph may imply. An example is depicted in Figure 33 in which the joints of the outer loop are highlighted in both the mechanism and its SCD graph. Only these outer, highlighted joints are oriented toward the highlighted spherical center; the joints of the interior sub-loop are not, but they are oriented to the non-highlighted spherical center enclosed by the sub-loop. This is difficult to depict in a two-dimensional connectivity graph and will be considered an exceptional case of SCD graphs.

3.4.3 Mechanism Reconstruction and Polyhedron Feature Counting

The SCD graph informs the reconstruction of the mechanism geometry in the polyhedron model. This is because the polyhedron model is the most generic representation of a mechanism, and its generic geometric and connectivity information is fully encoded in the SCD graph. Specifically, each degree-n vertex encodes a rigid link with n vertices connected by n external edges and $2n - 6$ internal edges to maintain rigidity. The lowest possible SCD vertex degree is three, which represents a triangular truss. The external edges of the polyhedra that connect to the other links are specified by the ordering of the adjacent open and connected edges of the SCD graph vertices. Loops with no internal open edges that surround a circled dot connect at a single physical vertex, and loops with internal edges that surround a circled dot have an implicit spherical center to which the loop joints are oriented. As a result, all polyhedral mechanism configurations with unique geometry and connectivity are encoded by unique SCD graphs.
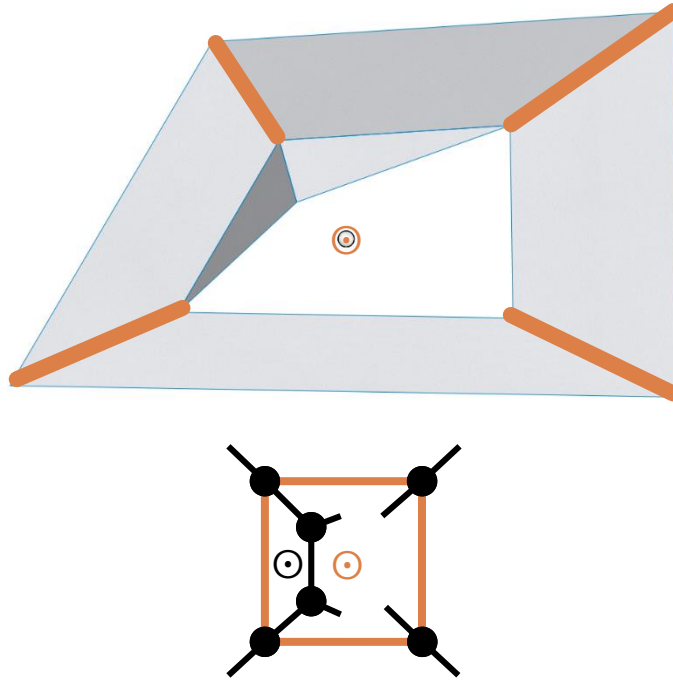
Figure 33. Spherical system mechanism with a sub-mechanism internal to a loop (top) and its SCD graph (bottom)
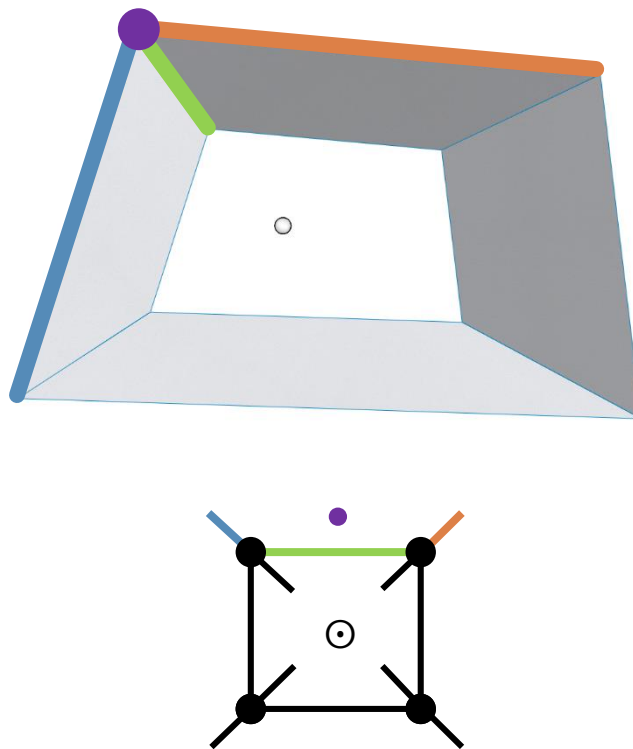
Figure 34. Spherical four-bar (top) with its SCD graph (bottom) with vertex highlighted

Identifying polyhedron vertices which are not spherical centers of loops using the SCD graph requires an extra step of interpretation. Polyhedron vertices are associated with paths in the SCD graph connecting two adjacent open edges that are in the same loop or external to all loops. An example is visualized in Figure 34 in which the highlighted polyhedron vertex is associated with the path on the SCD graph created by the three colored edges. The orientation of the corresponding colored joints on the rigid panel model are all coincident with this vertex in the mechanism. There is a polyhedron vertex between each adjacent open edge pair when traversing around the outside of the SCD graph or inside a loop. A result of this property is the total number of polyhedron vertices which are not spherical centers is equal to the total number of open edges on the SCD graph.

Based on the relation of the SCD graph to the polyhedron model due to their equivalent encoding of generic representation information, it is desirable to use the SCD graph to account for the number of vertices, implicit spherical centers, external edges, and internal edges of the polyhedron representation of a mechanism. This is analogous to the use of the SC graph to account for the number of links and joints in a mechanism and to identify the constraint space parameter. The variables extracted from the SCD graph can be used in a mobility formulation for the polyhedron model [13].

The accounting rules for determining the number of each feature in the polyhedron model of a mechanism from the SCD graph are as follows:

The number of vertices V is equal to the number of open edges in the SCD graph plus the number of circled dots in loops with no open edges internal to the loop

The number of implicit spherical centers C is equal to the number of circled dots in loops with open edges internal to the loop

The number of external edges E_{ext} is the total number of edges of the SCD graph

The number of internal edges E_{int} requires identifying all vertices with degree n greater than or equal to four and adding $2n - 6$ internal edges for each

---

3.4.4 Explicit Polyhedron Mechanism Graph Reconstruction

A direct method can be used to reconstruct the polyhedron model from an SCD graph. The process entails deriving a graph of the polyhedron vertices and edges visually from the SCD graph. An example is depicted in Figure 35. First, one draws all the polyhedron vertices associated with the pairs of open edges internal to each loop and external to all loops. Next, one draws all polyhedron vertices associated with spherical centers of loops with no internal edges. The union of these two sets of vertices are all of the polyhedron vertices, depicted as blue vertices in Figure 35. All external polyhedron edges can be identified and drawn such that each one intersects one SCD graph edge to connect adjacent polyhedron vertices. These edges are depicted as blue edges in Figure 35. Next, all spherical centers can be drawn as an open circle symbol ($\circ$) corresponding to circled dots in loops with internal open edges as depicted by the open circle in Figure 35. Finally, $2n - 6$ internal edges are added to non-adjacent vertices of each polyhedron developed from a vertex of degree n (greater than or equal to four). The internal edges are depicted as light blue edges in the final polyhedron graph in Figure 35. The polyhedron model is constructed from the graph by treating edges as rigid bars and vertices as spherical joints, then generalizing the dimensions without invalidating specified joint orientations. The polyhedron linkage developed in Figure 35 is the generic equivalent of that in Figure 32 as expected based on the equivalence of the SCD graphs.
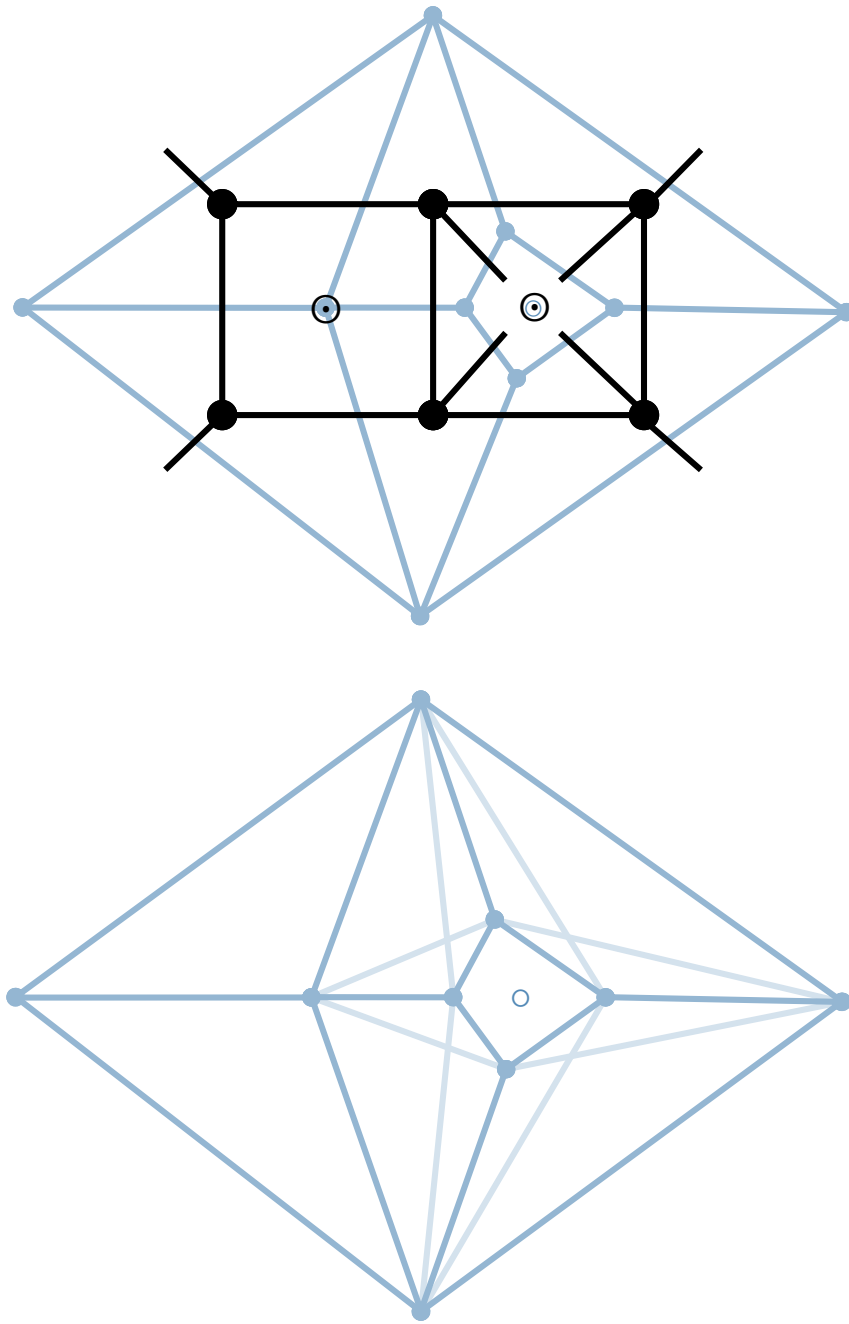
Figure 35. Explicit reconstruction of complete polyhedron model graph (bottom), developed from its SCD graph, overlaid (top)

3.5 EXAMPLES OF SPHERICAL SYSTEM MECHANISMS AND THEIR CONNECTIVITY GRAPHS

The following examples exemplify properties of the SC and SCD graph schemes using variations of mechanisms with comparable connectivities.

3.5.1 SC Graphs of Watt Six-Bar Variations

Variations of rigid panel six-bars which are all spherical system analogues of a Watt mechanism are presented in Table 2. The geometric variations demonstrate how the SC graph and the modified C-G-K parameter count does or does not change with modifications to the geometry. This can be contrasted to the SCD graph depictions of the comparable mechanisms in Table 3.

3.5.2 SCD Graphs of Watt Six-Bar Variations

Variations of rigid panel six-bars which are all spherical system analogues of a Watt mechanism are presented in Table 3. The geometric variations demonstrate how the SCD graph and the polyhedron feature count does or does not change with modifications to the geometry. This can be contrasted to the SC graph depictions of the comparable mechanisms in Table 2.
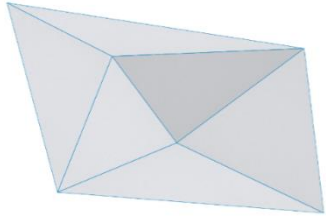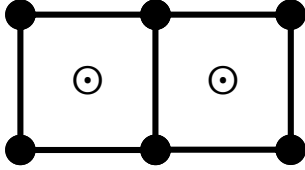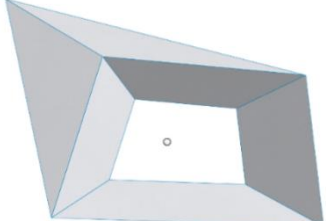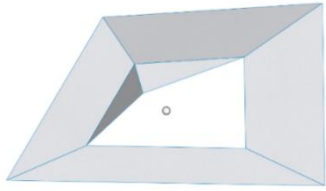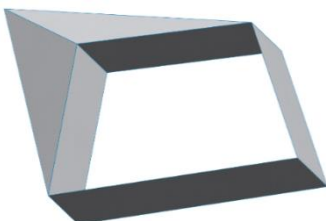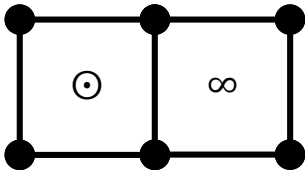
Rigid Linkage	Comment	SC Graph	Parameters
	The spherical centers of the two loops are both explicit vertices in the geometry		
	The spherical center of one loop is implicit in the geometry, but the graph is identical		$N = 6$ $J = 7$ $\lambda = 3$
	The connecting edges and vertex of two links has changed in the geometry, but the graph is identical		
	The spherical center of the planar loop is an infinite distance away due to the parallel axes. This is depicted in the graph explicitly		

Table 2. Spherical system six-bars with varying geometry and SC graphs
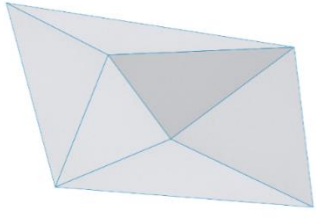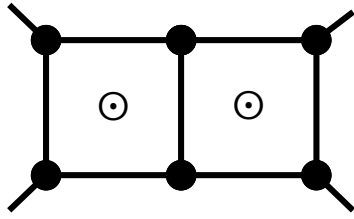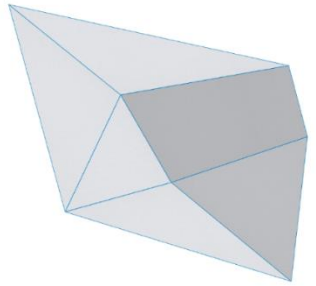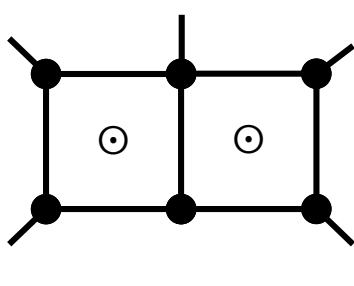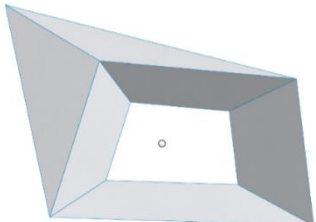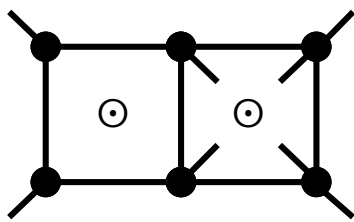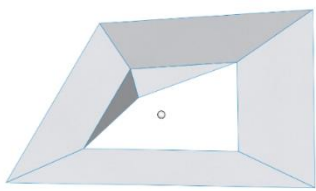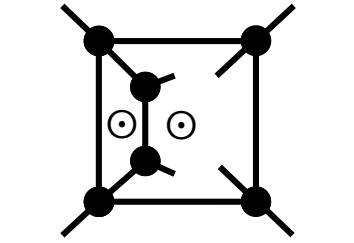
Rigid Linkage	Comment	SCD Graph	Parameters
	The links are trusses so they are all degree three. Four links have one external open edge each		$V = 6$ $C = 0$ $E_{ext} = 11$ $E_{int} = 0$
	One link has four edges, so its vertex is degree four, there is an additional external open edge, and there are two internal edges introduced		$V = 7$ $C = 0$ $E_{ext} = 12$ $E_{int} = 2$
	One loop has an implicit spherical center rather than a vertex, so there are four internal open edges and four degree-4 vertices introducing eight internal edges		$V = 9$ $C = 1$ $E_{ext} = 15$ $E_{int} = 8$
	The mechanism contains a sub-loop attached to edges internal to the outer loop, but the feature count does not change		

Table 3. Spherical system six-bars with varying geometry and their SCD graphs

3.5.3   SC Graph Equivalent of Vertex-Edge Classification Graphs (Bowen et al.)

Bowen et al. classify origami mechanisms using the characteristics of their vertex-edge graph [3]. The classifications have been converted to SC graphs in Table 4 and Table 5 to visualize the SC graphs associated with each classification type. The conversion is performed by converting the vertices of the vertex-edge graph to an SC graph spherical center, assigning the space between open edges on the vertex-edge graph vertices representing links on the SC graph, and connecting the SC graph vertices with edges which intersect the edges of the vertex-edge graph. The dashed edges on the vertex-edge graph correspond edges on the SC graph which belong to multiple loops. The SC graph is comparable to the dual of the vertex-edge graph but with the addition of the original vertices depicted explicitly. The patterns and periodicity with which Bowen et al. classify the systems are retained in the SC graph representation.
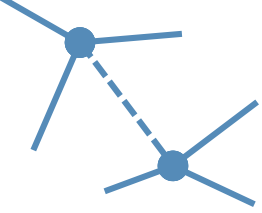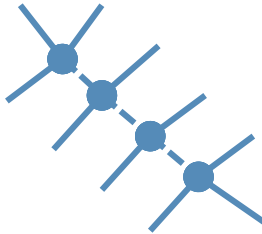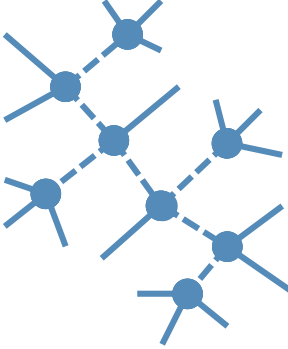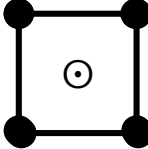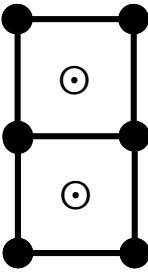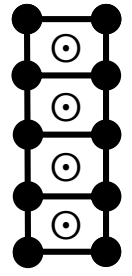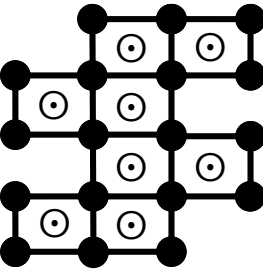
	Single	Coupled	N-Linear	Tree
Vertex-Edge Graph				
SC Graph				

Table 4. Conversion of vertex-edge graph to SC graph for spherical system open chains
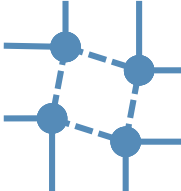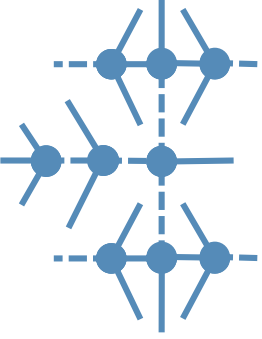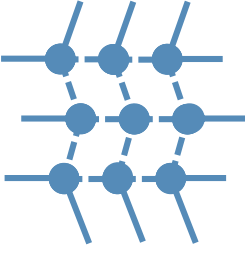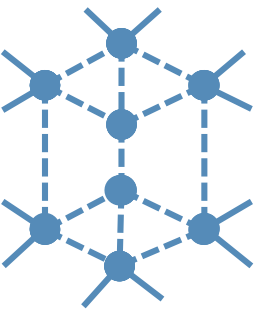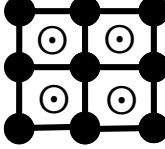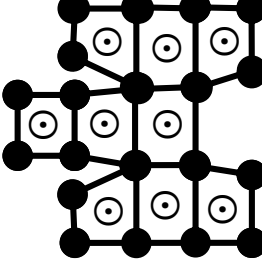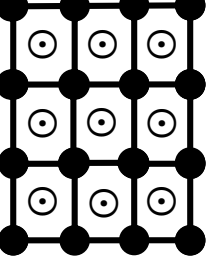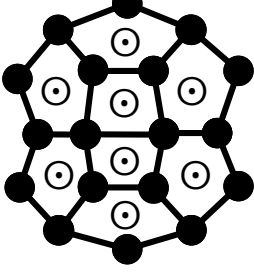
	Single Loop	1D Periodic	2D Periodic	Non-Periodic
Vertex-Edge Graph				
SC Graph				

Table 5. Conversion of vertex-edge graph to SC graph for spherical system networks

3.5.4 Spherical System Six-Bar Pop-Up Element

The source of inspiration for the identification and analysis of spherical system mechanisms is the prominence of the mechanism class in kinematic paper art. Element 1 utilizes the paper art domain to present the reader with an interactive spherical system analogue of a Watt mechanism. Figure 36 depicts the equivalent mechanism's SC graph, which indicates there is a planar loop associated with the parallel folds and a finite centered loop associated with the vertex developed by the intersection of creases on the pop-up strip.
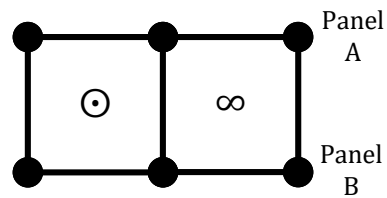
Figure 36. SC graph representation of six-bar pop-up element

Instructions:

1. Photocopy and print this diagram on a new sheet of paper
2. Cut along the solid black lines (don't cut anywhere else)
3. Crease the dashed lines (– – – – –) as valley folds, meaning the "peak" faces away from you
4. Crease the dot-dash lines (– · – · – ·) as mountain folds, meaning the "peak" faces toward you
5. Make sure the creases between Panel A and Panel B extend to the edges of the paper
6. Actuate the mechanism by changing the angle between Panel A and Panel B

Crease to edge of paper

Panel A

Panel B
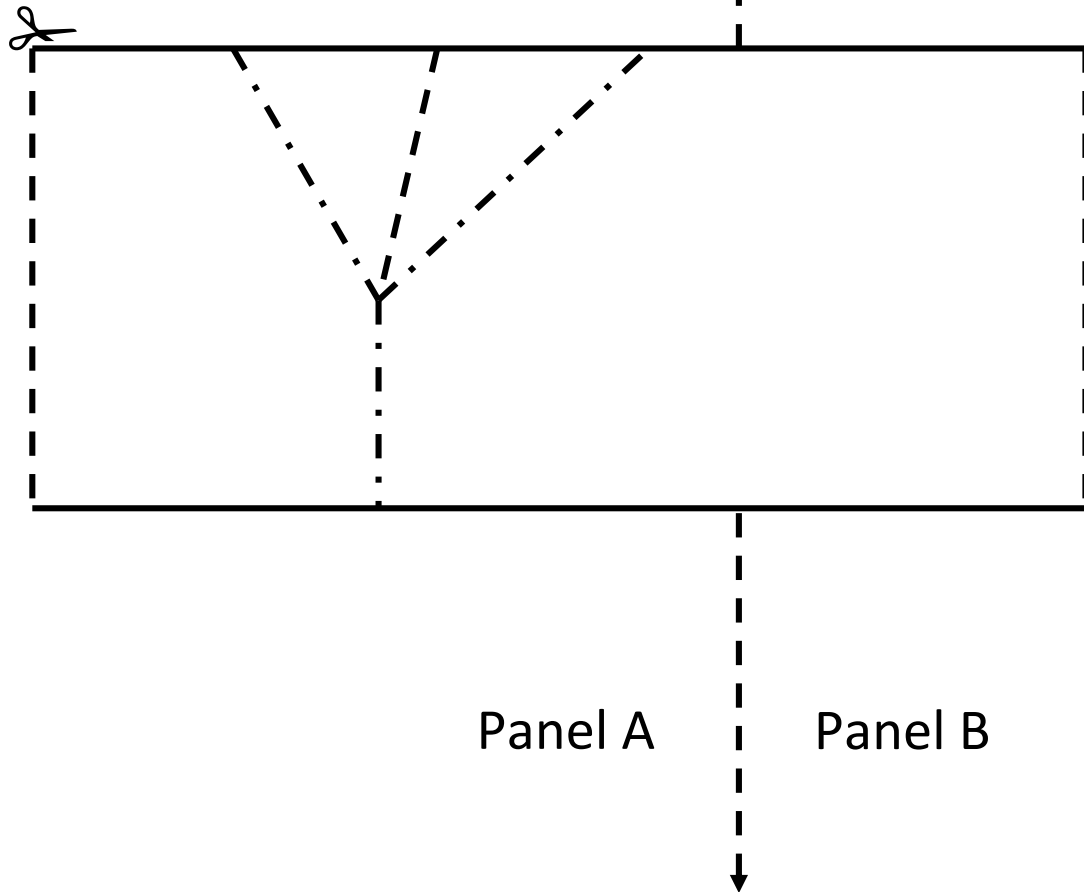
Element 1. Spherical system six-bar pop-up element

3.6 VALUE OF SPHERICAL SYSTEM CONNECTIVITY GRAPHS

The spherical system connectivity graph schemes proposed in this section address the shortcomings of the existing graph schemes by incorporating salient features of spherical systems which are not represented in traditional linkages. The ability to develop the graph stems from the recognition of spherical systems as a generalized class of mechanism, and the two schemes each encode specific information which may be leveraged depending on the analysis needed. The SC graph scheme simply encodes link-joint connectivity and spherical center orientation data. This scheme is the minimal, generic representation of a spherical system's connectivity and informs analysis under the assumption that spherical system status is maintained in the linkage. On the other hand, the SCD graph scheme adds link geometry and specific joint connectivity which informs the polyhedron model, the most generalized physical representation of a linkage. This richer information can inform analysis of spherical systems, spherical/spatial hybrid mechanisms, and fully spatial mechanisms. The trade-off between to two schemes is the robustness of the analysis capability vs. the quantity of data that must be encoded.

4 SPHERICAL SYSTEM MOBILITY AND ADJUNCT ADDENDA

4.1 GENERIC MOBILITY EQUATIONS

4.1.1 Spherical System Mobility Equation

The modified C-G-K equation for spherical system mechanisms established in (Eqn. 2) holds under the condition that all loops of a mechanism's SC graph contain a spherical center with no concentric loops and where one link is taken to be grounded. It does not matter whether the spherical centers are all unique, some are coincident, or all are coincident. The equation is not valid if there are both spherical and spatial loops in a single mechanism, but the modified C-G-K equation for spatial mechanisms can be used to predict generic mobility if all loops are spatial. Applying the modified C-G-K equation to a subset of paper art-inspired spherical system mechanisms which meet certain connectivity criteria permits simplification of the equation to fewer parameters.

The modified C-G-K equation for spherical systems can be reduced to fewer parameters under the assumptions that a mechanism has a spherical center for every loop in its SC graph and consists entirely of revolute joints, which is the case in most kinematic paper art. As a result of the spherical center condition, the constraint space parameter λ is fixed as 3 DOF, and as a result of the all-revolute joint condition, the mobility of each joint f_i is 1 DOF. Thus, the Modified C-G-K equation can be reduced to the spherical system mobility equation expressed in (Eqn. 3) [13]. Assuming the connectivity criteria are met, its parameters are completely informed simply by counting the relevant features of the SC graph.

$$M = 3N - 2J - 3 \qquad \textit{(Eqn. 3)}$$

$M = generic\ mobility\ of\ revolute, spherical\ system\ mechanism$
$N = number\ of\ links$
$J = number\ of\ joints$

This equation only holds for the limited case of mechanisms that meet the strict definition of revolute-only spherical system linkages. The benefit derived from the limited utility of the equation is that it requires a very simple count of links and joints from an SC graph without the need to know any geometric properties assuming the connectivity criteria are met. On the other hand, generalized mechanisms which consist of both spherical and spatial loops (spherical/spatial hybrid mechanisms) require a more robust equation which account for specific connectivity and geometric features which are not encoded in the SC graph. The features of the polyhedron model and SCD graph are needed to develop a robust generic mobility equation for these mechanisms.

4.1.2   Polyhedron Model Mobility Equation

Along with the polyhedron representation of a mechanism, Wampler et al. develop a mobility equation utilizing the features of the polyhedron model which provides a generalized mobility formulation for spherical/spatial hybrid mechanisms [13]. The equation covers more connectivity cases than the modified C-G-K equation and spherical system equation as it does not require all loops to be all spherical or all spatial; thus, it can be used in spherical systems in which all loops contain a spherical center, in hybrid linkages with both spherical and spatial loops, and in spatial linkages with all spatial loops. The polyhedron equation as stated in (Eqn. 4) predicts the generic mobility in the cases where all joints are revolute and the loops may be any combination of spatial or spherical with no concentricity, assuming no additional special geometric features [13]. This covers all but the most exceptional configurations of kinematic paper art and its generalized class of

75

spherical/spatial hybrid mechanisms. The equation's parameters are completely informed

by counting the connectivity features of the polyhedron model, which can be done via the SCD

graph.

$$M = 3(V + C) - E - 6$$

$M = generic\ mobility\ of\ revolute\ spherical/$
$\qquad\qquad spatial\ hybrid\ mechanism$
$V = number\ of\ polyhedron\ vertices$
$C = number\ of\ implicit\ spherical\ centers$
$E = E_{ext} + E_{int} = total\ number\ of\ polyhedron\ edges$
$\qquad\qquad (external\ and\ internal)$

The SCD graph provides a shortcut to encode the number of each relevant feature in

the polyhedron model, and therefore the SCD graph is sufficient information to calculate the

mechanism mobility. Because the polyhedron mobility equation covers a much more general

class of mechanisms than the spherical system mobility equation, the SCD graph is shown to

be valuable for the analysis of mechanisms with any combination of spherical and spatial

loops. The cost of the SCD graph's robustness is the need to encode the extra

geometric/connectivity information and implement a more complex counting process than

that associated with the SC graph and the simple spherical system mobility equation.

4.1.3   Comparison of Utility of Mobility Equations

The three cases of all-revolute mechanisms which may be encountered in the context

of mechanisms inspired by kinematic paper art are spherical system mechanisms,

spherical/spatial hybrid mechanisms, and fully spatial mechanisms. For a spherical system

mechanism, the strict constraints permit the use of the simpler spherical system mobility

equation informed by parameters encoded in the simple SC graph as a sufficient means of

calculating the generic mobility. For a fully spatial mechanism, the modified C-G-K equation

for spatial mechanisms informed by parameters encoded in the simple SC graph is a sufficient

means of calculating the generic mobility. For a spherical/spatial hybrid mechanism, the polyhedron mobility equation informed by parameters encoded in the more complex SCD graph is the only means of calculating the generic mobility. The identification of a given mechanism as one of these classes permits identification of the simplest, sufficient means of encoding the mechanism in a graph and the simplest means of calculating the generic mobility, as summarized briefly in Figure 37.

On the other hand, there is overlap in the connectivity classes which each analysis technique covers as summarized in Table 6. The traditional C-G-K equation only covers the cases where a mechanism is fully spherical/planar or fully spatial. The modified C-G-K equation generalization covers these cases as well as the broader class of spherical system mechanisms, thus overriding the utility of the traditional C-G-K equation. The spherical system mobility equation, in contrast, covers only a subset of mechanisms which meet the strict criteria of revolute-only spherical systems. Finally, the polyhedron mobility equation is sufficient to cover all cases because it includes hybrid mechanisms, and it is the most robust equation of all. The trade-off for this robustness is the need for the SCD graph of the mechanism which includes all polyhedron geometry information. Therefore, given an SCD graph, the polyhedron equation is the most reliable equation to use in any situation. Given an SC graph, the modified C-G-K equation is appropriate to use if the mechanism is every loop is spherical or every loop is spatial, and the spherical system equation is only appropriate to use for a mechanism that is known to be an all-revolute spherical system.
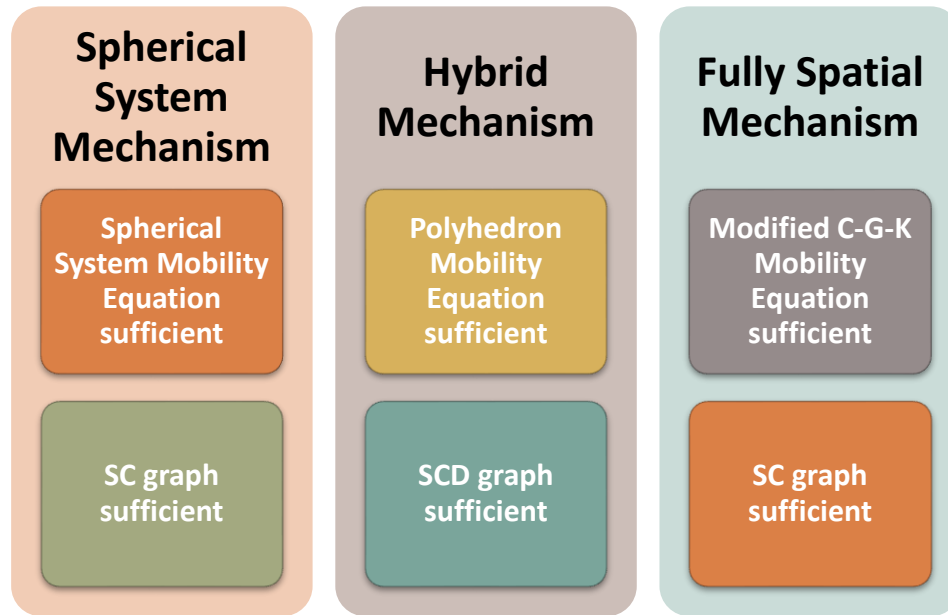
Figure 37. Summary of sufficient analysis technique for each mechanism class

Mobility Equation	Required Graph	Spherical/Planar Mechanism	Spherical System Mechanism	Hybrid Mechanism	Fully Spatial Mechanism
Traditional C-G-K Equation (Eqn. 1)	Link-Joint graph	✓			✓
Modified C-G-K Equation (Eqn. 2)	SC graph	✓	✓		✓
Spherical System Equation (Eqn. 3)	SC graph	✓	✓		
Polyhedron Model Equation (Eqn. 4)	SCD graph	✓	✓	✓	✓

Table 6. Summary of applicable mechanism classes for each analysis technique

4.1.4 Examples of Generic Mobility Calculation

The following examples depict various paper art-mimetic mechanisms with their SC and/or SCD graphs as appropriate. The generic mechanism mobility is calculated using the spherical system mobility equation, the polyhedron mobility equation, and/or the modified C-G-K equation for fully spatial mechanisms as appropriate.

4.1.4.1 Two Loop Six-bar Mobility

Rigid Panel Linkage   SC Graph   SCD Graph
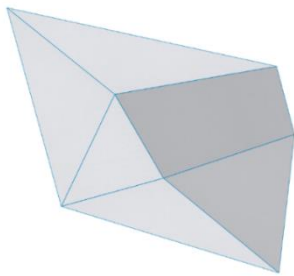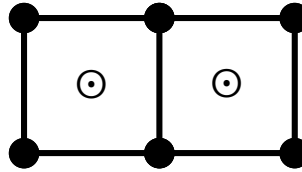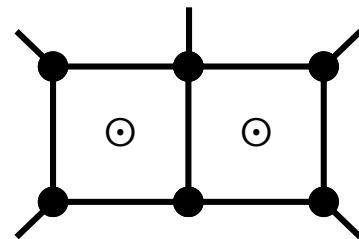
Spherical system
$N = 6; \ J = 7; \ \lambda = 3$
$M = 3N - 2J - 3 = 1$
$\boxed{M = 1 \ DOF}$

Polyhedron
$V = 7; \ C = 0; \ E = (12)_{ext} + (2)_{int} = 14$
$M = 3(V + C) - E - 6 = 1$
$\boxed{M = 1 \ DOF}$

4.1.4.2 Three Loop Eight-bar Mobility

Rigid Panel Linkage   SC Graph   SCD Graph
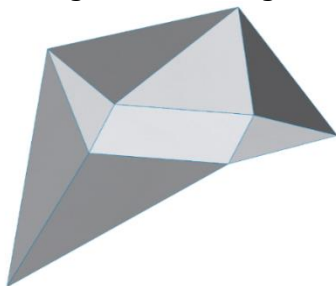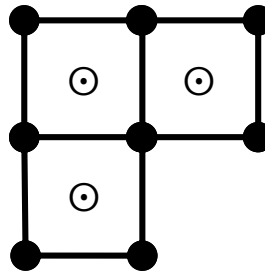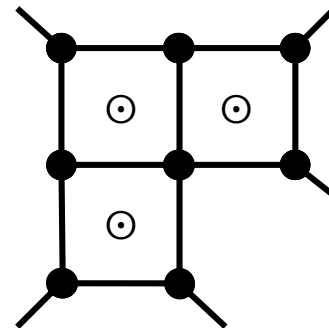
Spherical system
$N = 8; \ J = 10; \ \lambda = 3$
$M = 3N - 2J - 3 = 1$
$\boxed{M = 1 \ DOF}$

Polyhedron
$V = 8; \ C = 0; \ E = (15)_{ext} + (2)_{int} = 17$
$M = 3(V + C) - E - 6 = 1$
$\boxed{M = 1 \ DOF}$

79

4.1.4.3 Three Link Spatial Chain Mobility
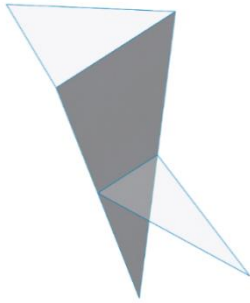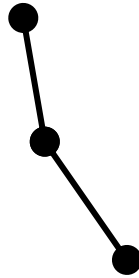
Rigid Panel Linkage　　　SC Graph　　　Polyhedron Linkage　　　SCD Graph
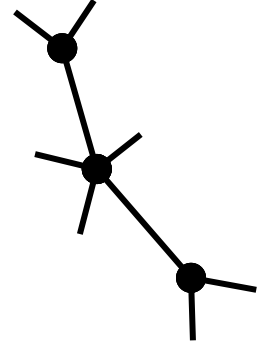
Spatial
$N = 3;\ J = 2;\ \lambda = 6;\ f_i = 1$
$M = \lambda(N - J - 1) + \sum f_i = 2$
$\boxed{M = 2\ DOF}$

Polyhedron
$V = 7;\ C = 0;\ E = (9)_{ext} + (4)_{int} = 13$
$M = 3(V + C) - E - 6 = 2$
$\boxed{M = 2\ DOF}$

4.1.4.4 Five Loop Eight-Bar (Fortune Teller) Mobility

Rigid Panel Side View　　　　　　　　Rigid Panel Top View
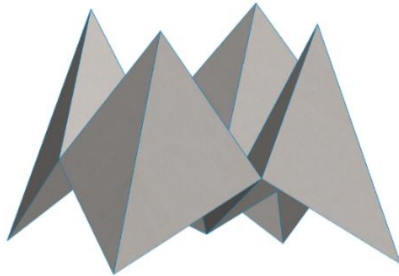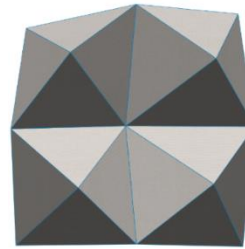
SC Graph　　　　　　　　SCD Graph
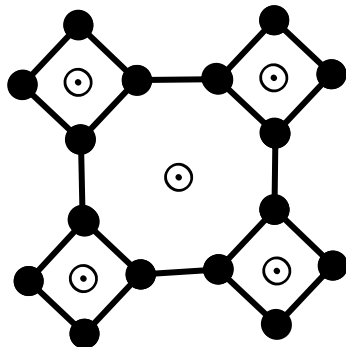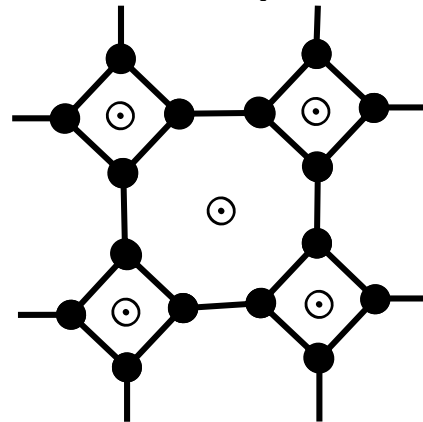
Polyhedron
$V = 13; \ C = 0; \ E = (28)_{ext} = 28$
$M = 3(V + C) - E - 6 = 5$
$M = 5 \ DOF$

4.1.4.5 Nine-Bar Mesh Mobility

Rigid Panel Linkage	SC Graph	SCD Graph
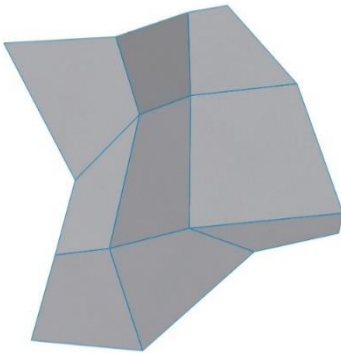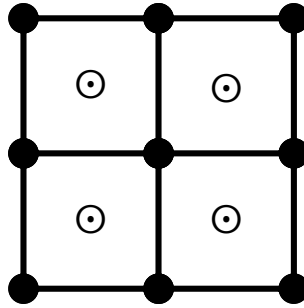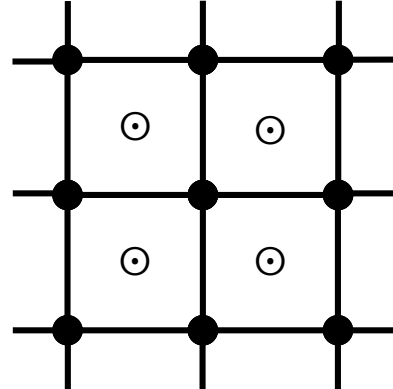
Spherical system
$N = 9; \ J = 12; \ \lambda = 3$
$M = 3N - 2J - 3 = 0$
$M = 0 \ DOF$

Polyhedron
$V = 16; \ C = 0; \ E = (24)_{ext} + (18)_{int} = 42$
$M = 3(V + C) - E - 6 = 0$
$M = 0 \ DOF$

4.1.4.6 Two Loop Spherical/Spatial Hybrid Ten-bar Mobility

Polyhedron Model	SCD Graph
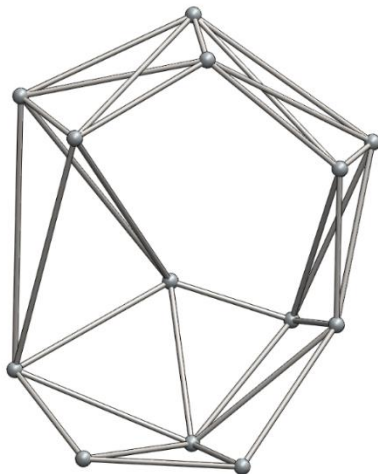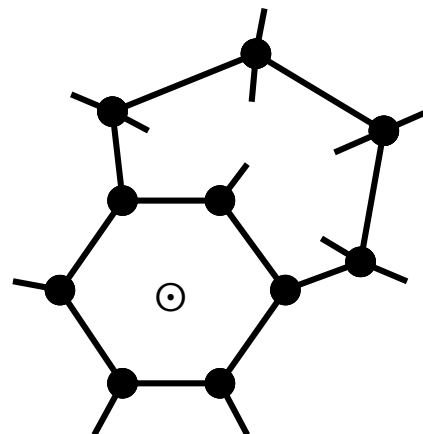
Polyhedron
$V = 13; \ C = 0; \ E = (23)_{ext} + (8)_{int} = 31$
$M = 3(V + C) - E - 6 = 2$
$M = 2 \ DOF$

4.2 RELATIVE MOBILITY EQUATIONS

4.2.1 Mechanism Addenda and Modifications

4.2.1.1 Bottom-Up Approach

In the case where a mechanism has a known graph and mobility, the developed mobility equations can be adapted to account for a mechanism's change in mobility resulting from additions to the original mechanism, called linkage addenda, or changes to the mechanism features, called linkage modifications. Addenda and modifications can be designed such that the overall generic mechanism mobility increases, decreases, or is not changed. This is accomplished by the net number of links and joints or vertices and edges introduced or removed by the change. The quantification of the change in mobility is called the relative mobility. The relation between the initial, relative, and final mobility is described in (Eqn. 5).

$$M = M_0 + \Delta M \qquad \textit{(Eqn. 5)}$$

$M = generic\ mobility\ of\ final\ mechanism$
$M_0 = generic\ mobility\ of\ initial\ mechanism$
$\Delta M = relative\ mobility\ of\ the\ addendum\ or\ modification$

The framing of the relative mobility equation encourages the utility of a bottom-up design technique in which addenda expands a base mechanism. This process reflects the design techniques of pop-up books which often have one large driving mechanism with smaller addenda driven by the larger [5], often without changing the overall mobility. Generalizing the design methodology to spherical system mechanisms encourages connecting addenda such that a closed loop chain of linkages can be developed to perform complex actions while maintaining simple generic mobility and actuation inputs.

4.2.1.2   Relative Mobility Equations

The relative mobility terms are derived by taking the differential of the spherical system and polyhedron mobility equations under the assumption that the connectivity characteristics which permit the use of each of the mobility equations are maintained. The change in mobility is given in terms of the change in the number of salient features of each equation. The relative mobility equations for spherical center and polyhedron analyses are stated in (Eqn. 6) and (Eqn. 7), respectively.

$$\Delta M = 3\Delta N - 2\Delta J \qquad \textit{(Eqn. 6)}$$

$\Delta M = relative\ mobility\ of\ the\ addendum\ or\ modification$
$\Delta N = change\ in\ number\ of\ links$
$\Delta J = change\ in\ number\ of\ joints$

$$\Delta M = 3(\Delta V + \Delta C) - \Delta E \qquad \textit{(Eqn. 7)}$$

$\Delta M = relative\ mobility\ of\ the\ addendum\ or\ modification$
$\Delta V = change\ in\ number\ of\ vertices$
$\Delta C = change\ in\ number\ of\ implicit\ spherical\ centers$
$\Delta E = \Delta E_{ext} + \Delta E_{int} = change\ in\ number\ of\ total\ polyhedron$
$edges\ (external\ and\ internal)$

4.2.1.3   Addendum Connectivity Requirements

For the relative mobility analyses to be valid, none of the conditions of the mobility equation used may be invalidated by the addition of the addendum features to the base. For example, loops may not be introduced which create a contradiction in joint orientation, and concentricity may not be introduced. As a result, the most straightforward way of developing an addendum loop which behaves well under spherical system analysis, for example, is by affixing it to two adjacent vertices on the SC graph such that the joint axis shared by those links is oriented to the new loop's spherical center without changing any other orientation constraints. An example is depicted in Figure 38 where three links are appended to two adjacent links in the base mechanism forming a new spherical loop about vertex b without

impacting the spherical loop about vertex a. The equivalent SC graphs are depicted in Figure 39. This method of appending generally maintains a mechanism's status as a spherical system mechanism.

In contrast, an addendum resulting in a hybrid mechanism does not need to maintain the closure properties of a spherical system as long as polyhedron mobility analysis is used and the SCD graph is known. If this is the case, the addendum can be spatial and significantly more complex due to the robustness of the polyhedron analysis. It is generally simpler to analyze addenda which maintain spherical system properties with the spherical system equations and SC graph if possible, but it is more comprehensive and robust to analyze addenda with the polyhedron equations and SCD graph if known. An example of a skew, spatial addendum loop which results in a spherical/spatial hybrid mechanism is depicted in Figure 40, and its equivalent SCD graph is depicted in Figure 41.
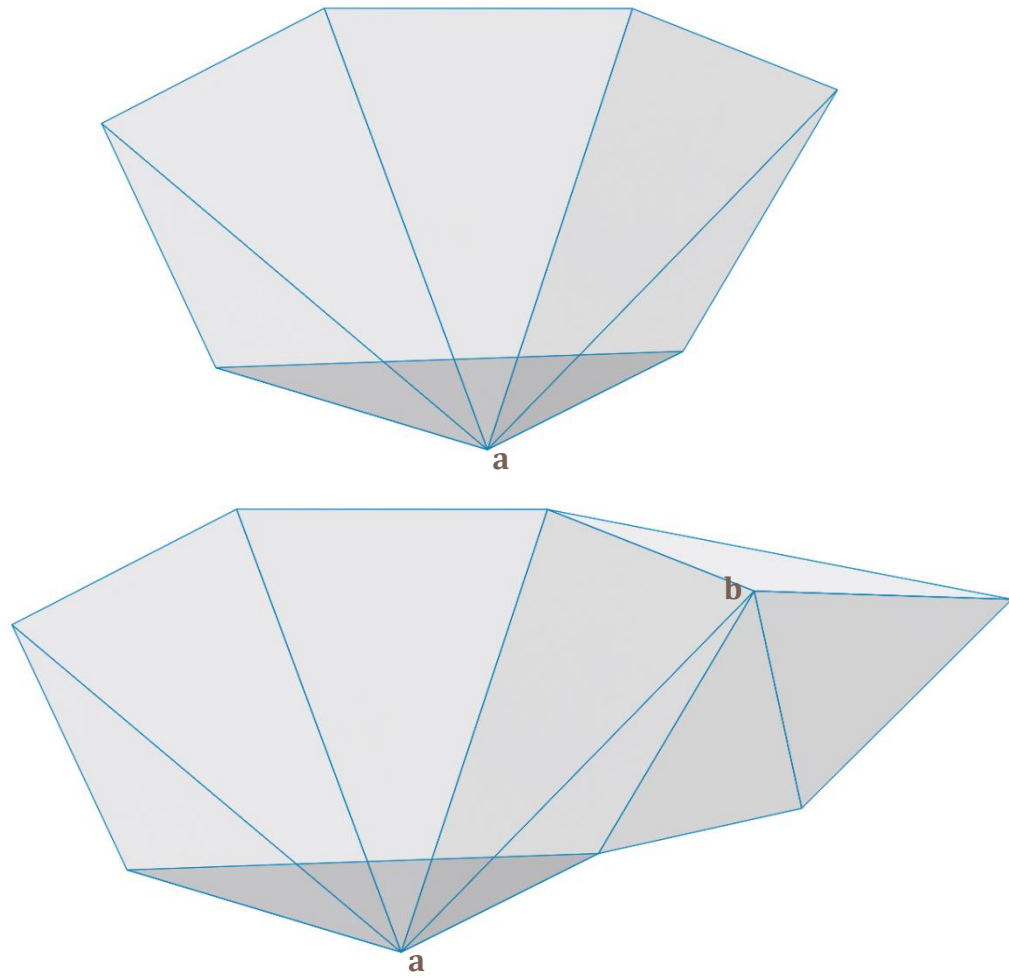
Figure 38. Rigid panel spherical six-bar base mechanism (top), with an addendum loop (bottom)
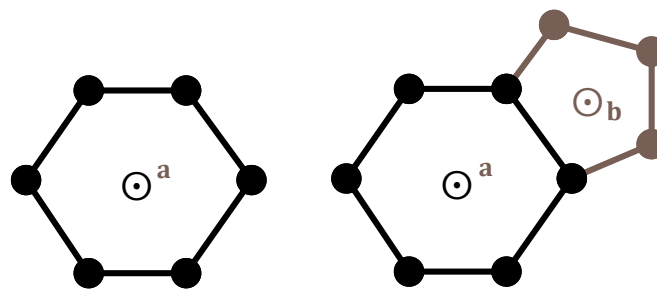
Figure 39. Spherical six-bar base SC graph (left), with an addendum loop (right)
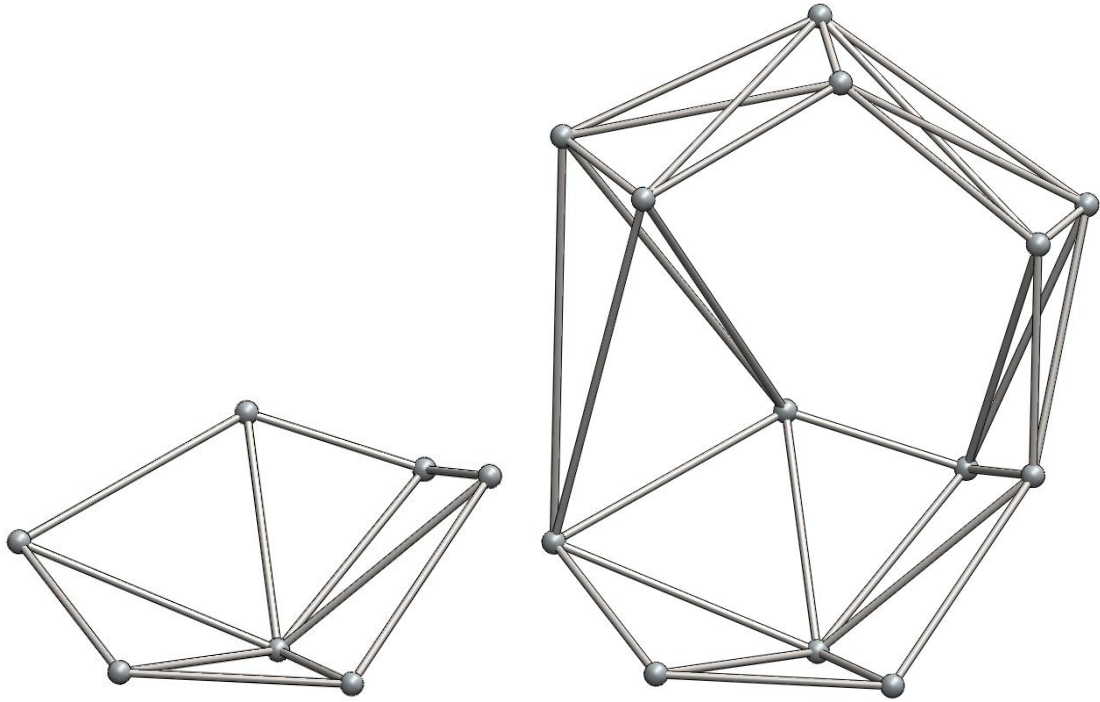
Figure 40. Polyhedron spherical six-bar base mechanism (left), with a spatial addendum loop (right)
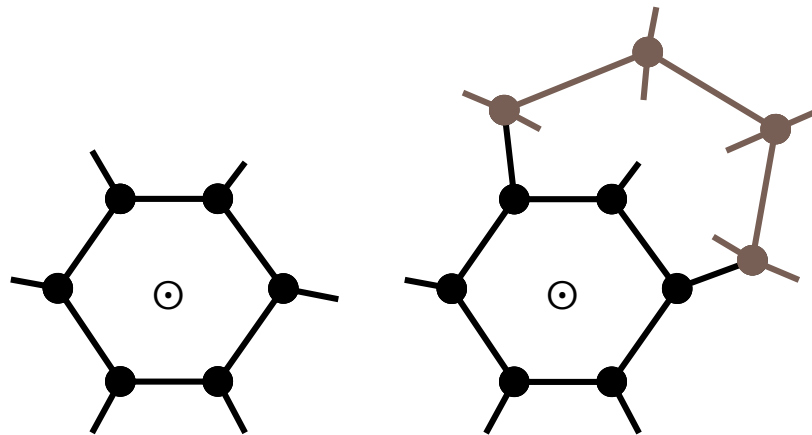
Figure 41. Spherical six-bar base SCD graph (left), with a spatial addendum loop (right)

4.2.2   Case Study: Introduction of Revolute Joints

One fundamental application for the relative mobility equation is the introduction of revolute joints to a mechanism, which is equivalent to introducing creases to a panel between vertices (as depicted in Figure 42) without invalidating the spherical system constraints. Intuitively, adding one crease is equivalent to directly introducing one additional degree of freedom to a mechanism, which analysis corroborates.

In the link-joint analysis of the introduction of one revolute joints to a mechanism, each crease turns one link into two and adds a joint between them. Thus the change in number of links and the change in number of joints terms both equal the number of revolute joints introduced. As a result, the change in mobility is equal to 1 DOF for each crease introduced.

$$\Delta N = 1; \qquad \Delta J = 1$$
$$\Delta M = 3\Delta N - 2\Delta J = 1$$

$$\boxed{\Delta M = 1 \; DOF \; for \; each \; crease \; introduced}$$

In the vertex-edge analysis of the introduction of one revolute joint to a mechanism, there are two geometric cases. Introducing a crease in a triangular truss adds one vertex and two edges to form two trusses with one shared edge. When introducing a crease in a polyhedron with more than three external edges, the change in the number internal edges must be accounted for. The revolute joint turns one rigid k-sided polyhedron into one n- and one m-sided rigid polyhedron connected by one edge between two shared vertices. This establishes the relationship that the sum of the number of sides in the subdivided polyhedra is $k + 2$. The total number of vertices is not changed by the crease, but the new total number of edges is found by adding one external edge between the shared vertices, removing all the internal edges of the k-sided mechanism, and adding the appropriate number of internal edges to the newly established n- and m- sided polyhedra. Due to the relationship between

n, m, and k, the change in mobility is equal to 1 DOF for each crease introduced in all geometric cases.

$k = 3$

$\Delta V = 1; \qquad \Delta C = 0; \qquad \Delta E = \Delta E_{ext} + \Delta E_{int} = (2)_{ext} = 2$
$\Delta M = 3(\Delta V + \Delta C) - \Delta E = 1$

$k > 3; \qquad n, m \geq 3; \qquad n + m - 2 = k$

$\Delta V = 0; \qquad \Delta C = 0$
$\Delta E = \Delta E_{ext} + \Delta E_{int} = (1)_{ext} + \big(-(2k-6) + (2n-6) + (2m-6)\big)_{int} = -1$
$\Delta M = 3(\Delta V + \Delta C) - \Delta E = 1$

$\boxed{\Delta M = 1 \; DOF \; for \; each \; crease \; introduced}$
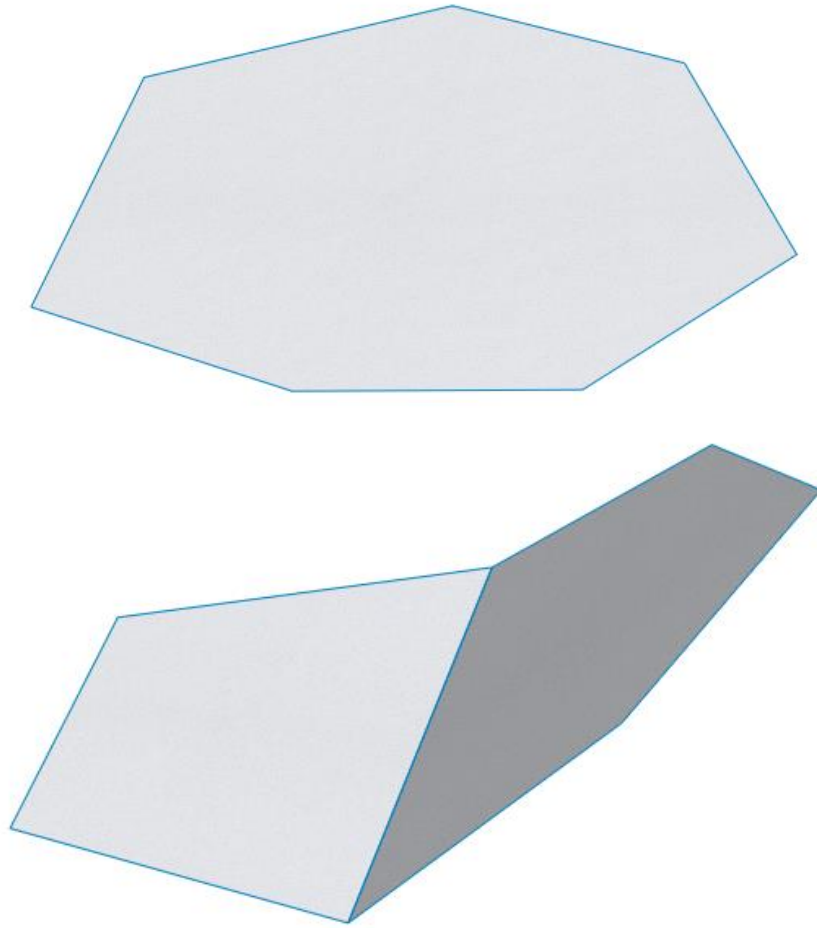
Figure 42. Rigid panel (top), with revolute crease introduced (bottom)

4.2.3　Case Study: Interchangeability of Implicit Spherical Center and Vertex

Another useful application of the relative mobility equations is demonstrating the interchangeability between a vertex and an implicit spherical center as depicted in Figure 43. This is accomplished in the polyhedron model by taking a polyhedron vertex of n intersecting rigid polyhedra and converting it to an implicit spherical center surrounded by n rigid polyhedra with the same joint alignment but with n internal open edges introduced.

The SCD graph equivalent of this is taking a loop of n graph vertices with no internal open edges and introducing n internal edges without making any other changes as depicted in Figure 44. This modification is accounted for by the removal of the loop vertex in favor of a spherical center, and the addition of n vertices associated with the new internal open edges. The change in the number of edges is equal to the additional n internal open edges plus an additional two internal edges per link to maintain rigidity in the n polyhedra whose number of sides each increased by one. As a result of all of these modifications, the change in mobility is zero, indicating a vertex and an implicit spherical center have equal mobility and are interchangeable.

$$\Delta V = n - 1; \quad \Delta C = 1; \qquad \Delta E = \Delta E_{ext} + \Delta E_{int} = (n)_{ext} + (2n)_{int} = 3n$$
$$\Delta M = 3(\Delta V + \Delta C) - \Delta E = 3(n - 1 + 1) - 3n = 0$$

$$\boxed{\Delta M = 0 \; DOF \; for \; any \; vertex \; converted \; to \; an \; implicit \; spherical \; center}$$
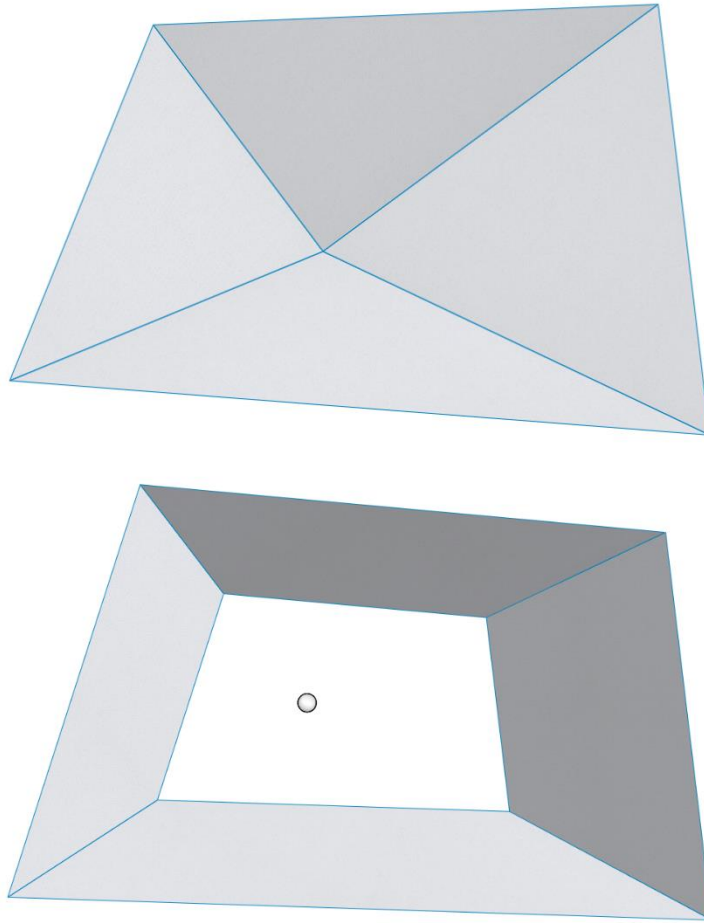
Figure 43. Rigid panel spherical four-bar with a vertex (top) and with an implicit spherical center (bottom)
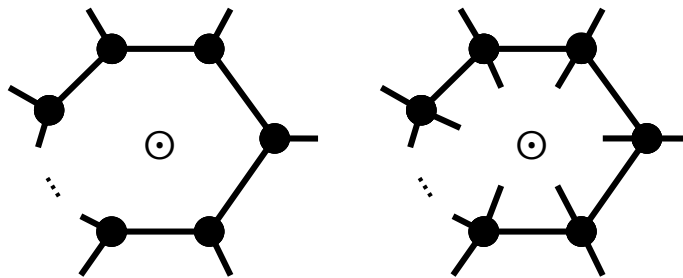
Figure 44. SCD graph of arbitrary spherical loop with a vertex (left) and with an implicit spherical center (right)

4.2.4 Adjunct Addenda

4.2.4.1 Definition

Beatini and Korkmaz identify that a mechanism which features a "two-strip" addendum chain (depicted in Figure 45) maintains the original mobility of the base mechanism [12]. This observation is an example of what is dubbed an adjunct addendum to a mechanism, which is defined as an addendum to a base mechanism created out of a chain of simple addendum cells with zero relative mobility. Adjunct addenda have no impact on the overall mechanism mobility but may allow for complex motion in space along the chain of addenda when actuated.

4.2.4.2 Ride-Along Addendum Definition

To develop an adjunct addendum, one must first identify the simplest addendum which maintains zero relative mobility, which is the building block with which adjunct addenda are developed. It is found that when two links are appended to two extant links in a base mechanism such that the four links meet at a vertex or implicit spherical center without changing the joint orientation of the base mechanism, this is accomplished. The SC graph representation is depicted in Figure 46, and a rigid panel example is depicted in Figure 47. The simplest relative mobility calculation demonstrates that with an increase of links by two and an increase of joints by three, the relative mobility is zero in a spherical system. Their actuation is dependent only on the actuation between the links on the base mechanism to which they attach. These addenda are called ride-along addenda, as their presence does not impact the base mechanism and they are simply "along for the ride." The relative mobility of zero implies that any amount of these can be appended to any link pair of a mechanism as long as the spherical center criteria are met, and the overall mobility will not change.
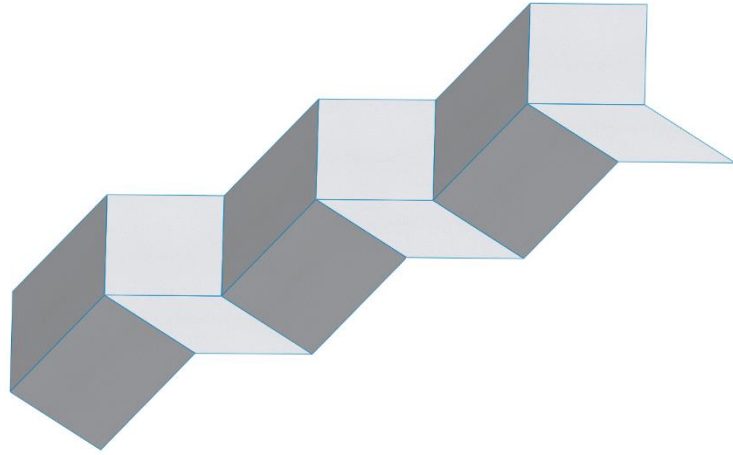
Figure 45. Two-strip addendum chain (Beatini et al.)
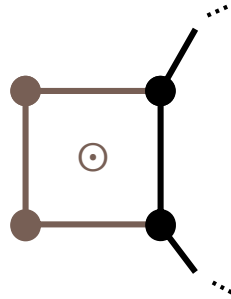
Figure 46. Ride-along addendum (highlighted) appended to a section of an arbitrary linkage
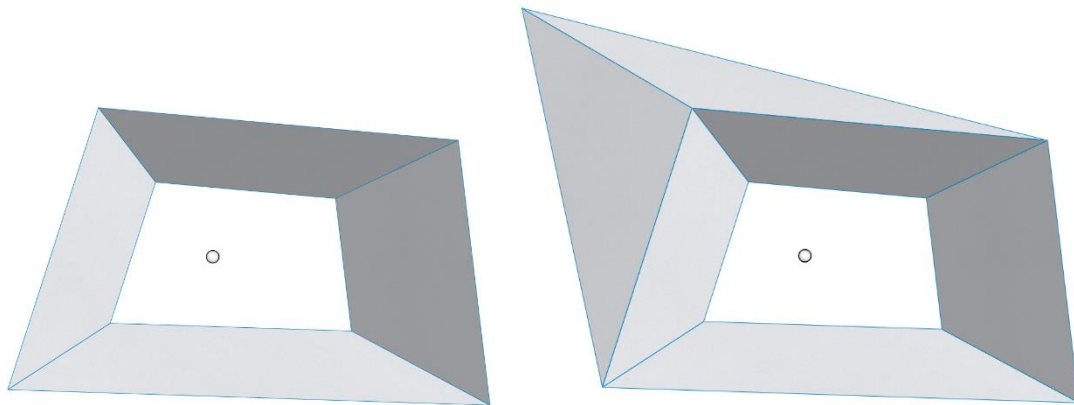
Figure 47. A spherical four-bar (left), with a ride-along addendum attached (right)

4.2.4.3 Ride-Along Addendum Mobility Analysis

In the link-joint analysis of a ride-along addendum to a spherical system mechanism, the addendum will not violate the spherical system constraints due to its requirement of connecting at a vertex or implicit spherical center. Two links are introduced with one joint between them and two joints connecting them to the base mechanism. As expected, there is no change in mobility.

$\Delta N = 2; \qquad \Delta J = 3$
$\Delta M = 3\Delta N - 2\Delta J = 0$

$\boxed{\Delta M = 0 \; DOF \; for \; a \; ride \; along \; addendum}$

In the vertex-edge analysis of the ride-along addendum, the two links are taken to be n- and m-sided polyhedra connecting to the base mechanism at a vertex (although the vertex can be interchanged for an implicit spherical center with no change in mobility). The net change in vertices is the sum of the vertices in the addendum polyhedra minus the two shared vertices of the polyhedra minus the three shared vertices connecting the addendum to the base mechanism. The net change in edges is the sum of the external edges in the addendum polyhedra plus the number of internal edges in those polyhedra minus one shared edge between them minus two shared edges connecting the addendum to the base mechanism. As expected, there is no change in mobility.

$n, m \geq 3$

$\Delta V = n + m - 5; \qquad \Delta E = (3n - 6) + (3m - 6) - 3 = 3n + 3m - 15$
$\Delta M = 3(n + m - 5) - 3n + 3m - 15 = 0 \; DOF$

$\boxed{\Delta M = 0 \; DOF \; for \; a \; ride \; along \; addendum}$

4.2.4.4 Reduced Mobility Analysis

Due to the zero relative mobility of ride-along addenda, if an isolated ride-along addendum is identified on an SC graph, the addendum can be eliminated with no impact on the mobility of that mechanism. As a result, a reduced graph can be used for mobility analysis

with equivalent generic mobility. A practical example of this reduction is drawn from the fortune teller origami fold depicted in Figure 48. The mechanism is a spherical eight-bar loop with flaps creating four ride-along addenda outside the eight-bar. Reducing the SC graph by eliminating the ride-along addenda leaves a single spherical eight-bar loop, a simpler mechanism with equal mobility to the fortune teller.

4.2.4.5   Adjunct Linkages Construction

Using the definition of ride-along addenda and leveraging their ability to be appended to any two adjacent links at a vertex, adjunct addenda are created by serially connected chains of ride-along addenda. This includes Beatini and Korkmaz's "two-strip" addendum as well as all other chains which may be connected in a non-linear pattern such as the example depicted in Figure 49. Adjunct addenda do not impact the mobility of the mechanism, but they can undergo complex motion in three dimensions with fewer actuation inputs required by an open chain, which indicates their potential to be designed as complex, closed loop actuating elements in spherical system mechanisms.
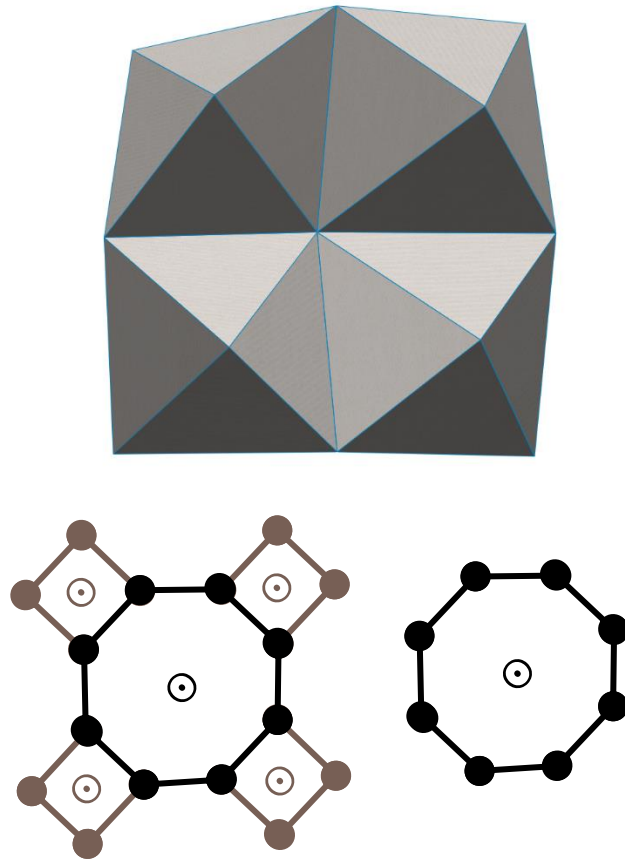
Figure 48. Rigid panel mechanism (top), its SC graph with ride-along addenda highlighted (bottom, left), and its reduced SC graph with ride-along addenda eliminated (bottom, right)
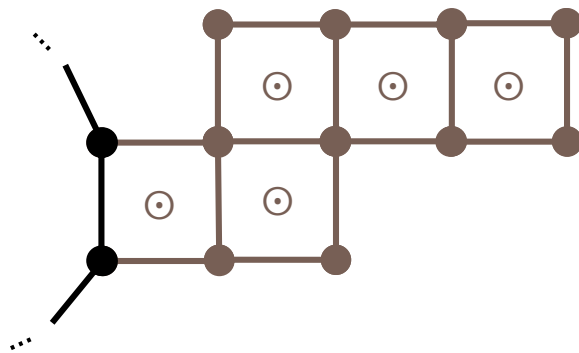
Figure 49. Example adjunct linkage (highlighted) developed from ride-along addenda and appended to a section of an arbitrary linkage

4.2.5   Examples of Relative Mobility Calculation

4.2.5.1   *Spherical Loop Addendum*

The base mechanism is a spherical six-bar loop with a known mobility of 3 DOF. In the final mechanism, a spherical loop consisting of three new links (highlighted in the SC graph) is appended to two adjacent links of the base mechanism.

<div align="center">
Base Rigid Panel Mechanism   Final Rigid Panel Mechanism
</div>
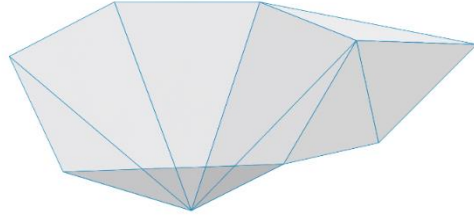
<div align="center">
Base SC Graph   Final SC Graph
</div>
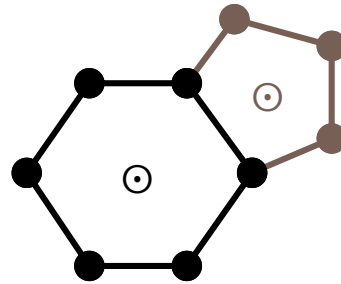
Spherical system
$M_0 = 3\ DOF$
$\Delta N = 3;$ $\Delta J = 4;$ $\lambda = 3$
$\Delta M = 3\Delta N - 2\Delta J = 1;$ $M = M_0 + \Delta M$
$\boxed{\Delta M = 1\ DOF;\quad M = 4\ DOF}$

4.2.5.2   *Spatial Loop Addendum*

The base mechanism is a spherical six-bar loop with a known mobility of 3 DOF. In the final mechanism, a spatial loop consisting of four skew, four-sided polyhedra (highlighted in the SC graph) is appended to two non-adjacent links of the base mechanism.

Base Polyhedron Mechanism   Final Polyhedron Mechanism
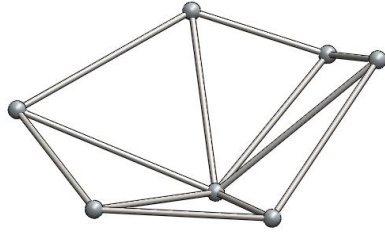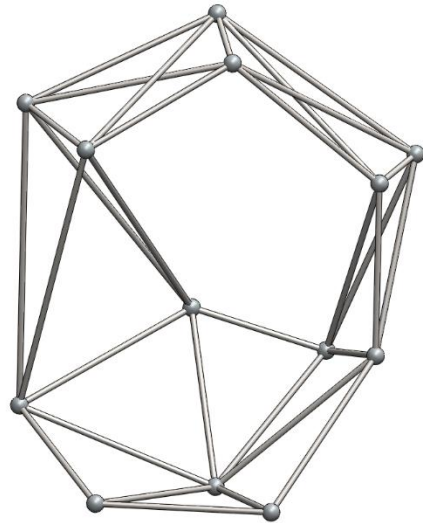
Base SCD Graph   Final SCD Graph
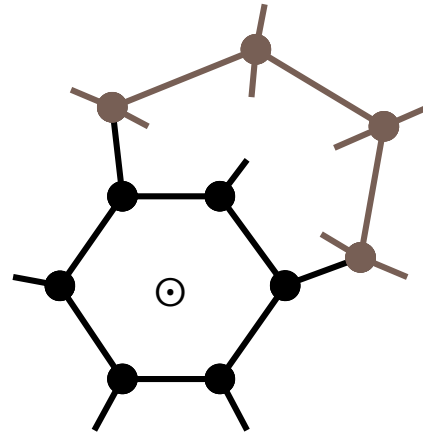
Polyhedron
$M_0 = 3\ DOF$
$\Delta V = 6;$ $\Delta E = \Delta E_{ext} + \Delta E_{int} = (11)_{ext} + (8)_{int} = 19$
$\Delta M = 3\Delta V - 2\Delta E = -1;$ $M = M_0 + \Delta M$
$\boxed{\Delta M = -1\ DOF;\quad M = 2\ DOF}$

4.2.5.3   Ride-Along Reduction

This mechanism is recognized to have a ride-along addendum (highlighted in the SC graph), which can be eliminated in the SC graph with no impact on mobility calculation. As a result, the mechanism mobility is equal to that of a spherical four-bar.

Rigid Panel Linkage   SC Graph   Reduced SC Graph
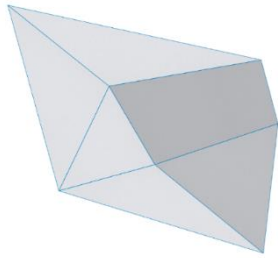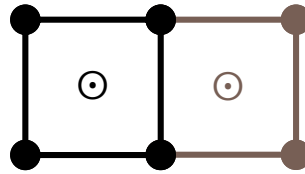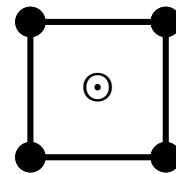
Spherical system
$N = 4; J = 4; \lambda = 3$
$M = 3N - 2J - 3 = 1$
$\boxed{M = 1 \, DOF}$

4.2.5.4 Adjunct Chain Reduction

This mechanism is recognized to have a ride-along addendum (highlighted in the SC graph), which can be eliminated in the SC graph with no impact on mobility calculation. The resulting reduced SC graph is also recognized to have a ride-along addendum, which can also be eliminated. As a result, the mechanism mobility is equal to that of a spherical four-bar.
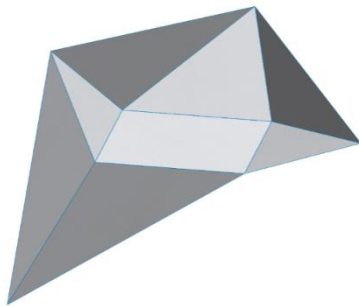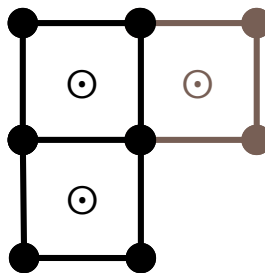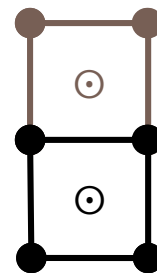
Rigid Panel Linkage   SC Graph   Reduced SC Graph   Fully Reduced SC Graph
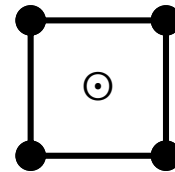
Spherical system
$N = 4; J = 4; \lambda = 3$
$M = 3N - 2J - 3 = 1$
$\boxed{M = 1 \, DOF}$

4.2.5.5   Double-Strip Chain Reduction

This mechanism is recognized to have a double-strip chain addendum developed from serially connected ride-along addenda (highlighted in the SC graph), which can be eliminated in the SC graph with no impact on mobility calculation. As a result, the mechanism mobility is equal to that of a spherical four-bar.

Rigid Panel Linkage   SC Graph   Reduced SC Graph
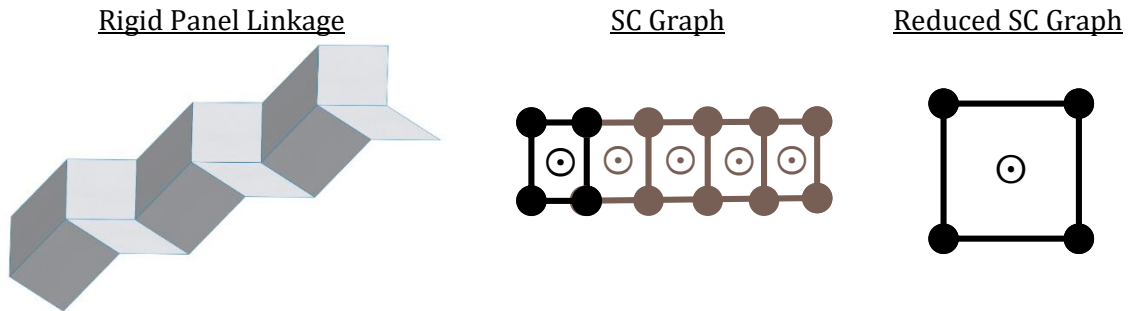
Spherical system
$N = 4; J = 4;\ \ \lambda = 3$
$M = 3N - 2J - 3 = 1$
$\boxed{M = 1\ DOF}$

4.2.5.6   Fortune Teller Ride-Along Reduction

This mechanism is recognized to have four ride-along addenda (highlighted in the SC graph), which can be eliminated in the SC graph with no impact on mobility calculation. As a result, the mechanism mobility is equal to that of a spherical eight-bar loop.

Rigid Panel Linkage   SC Graph   Reduced SC Graph
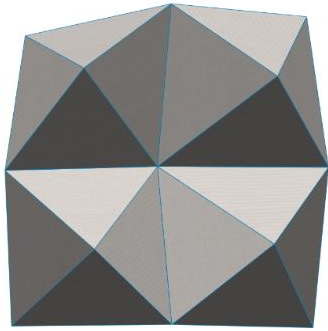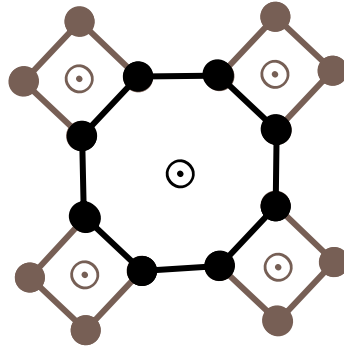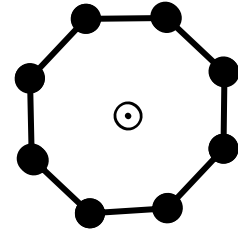
Spherical system
$N = 8; J = 8; \quad \lambda = 3$
$M = 3N - 2J - 3 = 5$
$\boxed{M = 5\ DOF}$

5 ORIGAMI-INSPIRED N DOF SPATIAL CHAIN

5.1 MAPPING JOINTS

5.1.1 Motivation

In paper art inspired kinematics, all joints are taken to be revolute due to the direct mapping to a crease. Other joints such as prismatic sliders and cylindrical joints can be developed in the paper art domain [5] and the polyhedron domain [13], but these joints do not map as simply as creases to revolute joints. Thus, it is desirable to develop a framework for the conversion of certain joint combinations to all-revolute equivalents. A useful application of this process is in open chain manipulators.

5.1.2 Mappings

5.1.2.1 Equivalent Joints

An all-revolute, rigid panel 3 DOF spherical (S) joint has been identified by Winder et al. [5] as two isosceles right triangular panels connected at the right angled vertices sharing one edge and affixed to two rigid bodies by the open edges which connect to the vertex. Rotation about the three orthogonal axes intersecting at the vertex provide the $\{\theta_x, \theta_y, \theta_z\}$ degrees of freedom associated with a spherical joint. The spatial and rigid panel spherical joints are depicted in Figure 50. Similarly, an all-revolute, rigid panel 2 DOF universal (U) joint can be developed with a single right triangle connecting two bodies on the edges which connect to the vertex. Rotation about the two orthogonal axes intersecting at the vertex provide the $\{\theta_x, \theta_y\}$ degrees of freedom associated with the universal joint. The spatial and rigid panel universal joints are depicted in Figure 51.
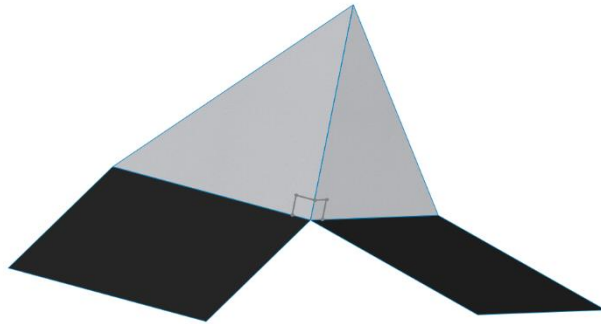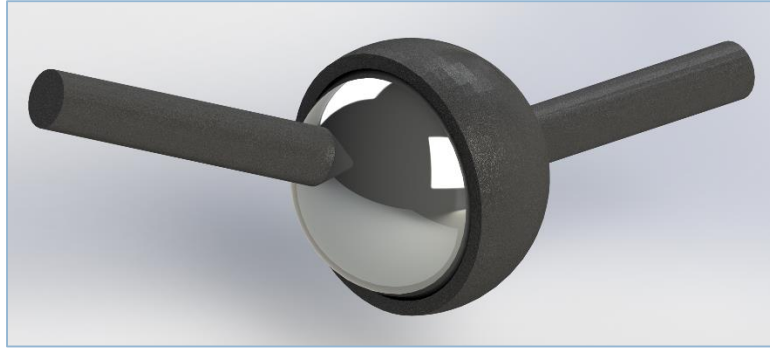
Figure 50. Spherical joint (top) and its rigid panel representation (bottom)
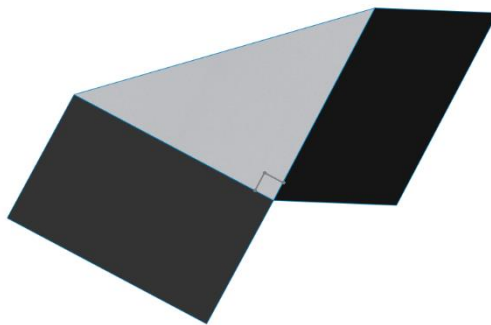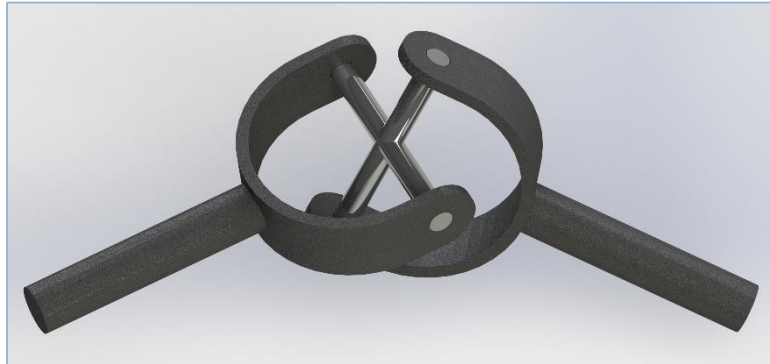
Figure 51. Universal joint (top) and its rigid panel representation (bottom)

A prismatic slider cannot be directly mapped from revolute joints, however, a revolute-prismatic-revolute (RPR) chain (assuming parallel revolute joints) can be simulated with two identical rectangular panels connected at a crease where each rectangle connects a rigid body at the edge opposite the shared edge. The spatial and rigid panel RPR chains are depicted in Figure 52. The outer edges connecting the rectangles to the bodies map to the parallel revolute joints. The edge connecting the rectangular panels simulates a prismatic slider as its actuation controls the distance between the rigid bodies with one degree of freedom, simulating linear actuation. The range of distances the prismatic analogue can achieve is established by the lengths of the rectangles. Assuming the rectangle lengths are both equal to l, the maximum distance between rigid bodies is $2l$ when the angle between rectangles is 180°, and the minimum distance is 0 when the angle between rectangles is 0°.

5.1.2.2   *Rigid Panel Notation*

A specific rigid panel notation is established for the case where a rigid panel chain consists of combinations of right triangles connected by the edges which connect to the right angled vertex and rectangles connected by their opposite, parallel edges. In this notation scheme, a chain of rectangles and right triangles is described by a string of characters from the set $\{R, -\}$. A string of "$RR \ldots R$" is used to describe a chain of right triangles connected at the right angled vertex (i.e. a chain of revolute joints connected orthogonally with a common spherical center) where inner Rs represent the connected revolute edges in the chain and the two outer Rs represent the available right triangle edges which intersect the vertex. An example is depicted in Figure 53. A string of "$R - R \ldots - R$" is used to describe a chain of rectangles connected at opposite edges with parallel orientation (i.e. a chain of revolute joints connected with parallel orientation) where inner Rs represent the connected revolute edges in the chain, each "$-$" corresponds to the face of a rectangle, and the two outer Rs represent

the two available rectangle edges with parallel orientation. An example is depicted in Figure 53. When any two rigid panel chains are combined, one outer R from each chain are merged into a single R, representing a shared edge, and the remainder of the strings are concatenated in the appropriate order to represent the combined mechanism chain.
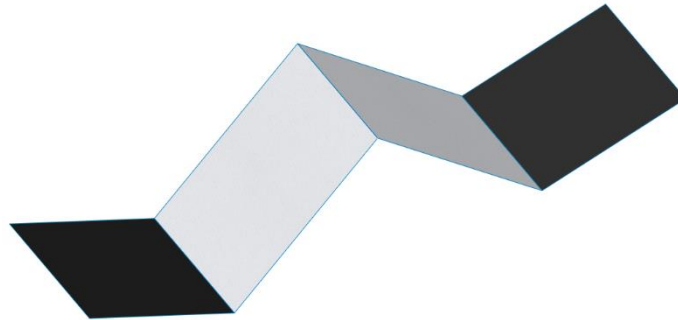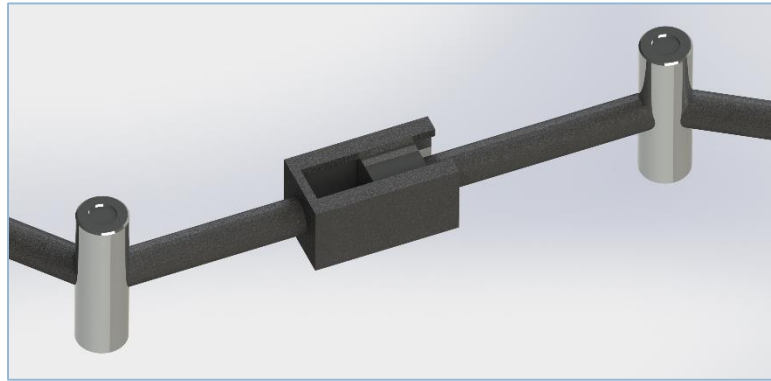
Figure 52. Revolute-prismatic-revolute chain (top) and its rigid panel equivalent (bottom)
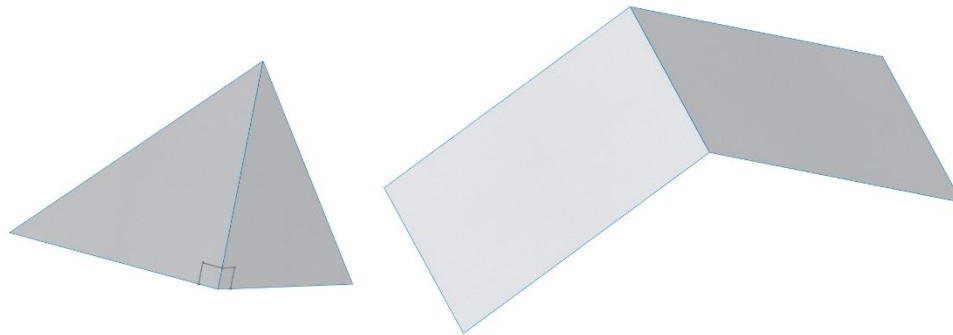
Figure 53. Rigid panel RRR chain (left) and R − R − R chain (right)

5.2 DEVELOPMENT OF 6 DOF SPATIAL CHAIN

5.2.1 Motivation

It is desirable to develop a rigid panel mechanism which is equivalent to an open chain manipulator with six degrees of freedom. Proper implementation of this chain would have the capability of connecting any two edges at any relative orientation in space as its degrees of freedom permit it to actuate its open edges into any relative position and orientation in a 6 DOF spatial constraint space.

5.2.2 Identification of UPS Chain

A simple, traditional 6 DOF spatial mechanism which is capable of connecting two bodies in space at any relative position and orientation is a universal-prismatic-spherical (UPS) joint chain. The joints provide two, one, and three degrees of freedom, respectively [28], and the sum of these degrees of freedom is six if there is no loop closure. The physical representation of the degrees of freedom between the bodies this chain connects can be visualized as a vector with 3 DOF $\{x, y, z\}$ that establishes the relative position between the bodies and a rotation with 3 DOF $\{\theta_x, \theta_y, \theta_z\}$ which establishes the relative orientation between the bodies. The two degrees of freedom of the universal joint establish the direction of the position vector, the one degree of freedom of the prismatic joint establishes the length of the position vector, and the three degrees of freedom in the spherical joint establish the relative orientation. The degrees of freedom account for all six degrees of freedom in the spatial constraint space $\{x, y, z, \theta_x, \theta_y, \theta_z\}$. A spatial mechanism representation of the UPS chain is depicted in Figure 54.
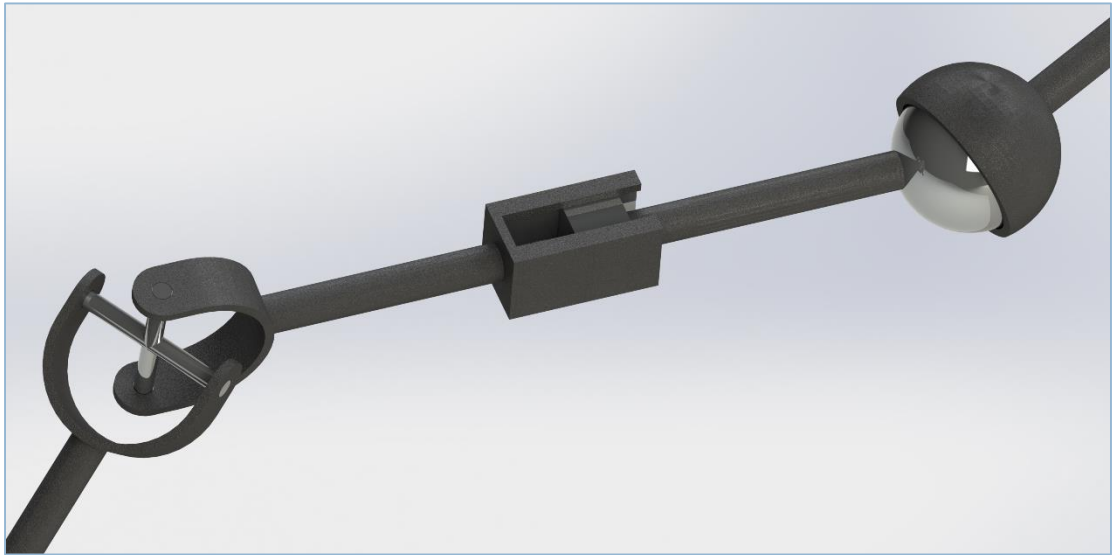
Figure 54. Spatial universal-prismatic-spherical chain connecting two rigid bodies
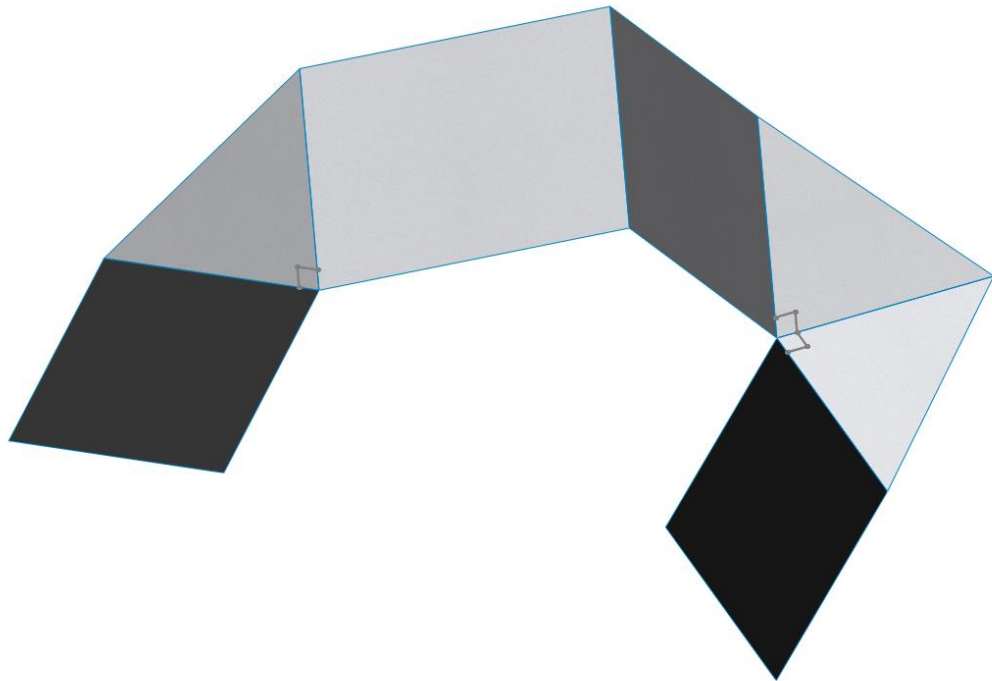
Figure 55. Rigid panel universal-prismatic-spherical chain (RR — R — RRR) connecting two rigid bodies

5.2.3 Conversion to Rigid Panel

5.2.3.1 Rigid Panel UPS Chain

By concatenating the rigid panel equivalents of the universal joint, the revolute-prismatic-revolute chain, and the spherical joint, one develops a rigid panel equivalent of the 6 DOF UPS chain. Representation of this mechanism requires use of the rigid panel notation with the character set $\{R, -\}$. From the notation definitions, a universal joint is represented by the string RR as it is just one right triangle with two available edges. A spherical joint is represented by the string RRR as it is two right triangles with one shared edge and two available edges. A revolute-prismatic-revolute joint is represented by the string $R - R - R$ as it is two rectangles with one shared edge and two available edges. Concatenating these strings and merging outer edges into shared edges represents the UPS mechanism with the string $RR - R - RRR$, which is the rigid panel 6 DOF spatial chain, depicted in Figure 55. This mechanism is capable of establishing relative position and orientation between any two rigid bodies (within the distance constraint established by the rectangle dimensions) using the same degrees of freedom as the original UPS mechanism.

5.2.3.2 Enumeration of Rigid Panel 6 DOF Spatial Chains

The UPS mechanism utilized to develop the $RR - R - RRR$ mechanism was specifically selected to easily visualize of the six degrees of freedom in terms of a position vector and relative orientation. It is recognized that the six degrees of freedom are not dependent on the specific ordering of the components and that any permutation of the $RR - R - RRR$ string which obeys certain constraints would provide the same 6 DOF mobility. These chains are found by permuting the ordering of the string within certain bounds.

The constraints on the permutations are as follows. The number of each character must remain the same because the number and types of links do not change. The outer

characters of the string must remain R as there must be available outer edges. Two "$-$" characters must be separated by at least one R as two adjacent rectangles must share a revolute edge. A chain of triangles can be at most three (RRR) at a single vertex (i.e. in between "$-$" characters) as all possible rotational degrees of freedom at a single vertex are accounted for with three orthogonal edges. Strings which are equal when one is reversed are not considered unique. The constraints and the permutation algorithm are encoded in Appendix B: N DOF Spatial Chain Matlab Code.

The resulting valid permutations which represent 6 DOF spatial chains are listed below. Each of these chains is capable of establishing relative position and orientation between any two rigid bodies within the distance constraint established by the rectangle dimensions.

$$
\begin{array}{|l|}
\hline
R - RR - RRR \\
R - RRR - RR \\
RR - R - RRR \\
RR - RR - RR \\
\hline
\end{array}
$$

5.2.3.3 Modes

Connecting right triangles to each other does not allow for choice in connection orientation because the right angled vertices must be coincident. However, affixing the right triangles to the rectangles permits a choice of rectangular vertex to attach the right angled vertex because either orientation maintains the parallel orientation of the connecting edges across the rectangle. When right triangles are connected on either side of a chain of rectangles, the right angle vertices may connect to vertices on the same side of the rectangle or diagonally across the rectangle. These different connectivities result in different modes of connection of the mechanism. All unique modes of each 6 DOF spatial chains are depicted in Table 7 based on the combinations of vertex pairs spanning a rectangle's diagonal.

110

R − RR − RRR	
I	*II*
R − RRR − RR	
I	*II*
RR − R − RRR	
I	*II*

RR − RR − RR		
I	*II*	*III*

Table 7. Unique modes of each rigid panel 6 DOF spatial chain

111

5.2.4 Degrees of Freedom Analysis

5.2.4.1 *Spatial Mechanism Analysis*

The $RR - R - RRR$ spatial chain can be depicted with an SC graph (equivalent to a spatial link-joint graph because of the lack of a closed loop), in which the five links and six edges are connected to two arbitrary rigid bodies as depicted in Figure 56. The total number of each feature in the spatial constraint space permits calculation of the degrees of freedom between the two rigid bodies using the modified C-G-K equation for spatial mechanisms. As expected, the mobility is 6 DOF.

$$\lambda = 6; \;\; N = 7; J = 6; \;\; f_i = 1$$
$$M = \lambda(N - J - 1) + \sum f_i = 6(0) + 6 = 6$$

$$\boxed{M = 6\,DOF}$$

5.2.4.2 *Polyhedron Model Analysis*

The $RR - R - RRR$ spatial chain can be depicted with an SCD graph (which encodes the linkage geometry) where the number of sides in a link is indicated by the vertex degree. The spatial chain connects arbitrary n- and m- sided rigid polyhedra as depicted in Figure 57. The counting for the polyhedron mobility formula is more involved. The number of vertices is the number of open edges, which is seven from the chain and $n - 1$ and $m - 1$ from the two rigid bodies. The number of external edges is $n + m$ from the rigid bodies and eleven accounted for by the chain. The number of internal edges is $2n - 6$ and $2m - 6$ from the rigid bodies and four total from the two rectangles in the chain. As expected, the mobility is 6 DOF.

$$n, m \geq 3$$

$$V = (n - 1) + (m - 1) + 7 = n + m + 5; \qquad C = 0$$
$$E = E_{ext} + E_{int} = (n + m + 11)_{ext} + ((2n - 6) + (2m - 6) + 4)_{int} = 3n + 3m + 3;$$
$$M = 3(V + C) - E - 6 = 3(n + m + 5) - (3n + 3m + 3) - 6 = 6$$

$$\boxed{M = 6\,DOF}$$
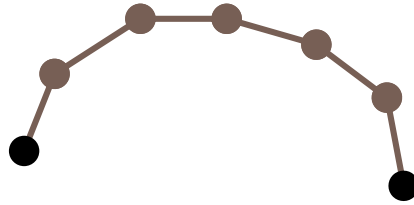
Figure 56. SC graph of RR − R − RRR chain connecting two arbitrary rigid bodies
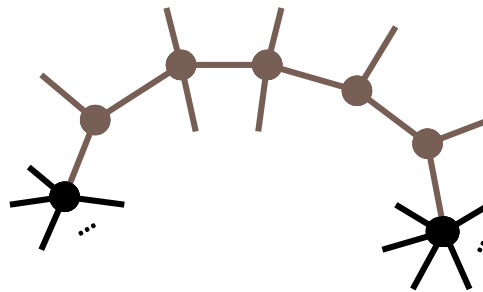
Figure 57. SCD graph of RR − R − RRR chain connecting two arbitrary rigid bodies

5.2.5 6 DOF Spatial Chain Pop-Up Element

The purpose of the development of the rigid panel 6 DOF spatial chain is presenting a useful spatial mechanism and its mapping to the kinematic paper art domain. Element 2 utilizes the paper art domain to present the reader with an interactive $RR - R - RRR$ rigid panel spatial chain capable of 6 DOF. Manipulation of this element tangibly demonstrates its spatial degrees of freedom.

Instructions:

1. Photocopy and print this diagram on a new sheet of paper
2. Cut along the solid black lines (don't cut anywhere else)
3. Crease the dashed lines thoroughly such that they can be folded back and forth
4. Hold Rigid Body B and position it relative to Rigid Body A without allowing the links to curve
5. Observe how any position and orientation of Rigid Body B can be achieved with the appropriate crease angles in the chain

Rigid Body B

Rigid Body A
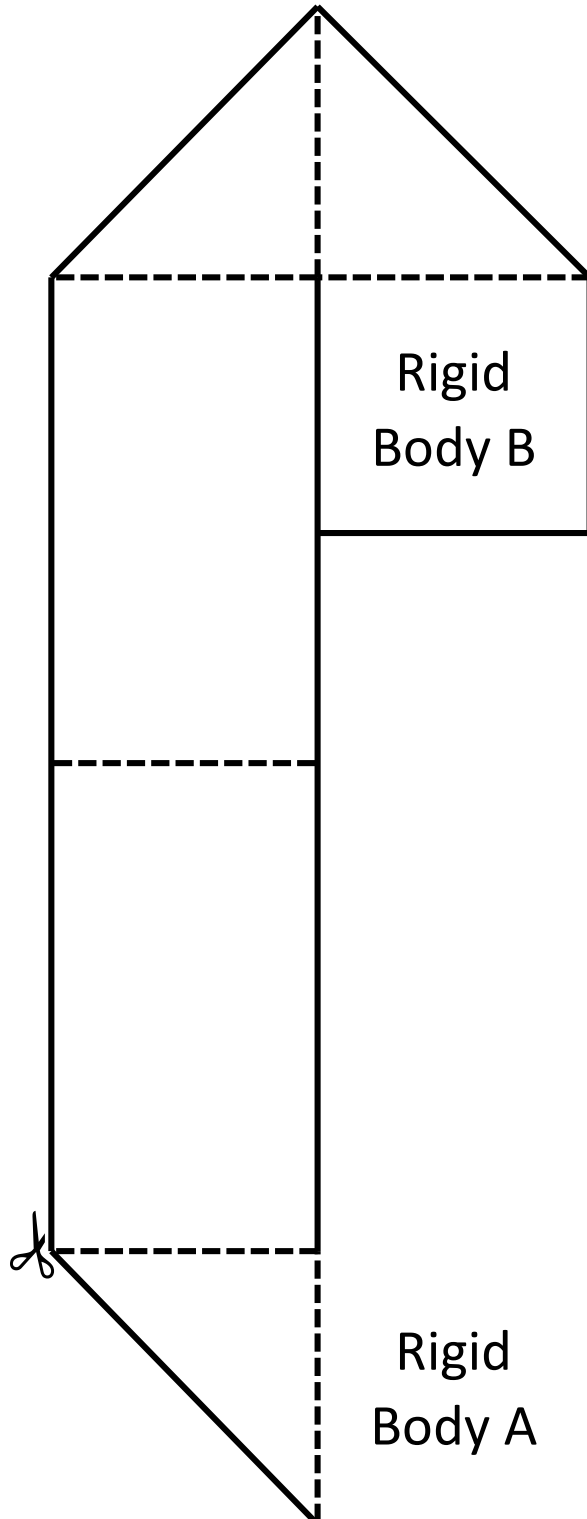
Element 2. 6 DOF spatial chain pop-up element

5.3 DEVELOPMENT OF N DOF SPATIAL CHAIN

5.3.1 Top-Down Design Approach

5.3.1.1 *Motivation*

Using the same rigid panel links, notation, and constraints as the 6 DOF spatial chain case, the methodology to find the 6 DOF permutations can be generalized to find all valid N DOF permutations of a spatial chain, where $N \leq 6$. The results of this analysis are all meaningful combinations of the rectangular and right triangular panels with mobilities ranging from 1 DOF to 6 DOF.

5.3.1.2 *Algorithm*

The algorithm was refined from the 6 DOF case such that the number of "R" and "$-$" characters in a string could be reduced from the initial quantities taken from the UPS mapping. This represents determining all combinations of removed and rearranged links to methodically suppress all combinations of degrees of freedom without breaking the constraint rules. This method enumerates the valid combinations of the specified links into chains which have one to six degrees of freedom. The algorithm is encoded in Appendix B: N DOF Spatial Chain Matlab Code.

5.3.2 Enumeration of Rigid Panel N DOF Spatial Chains

The output of the algorithm was compiled into Table 8 and analyzed. The mobility of the mechanism is equal to the number of Rs in the string by inspection of the modified C-G-K equation for spatial mechanisms. Whether the distance constraint between rigid bodies is coincident, fixed, or variable is determined by whether there are zero, one, or two rectangular panels, respectively. The variable distance is permitted by the prismatic joint analogue of two rectangular panels. Determination of the equivalent spatial mechanism treats rectangles as

connecting links and translates an isolated R to a revolute joint (R), an isolated RR to a universal joint (U), and an isolated RRR to a spherical joint (S) per the rigid panel definitions of these joints. It is notable that the output permutations include the definitions of revolute, universal, and spherical joints as well as all 6 DOF spatial chains. Finally, the output includes the SS mechanism established by Winder et al. [5], which has six degrees of freedom, but one of which is degenerate rotation of the link between the spherical joints. The SS mechanism as presented by Winder et al. is a mode of the $RRR - RRR$ class in which the spherical vertices are attached diagonally across the rectangular panel.

DOF	Distance Constraint	Panel Notation Representation	Spatial Mechanism	Comment
1	Coincident	R	R	Revolute joint
2	Coincident	RR	U	Universal joint
	Fixed	$R-R$	RR	Note: all revolute joints parallel
3	Coincident	RRR	S	Spherical joint
	Fixed	$R-RR$	RU	—
	Variable	$R-R-R$	RPR	Note: all revolute joints parallel
4	Fixed	$R-RRR$	RS	—
		$RR-RR$	UU	
	Variable	$R-R-RR$	RPU	—
		$R-RR-R$	RUR	
5	Fixed	$RR-RRR$	US	—
	Variable	$R-R-RRR$	RPS	—
		$R-RR-RR$	RUU	
		$R-RRR-R$	RSR	
		$RR-R-RR$	UPU	
6	Fixed	$RRR-RRR$	SS	Winder et al. SS mechanism; extraneous DOF
	Variable	$R-RR-RRR$	RUS	6 DOF spatial chains
		$R-RRR-RR$	RSU	
		$RR-R-RRR$	UPS	
		$RR-RR-RR$	UUU	

Table 8. Enumeration of rigid panel N DOF spatial chains

6 MISCELLANEOUS OBSERVATIONS ON PAPER ART

6.1 MOBILE OVERCONSTRAINT

6.1.1 Identification of Overconstraint

6.1.1.1 Definition

Overconstraint is a property of a mechanism connectivity in which the predicted generic mobility is zero (or negative). This implies that the mechanism's position is fully defined with no degrees of freedom, so the mechanism is a structure. In the case of a mobile overconstrained mechanism, the generic mobility equation does not output the actual value of the mechanism's mobility; the mobility equation predicts zero degrees of freedom, but the actual mechanism has positive mobility due to a combination of special geometric characteristics such as symmetry, special angle relationships, or other unique properties [30]. Often the identification of a mobile overconstrained mechanism is dependent on experimental observation rather than a methodical analysis approach. Some mobile overconstrained mechanisms are well known in the origami domain, and these are used to inform a preliminary study of the characteristics which permit mobility in overconstrained mechanisms.

Specific dimensions of links are the source of mobile overconstraint in mechanisms, so it is critical to note that this requires mathematically perfect geometry. Any variation in the dimensions through, for example, machining with a high tolerance removes the mobile overconstraint, creating an overconstrained mechanism which has no mobility. This sensitivity to dimensional error introduces a challenge in physically implementing overconstrained mechanisms. Conversely, high degrees of precision, symmetry, and other aesthetic features in an implemented design may introduce mobility when immobile

overconstraint is expected; this may lead to safety issues in design spaces such as architecture if a structure is expected but the bodies have unexpected, overconstrained mobility [31].

6.1.1.2 Mobile Overconstraint Quantification

Beatini and Korkmaz address the quantification of overconstraint in a mobile overconstrained mechanism using a term which accounts for the difference between the predicted and observed mobility [12] as stated in (Eqn. 8).

$$M_{actual} = M + h_{geom}$$
<div align="right">(Eqn. 8)</div>

The overconstraint term is the number of degrees of freedom which are accounted for by geometric properties rather than the mechanism connectivity. This value can also be interpreted as the number of 1 DOF revolute folds that need to be introduced to allow mobility in the generic mechanism.

6.1.2 Miura-Ori Analysis

A famous mobile overconstrained origami fold is the Miura-ori [21], which is a specific variation of a mesh of quadrilaterals in which each panel is an identical parallelogram and the orientation of the panels are such that there are parallel planes of symmetry along the edges of each row of parallelograms and tessellation of the parallelograms along the planes, forming the specific mesh depicted in Figure 59. The simplest mesh is a single four-bar cell of parallelograms with a central plane of symmetry as depicted in Figure 58, and a larger mesh can be developed by tessellation of this cell. Typically mechanisms with meshing exhibit overconstraint and are structures; however, the special dimensions of the Miura-ori (i.e. the parallel edges and supplementary angles of the parallelogram) permit one degree of freedom in the mesh.
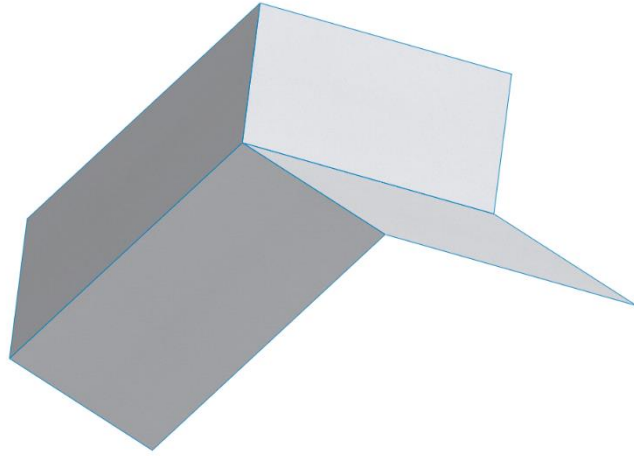
Figure 58. Miura-ori four-bar cell
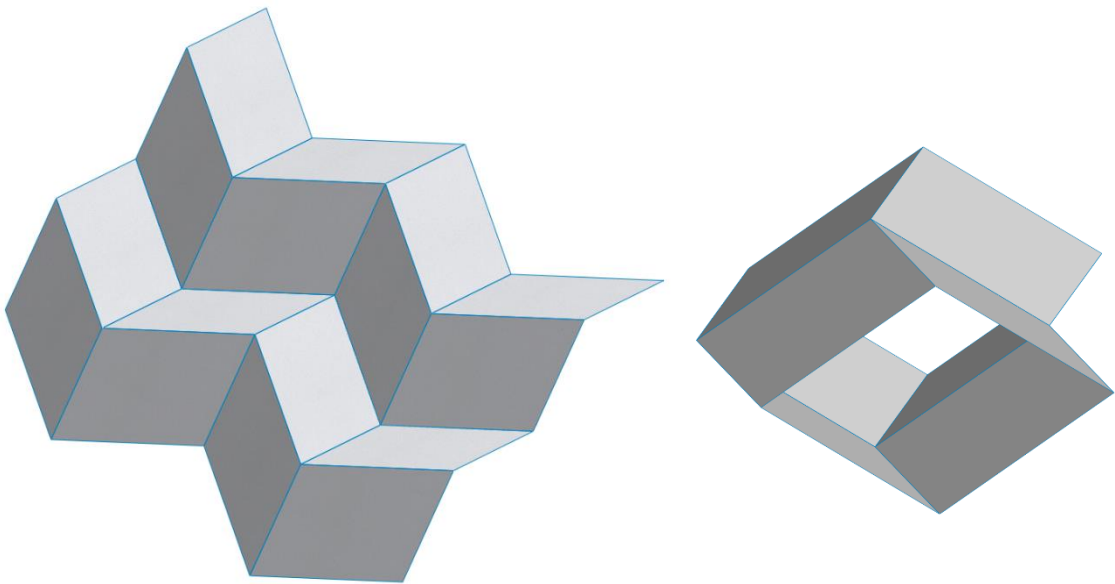
Figure 59. Mobile Miura-ori mesh (left) and tube element (right)

121

An analysis of the Miura-ori cell was undertaken to identify the source of mobility. A single four-bar cell of the tessellation was further reduced by symmetry [32] into a two-bar mechanism with edges constrained to a homokinetic plane about which there is reflective symmetry to form the other two links. The motion of the simplified two-bar model is fully defined by three dimensions of the parallelogram (the two side lengths and the angle between them) and the homokinetic xy plane constraint as depicted in Figure 60. From these parameters, vector analysis determines the parameterized motion of the mechanism (see Appendix A: Miura-Ori Vector Analysis). The analysis illustrates that the edges which emanate from the homokinetic xy plane are constrained to be parallel to the xz plane, perpendicular to the homokinetic plane. This permits tessellation of the Miura cell by translation over the xz plane. This property allows for the mating of any number of four-bar cells to form a two-dimensional mesh as depicted in Figure 59 while maintaining the same mobility of 1 DOF of the initial four-bar cell. The cell can also be reflected over the plane to form a tube shape as depicted in Figure 59, which can be further tessellated into a three-dimensional tube or cellular tessellation [21].

The Miura-ori can be depicted with an SC graph representing the connectivity of the parallelograms, and spherical system mobility analysis can be employed to calculate the generic mobility. Because the true mobility is known to be one, the overconstraint parameter of the Miura-ori can be calculated in terms of the SC graph mesh size.
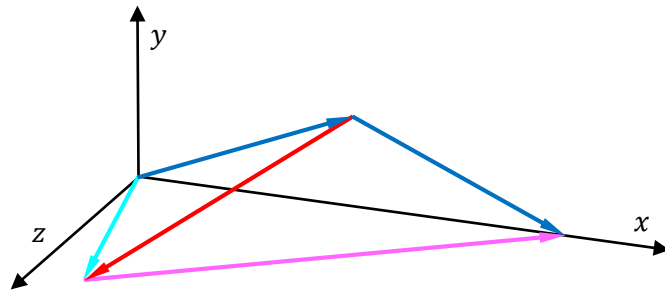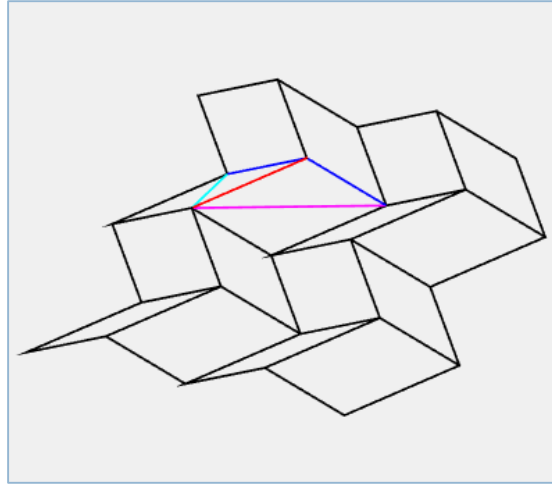
Figure 60. Miura-ori vector definition (top) and coordinate diagram (bottom)
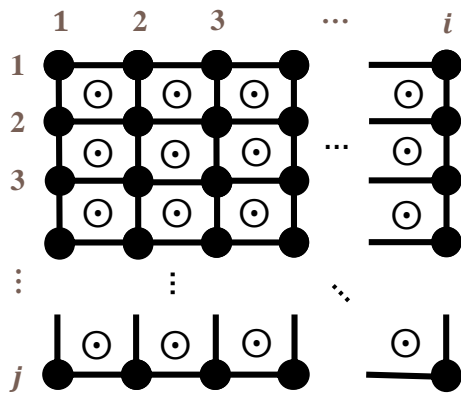
Figure 61. Miura-ori mesh SC graph of arbitrary mesh size

Figure 61 describes an arbitrary Miura-ori mesh consisting of i by j parallelograms. Because this is a spherical system with a known mobile overconstraint property and known actual mobility, spherical system mobility analysis can be used to quantify the degree of overconstraint in the mesh. The calculated quantity, $(i-2)(j-2)$ indicates that if i or j is two, there is a two-strip mechanism with no overconstraint and 1 DOF. Furthermore, in the corresponding mesh of polyhedra of arbitrary dimension, if $(i-2)(j-2)$ creases are introduced to the same number of panels, the resulting linkage will have 1 DOF.

$$N = ij; \qquad J = (i-1)j + (j-1)i = 2ij - i - j$$
$$M = 1 = 3N - 2J - 3 + h_{geom}$$
$$M = 1 = 3(ij) - 2(2ij - i - j) - 3 + h_{geom}$$
$$h_{geom} = ij - 2(i + j) + 4$$
$$\boxed{h_{geom} = (i-2)(j-2)}$$

6.1.3 Square Twist Analysis

Another well-recognized mobile overconstrained fold is the square twist fold [18], depicted in Figure 62. This mechanism is also a quadrilateral mesh which has a predicted generic mobility of zero, but the mechanism is observed to have one actual degree of freedom. A qualitative analysis can be employed to identify special dimensions which contribute to the mobility using the identified Miura-ori special dimensions as a base to compare. In the trapezoidal quadrilaterals in the mesh, adjacent angle pairs are supplementary, which asserts the opposite crease axes are parallel; furthermore, the angles of the corner rectangles are all right, which asserts orthogonal pairs of parallel crease axes. This permits the planes of the rectangular corner panels to all remain parallel to each other. Furthermore, the radial symmetry of the mechanism allows the tessellation to form a loop about the center square.
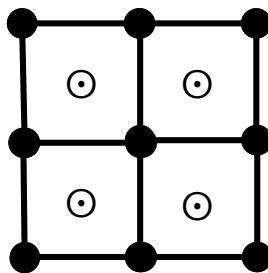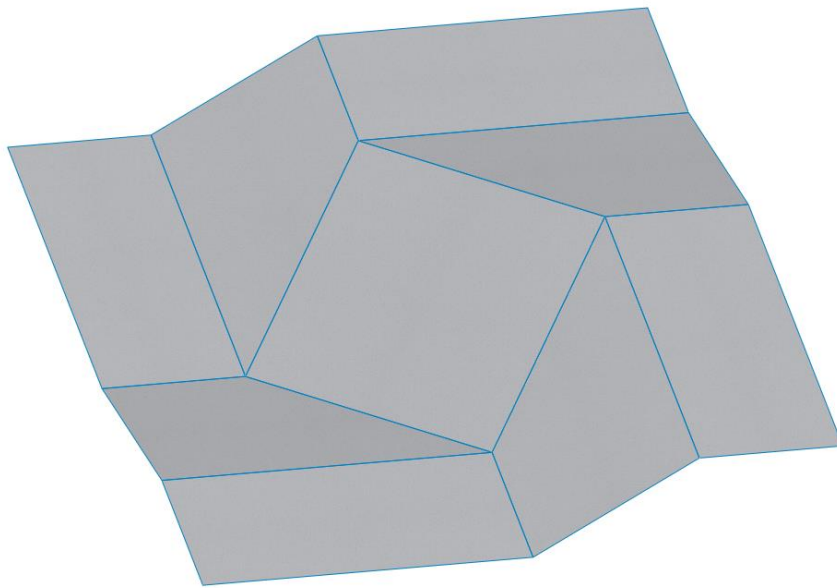
Figure 62. Square twist fold (top) and its SC graph (bottom)

6.1.4 Exceptional Closure Cases

Some linkages are single closed loops which do not have a single spherical center or have otherwise skew joint axes but which exhibit mobile overconstraint. A well-known example which maps readily to the rigid panel model is the Sarrus mechanism [33] depicted in Figure 63 which features two chains with all parallel joints connecting two parallel planar rigid bodies. This mechanism exhibits 1 DOF of vertical displacement between the parallel panels. Other mechanisms in this class include Bennett and Bricard mechanisms [33], [34], which can be represented by polyhedra with specific dimensional relationships. The geometric dimensions which permit the mobile overconstraint in this general class of mechanisms is not as obvious as in the spherical system cases of the Miura-ori and square twist. It is anticipated that the special geometric feature permitting mobility is the intersection of some combination joint axes of the loop to multiple distinct, moving spherical centers and/or infinite spherical centers with different axis directions. Wampler et al. identify a loop with similar exceptional properties and develop notation to address it [13] but still rely on mechanism observation to inform the overconstraint term. If a generalized property which permits this mobility is determined, the SCD graph scheme should be modified to incorporate it.
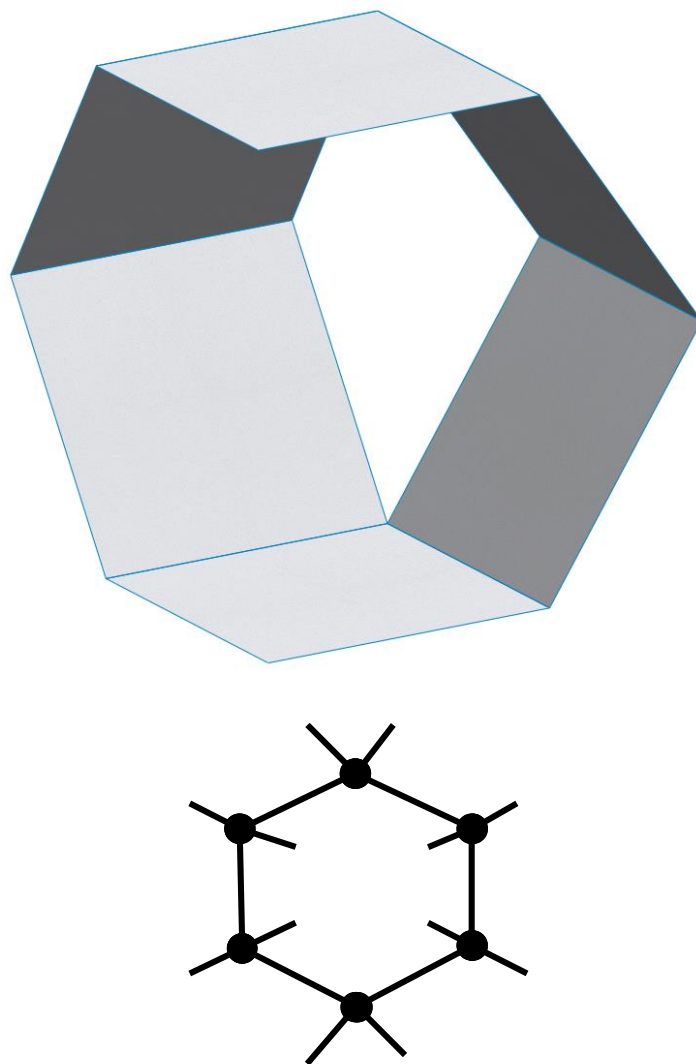
Figure 63. Rigid panel Sarrus mechanism (top) and its SCD graph (bottom)

6.2 ACTIVATING COMPLIANCE

6.2.1 Definition

Paper is inherently compliant due to its typical geometric properties. The ability to deform paper by hand is the reason for its use in origami. In rigid paper art, the paper links are treated as rigid bodies with ideal joints. Because paper does not consist of truly ideal joints in actuality, the mechanism equivalent actually has a stiffness associated with it [5] which is a nonlinear function that may change due to plastic deformation and other factors. Furthermore, in reality, paper's thin geometry permits deformation of the surface under small forces. The curvature of paper under compliant bending can be modeled with the PRBM model as a rigid joint with some stiffness [5]. A crucial observation regarding the nature of a joint with stiffness or PRBM representation is that the "spring" force has an equilibrium point in which the net force is zero and the system seeks to maintain, although due to complicated material properties and geometry of paper, the spring force may be highly nonlinear and the equilibrium position may change due to plastic deformation.

These properties inform characteristics of the various classes of compliant mechanisms. In the analysis of compliant mechanisms, various states of mechanisms are recognized based on their compliance properties and generic mobility properties. Transitions from one state to another define various classes of compliant mechanisms.

6.2.2 Classification

Two properties of a mechanism which can be combined in different ways are the compliance behaviors of the links and the mobility of the mechanism. The compliance of a link is "activated" when it is displaced from its equilibrium state by some force; if a compliant link remains in its equilibrium, it can be considered a rigid link. The mobility of the mechanism is the predicted generic mobility when all links are treated as rigid (i.e. compliant

links maintain equilibrium). These two binary properties can be combined into a matrix (Figure 64) that describes the state of a mechanism. Compliant mechanisms are capable of jumping between states by the activation or deactivation of compliance. Compliant mechanisms can be classified by the manner in which they transition through the states. Preliminary examples of common behaviors are described in the examples that follow.
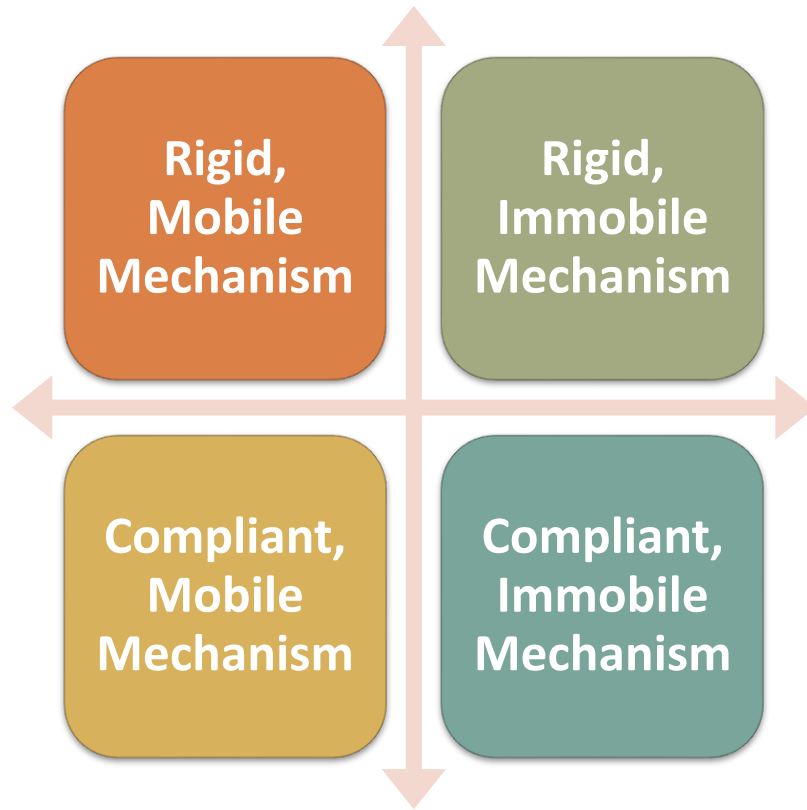
Figure 64. Matrix of mechanism's compliance and mobility properties

6.2.2.1 Compliant Mechanism

In this class of mechanism, the initial state is taken to be an immobile mechanism in which a compliant member behaves rigidly in its equilibrium, such as the truss featuring a compliant member in equilibrium in Figure 66, left. The compliance of the member is then activated which allows mobility, as depicted by the stretching of the compliant link permitting motion in Figure 66, right. This class of behavior is summarized in Figure 65.

6.2.2.2 Compliant Locking

In this class of mechanism, the initial state is taken to be mobile mechanism due to a member behaving compliantly, such as the two links connected by a compliant string in Figure 68, left. A limiting position of the compliant member is then reached, which locks the mechanism in some direction, such as the string's fully tensioned position in Figure 68, right. This class of behavior is summarized in Figure 67.

6.2.2.3 Variable Mobility Mechanism

In this class of mechanism, the initial state is taken to be rigid, mobile mechanism in which a compliant member behaves rigidly in its equilibrium state, such as the four-bar with its compliant member in equilibrium in Figure 70, left. The compliance of the member is then activated, which permits an additional degree of freedom, such as four-bar with the stretching compliant link in Figure 70, right. This class of behavior is summarized in Figure 69.
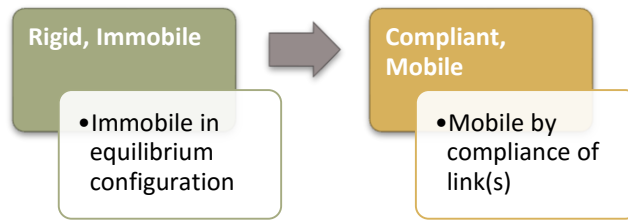
Figure 65. Compliant mechanism states
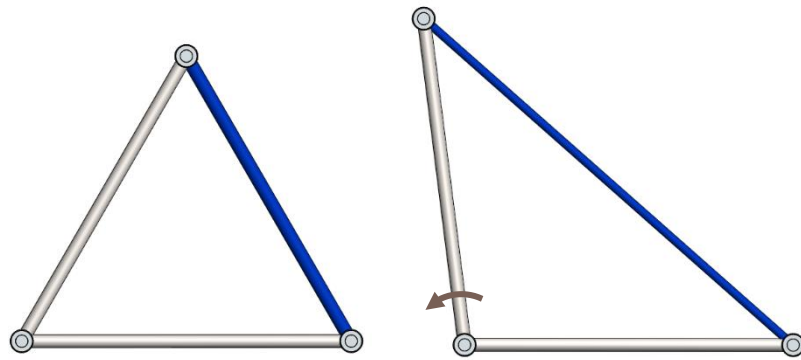
Figure 66. Compliant mechanism in its rigid, immobile state (left) and its compliant, mobile state (right) with its compliant member highlighted and mobility indicated with arrows
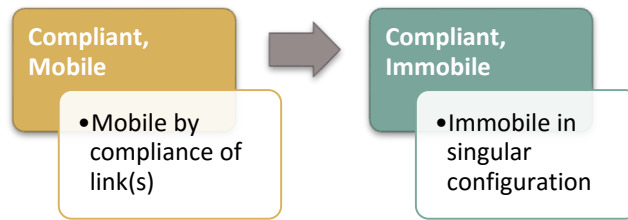
Figure 67. Compliant locking states
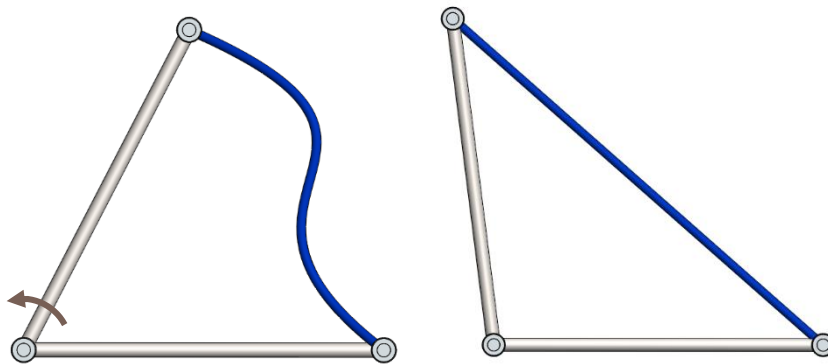
Figure 68. Compliant locking example in its compliant, mobile state (left) and its compliant, immobile state (right) with its compliant member highlighted and mobility indicated with arrows
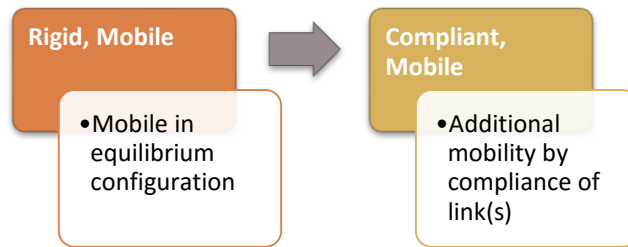
Figure 69. Variable mobility mechanism states
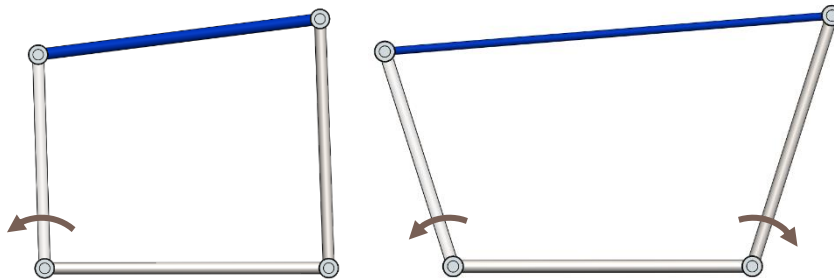
Figure 70. Variable mobility mechanism in its rigid, mobile state (left) and its compliant, mobile state (right) with its compliant member highlighted and mobility indicated with arrows

6.2.3 Compliance in Practice

6.2.3.1 Dynamical Modes

Because the PRBM model introduces spring dynamics which have stiffnesses and equilibria associated with them, the dynamical motion of paper art as compliant mechanisms may be considered. Mechanisms with multiple degrees of freedom with stiffnesses associated with creases and compliant action will have a net mechanism equilibrium as well as dynamical modes associated with each degree of freedom. An example of this property is found in the fortune teller fold, which is a spherical eight-bar with four ride-along mechanisms associated with it with a total of five degrees of freedom. The relative positions of links serve as inputs and outputs to the dynamical system and the stiffness of the creases determine the system response to inputs. The ride-along addenda further influence the net stiffnesses of the creases and can be designed to influence the modes of motion.

6.2.3.2 Neglecting Compliance

In the discussion of rigidity vs. compliance, a binary relationship was established between the two. In reality, all materials have compliance as there is always some material elasticity. Rigid links refer to materials with stiffnesses which are orders of magnitude larger than the forces that they will typically experience and whose elastic deformations are negligible. On the other hand, compliance arises when a material's stiffness is in a comparable order of magnitude of the forces. The "activation of compliance" occurs when the forces reach the range in which compliant deformation becomes significant. An example of a rigid material is a metal of sufficient thickness that cannot be bent by human hands alone in comparison to piece of cardboard that can be bent by human hands with low effort. The binary relationship of rigidity and compliance assumes a large enough gap between the stiffness and typical forces.

6.3 ACTIVATING CONSTRAINT

6.3.1 Discussion

Constraint is defined as the removal of a degree of freedom from a joint. Constraint can be evaluated in the generic case, where it is simply known that a joint's degree of freedom is eliminated, or in a specific case, where specific geometric characteristics are known which remove the degree of freedom. In a rigid linkage such as the four-bar in Figure 71, a critical constraining geometry is created when two adjacent links connected by a revolute joint become collinear or coplanar with some force keeping outward tension between them as in Figure 72, left. In this case, the revolute joints do not actuate along the rotational degree of freedom and are fixed at 180°. The removal of the revolute joint's degree of freedom constrains the joint, and no relative motion is permitted between the two links. In contrast, when the same singular, coplanar link relation occurs with some force applying inward compression between, the two links will tend to buckle at the joint and permit motion as in Figure 72, right.

The characteristic of links in a singular position constraining a revolute joint under tension and buckling under compression is analogous to the behavior of paper when treated as compliant. Due to paper's material and geometry properties, it is capable of bearing tension along its plane, however, it is not capable of bearing compression along its plane and will buckle very easily. The curvature of paper under compliant bending can be modeled with the PRBM model as a rigid joint with some stiffness [5]. By converting a sheet to a PRBM linkage, it is evident that a compliant paper link behaves as a rigid link in a singular position in both tension and compression.
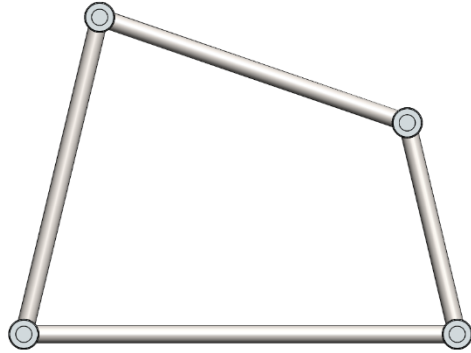
Figure 71. Four-bar mechanism with no constraining geometry
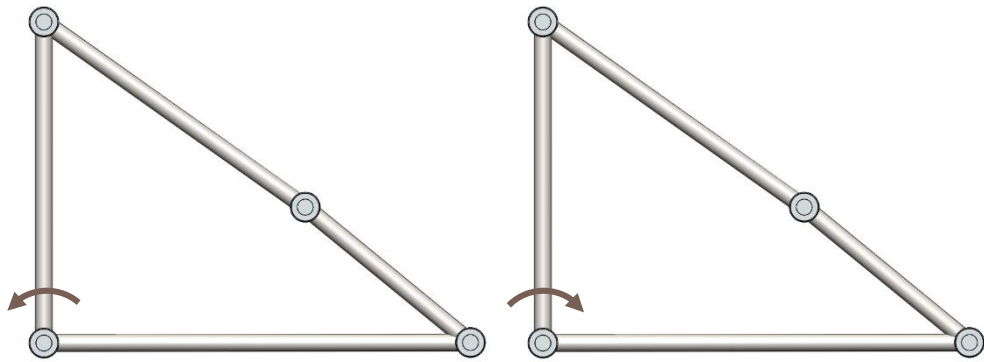
Figure 72. Four-bar mechanism with constraint in tension (left), at the onset of buckling in compression (right) with its direction of motion indicated by the arrows

6.3.2 Locking Ride-Along Addendum

Constraint can be represented on an SC graph by merging two vertices connected by an edge into a single vertex, representing the loss of the actuation of the joint between the bodies as depicted in Figure 73. This introduces a relative mobility of -1 due to the loss of the single degree of freedom of the revolute joint.

$$\Delta N = -1; \qquad \Delta J = -1$$
$$\Delta M = 3\Delta N - 2\Delta J = 3(-1) - 2(-1) = -1$$
$$\boxed{\Delta M = -1 \; DOF \; for \; each \; joint \; constrained}$$

An application of singular constraint in spherical system mechanisms including kinematic paper art is a locking feature which enforces an acceptable range of angles between links. This can be implemented by adding a ride-along mechanism to two adjacent links in a loop such that the ride-along becomes constrained in tension (as depicted in Figure 73) when a specific angle between links is established. This prevents motion beyond this angle due to the singularity, but it allows for motion within the range because the singularity will buckle.

Furthermore, because compliant paper can be interchanged for two links with a PRBM joint between them, a compliant ride-along mechanism may be introduced as a single piece of paper whose compliance is capable of actuating in the same motion that a rigid, jointed ride-along would provide. The compliant paper ride-along mechanism would also achieve locking singularity in tension due to the properties of paper.

6.3.3 Design Example: Radially Deployable Cylinder

A case study was introduced which implements a locking ride-along scheme to limit the angles of adjacent links. The motivating concept was the development of a deployable hand tool handle which is capable of collapsing to reduce storage space while exhibiting strength sufficient to apply torque. The design consists of radially symmetric panels each attached adjacently with a ride-along mechanism which reaches a singular position

138

corresponding to the angle which permits the outer links to open the full 360°, depicted in Figure 74. The locking ride-along addendum could be rigid or compliant. If the outer links are affixed to each other in the deployed position, the tension in the locked singular ride-along addenda ensure structural strength when torque is applied.
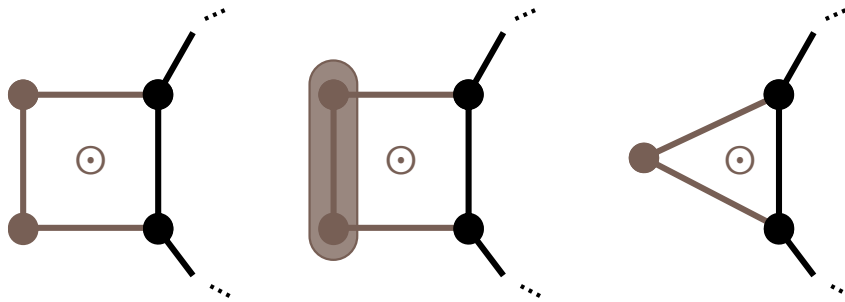
Figure 73. Activation of joint constraint converting a ride-along addendum (left) to a locked truss (right) by merging vertices (center) in SC graph notation
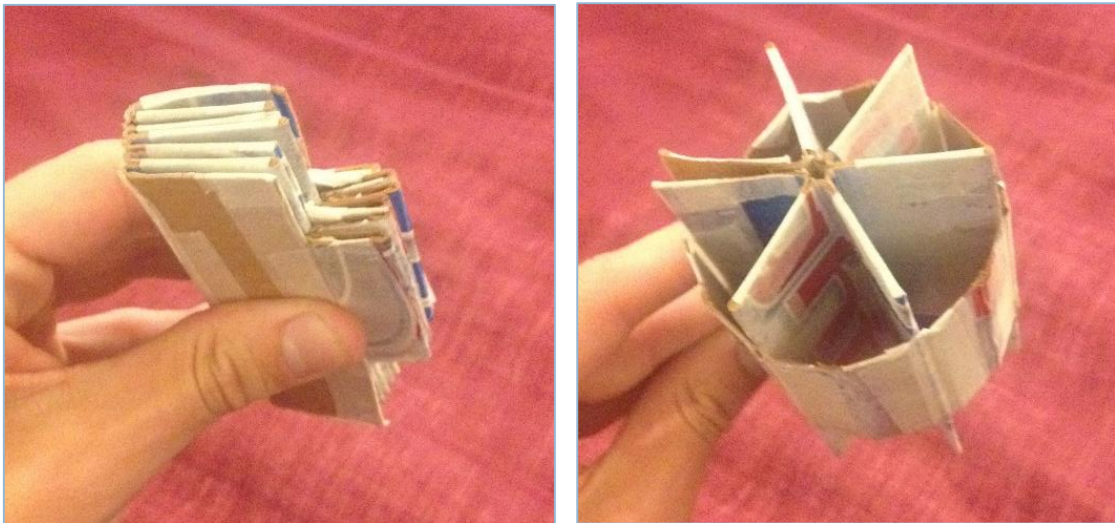
Figure 74. Radially deployable cylinder cardboard mock-up, collapsed (left) and deployed (right)

6.4 CONCLUSIONS DRAWN FROM THE STUDY OF KINEMATIC PAPER ART

This study of kinematic paper art was inspired by the recognition that paper art can be mapped to the mechanism domain and that the work of those who develop paper art can be mapped, studied, and generalized to develop a foundation for analysis of the broader class of mechanisms of which paper art is a subset. This was accomplished with the principles of de-aestheticization and generic analysis.

The goal of generalization of paper art in the mechanism domain was accomplished in two ways. The first was using properties of common paper art as the inspiration to classify the underlying mechanism class, the spherical system. The definition of spherical systems encompasses most kinematic paper art as well as traditional spherical and planar mechanisms as special cases, which motivated a reformulation of the Chebyshev-Grübler-Kutzbach generic mobility equation. Appropriate physical representations, connectivity graph representations, and C-G-K-based generic mobility analyses were developed for spherical system mechanisms based on the salient characteristics of the mechanism class.

The second level of generalization of paper art was identifying and analyzing spherical/spatial hybrid mechanisms, an overarching class of mechanism which includes spherical system mechanisms, fully spatial mechanisms, and combinations of the two. This class of mechanism is uncommon in kinematic paper art, but it is the broadest class of mechanism of which all kinematic paper art is a subset. Appropriate physical representations, connectivity graph representations, and polyhedron-based generic mobility analyses were adapted from Wampler et al. for spherical/spatial hybrid mechanisms based on the salient characteristics of the mechanism class.

The generic analyses which were developed rely only on the salient link connectivity properties encoded in the connectivity graphs to assess generic mobility. This basic analysis

141

uses minimal information about the mechanism to determine its fundamental properties and generic behavior. This analysis is insufficient for dimensional synthesis of a specific mechanism, but it informs the type synthesis process in which linkage connectivities can be synthesized exhaustively using an automated process with simple calculation of mobility. The connectivity graphs proposed encode all salient information for this process in the context of pure spherical systems and spherical/spatial hybrids.

In contrast with the generic approach, design of specific mechanisms in the spherical system domain can be informed by existing origami techniques. Whereas the generic analysis assumes de-aestheticized geometry, many mechanism applications are anticipated to require symmetry, rectilinear angles, planarity, and other special geometric features. Adapting the work of origamists to the mechanism domain is anticipated to be fruitful, and the generic foundation established in this analysis permits specific geometries as subsets of the generalized classes.

It is expected that the potential of spherical system mechanisms can be realized once the foundation for notation and analysis is further developed. There is a lot of potential for applications because the class of mechanisms exhibit motion in three-dimensional space while having an overall 3 DOF mobility constraint space, which means the mobility analysis is the same as a planar or spherical mechanism, but the final motion is not constrained to these surfaces. A simple example presented was the generalization of the Watt mechanism from a planar mechanism to a spherical system, which exhibits complex motion of the links the three-dimensional space. Further work which will allow for methodical design of spherical systems involves the development of robust multi-loop position analyses to develop synthesis techniques.

REFERENCES

[1]   D. Dureisseix, "An Overview of Mechanisms and Patterns with Origami," *Int. J. Sp. Struct.*, vol. 27, no. 1, pp. 1–14, Mar. 2012.

[2]   H. C. Greenberg, M. L. Gong, S. P. Magleby, and L. L. Howell, "Identifying links between origami and compliant mechanisms," *Mech. Sci.*, vol. 2, no. 2, pp. 217–225, Dec. 2011.

[3]   L. A. Bowen, C. L. Grames, S. P. Magleby, L. L. Howell, and R. J. Lang, "A Classification of Action Origami as Systems of Spherical Mechanisms," *J. Mech. Des.*, vol. 135, no. 11, p. 111008, Oct. 2013.

[4]   E. Demaine and J. O'Rourke, *Geometric Folding Algorithms*. New York: Cambridge University Press, 2007.

[5]   B. G. Winder, S. P. Magleby, and L. L. Howell, "Kinematic Representations of Pop-Up Paper Mechanisms," *J. Mech. Robot.*, vol. 1, no. 2, p. 021009, 2009.

[6]   J. S. Dai and J. R. Jones, "Kinematics and mobility analysis of carton folds in packing manipulation based on the mechanism equivalent," *Proc. Inst. Mech. Eng. Part C J. Mech. Eng. Sci.*, vol. 216, no. 10, pp. 959–970, Jan. 2002.

[7]   F. Massarwi, C. Gotsman, and G. Elber, "Papercraft Models using Generalized Cylinders," in *15th Pacific Conference on Computer Graphics and Applications (PG'07)*, 2007, pp. 148–157.

[8]   W. Yao and J. S. Dai, "Dexterous Manipulation of Origami Cartons With Robotic Fingers Based on the Interactive Configuration Space," *J. Mech. Des.*, vol. 130, no. 2, p. 022303, 2008.

[9]   G. Wei and J. Dai, "Geometry and kinematic analysis of an origami-evolved mechanism based on artmimetics," in *ASME/IFToMM International Conference on Reconfigurable Mechanisms and Robots*, 2009, pp. 450–455.

[10]   J. S. Dai and J. Rees Jones, "Mobility in Metamorphic Mechanisms of Foldable/Erectable Kinds," *J. Mech. Des.*, vol. 121, no. 3, p. 375, Sep. 1999.

[11]   A. G. Erdman, Ed., *Modern Kinematics: Developments in the Last Forty Years*. Wiley-Interscience, 1993.

[12]   V. Beatini and K. Korkmaz, "Shapes of Miura Mesh Mechanism with Mobility One," *Int. J. Sp. Struct.*, vol. 28, no. 2, pp. 101–114, Jun. 2013.

[13]   C. Wampler, B. T. Larson, and A. G. Erdman, "A New Mobility Formula for Spatial Mechanisms," in *Volume 8: 31st Mechanisms and Robotics Conference, Parts A and B*, 2007, no. 1, pp. 561–570.

[14]   A. Yellowhorse and L. L. Howell, "Creating Rigid Foldability to Enable Mobility of Origami-Inspired Mechanisms," *J. Mech. Robot.*, vol. 8, no. 1, p. 011011, Aug. 2015.

[15]   D. Balkcom, E. Demaine, M. Demaine, J. Ochsendorf, and Z. You, "Folding Paper Shopping Bags," in *Origami 4*, A K Peters/CRC Press, 2009, pp. 315–333.

[16]   T. Tachi, "Simulation of Rigid Origami," in *Origami 4*, vol. 4, A K Peters/CRC Press, 2009, pp. 175–187.

[17]   G. Wei and J. S. Dai, "Origami-Inspired Integrated Planar-Spherical Overconstrained Mechanisms," *J. Mech. Des.*, vol. 136, no. 5, p. 051003, Mar. 2014.

[18]   L. A. Bowen, W. L. Baxter, S. P. Magleby, and L. L. Howell, "A position analysis of coupled spherical mechanisms found in action origami," *Mech. Mach. Theory*, vol. 77, pp. 13–24, Jul. 2014.

[19]   T. Tachi, "Generalization of rigid foldable quadrilateral mesh origami," *J. Int. Assoc. Shell Spat. Struct.*, vol. 50, no. October, pp. 2287–2294, 2009.

[20]   T. Tachi, "Geometric Considerations for the Design of Rigid Origami Structures," in *Proceedings of the International Association for Shell and Spatial Structures (IASS) Symposium*, 2010, vol. 12, no. 10, pp. 458–460.

[21]   T. Tachi and K. Miura, "Rigid-foldable cylinders and cells," *J. Int. Assoc. Shell Spat. Struct.*, vol. 53, no. 174, pp. 217–226, 2012.

[22]   T. A. Evans, R. J. Lang, S. P. Magleby, and L. L. Howell, "Rigidly foldable origami gadgets and tessellations.," *R. Soc. open Sci.*, vol. 2, no. 9, p. 150067, Sep. 2015.

[23]   N. Makhsudyan, R. Djavakhyan, and V. Arakelian, "Comparative analysis and synthesis of six-bar mechanisms formed by two serially connected spherical and planar four-bar linkages," *Mech. Res. Commun.*, vol. 36, no. 2, pp. 162–168, Mar. 2009.

[24]   R. P. Dzhavakhyan, N. A. Makhsudyan, and V. G. Arakelyan, "Comparative analysis and synthesis of plane and spherical four-hinge mechanisms," *J. Mach. Manuf. Reliab.*, vol. 40, no. 5, pp. 423–429, Oct. 2011.

[25]   S. E. Wilding, L. L. Howell, and S. P. Magleby, "Spherical lamina emergent mechanisms," *Mech. Mach. Theory*, vol. 49, pp. 187–197, Mar. 2012.

[26]   G. Gogu, "Mobility of mechanisms: a critical review," *Mech. Mach. Theory*, vol. 40, no. 9, pp. 1068–1097, Sep. 2005.

[27]   O. Shai and A. Müller, "Computational Algorithm for Determining the Generic Mobility of Floating Planar and Spherical Linkages," in *Computational Kinematics: Proceedings of the 6th International Workshop on Computational Kinematics (CK2013)*, 2014, pp. 193–200.

[28]   G. N. Sandor and A. G. Erdman, *Advanced Mechanism Design: Analysis and Synthesis*. Englewood Cliffs: Prentice-Hall, Inc., 1984.

[29]   R. Norton, *Design of Machinery: An Introduction to the Synthesis and Analysis of Mechanisms and Machines*, 5th ed. McGraw-Hill Education, 2011.

[30]   C. Mavroidis and B. Roth, "New and Revised Overconstrained Mechanisms," *J. Mech. Des.*, vol. 117, no. 1, p. 75, Mar. 1995.

[31]   J. Eddie Baker, "An analysis of the Bricard linkages," *Mech. Mach. Theory*, vol. 15, no. 4, pp. 267–286, 1980.

[32]   M. Chew and P. Kumar, "Conceptual Design of Deployable Space Structures from the Viewpoint of Symmetry," *Int. J. Sp. Struct.*, vol. 8, pp. 17–27, 1993.

[33]   Y. Chen, "Design of Structural Mechanisms," University of Oxford, 2003.

[34]   P. W. Fowler and S. D. Guest, "A symmetry analysis of mechanisms in rotating rings of tetrahedra," *Proc. R. Soc. A Math. Phys. Eng. Sci.*, vol. 461, no. 2058, pp. 1829–1846, Jun. 2005.

APPENDICES

APPENDIX A: MIURA-ORI VECTOR ANALYSIS
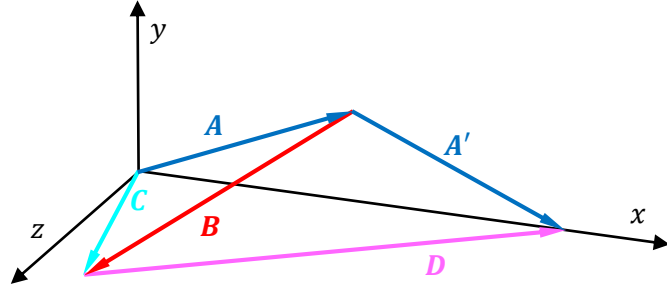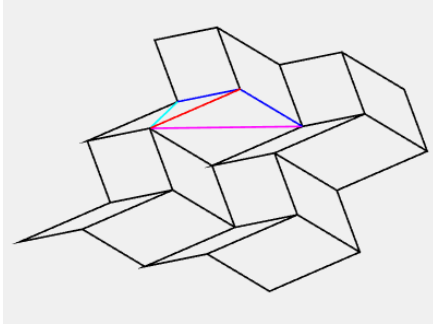
Known: length A, length B, angle θ between $\vec{A}$ and $\vec{B}$

Constraint: $\vec{A}, \vec{A}'$ constrained to xy plane

Input: angle ϕ between x-axis and $\vec{A}$

Unknown: orientation of $\vec{B}$ defined by azimuth angle α and elevation angle β

Vector definitions:

$$\vec{A} = A\begin{bmatrix} \cos\phi \\ \sin\phi \\ 0 \end{bmatrix}; \quad \vec{A}' = A\begin{bmatrix} \cos\phi \\ -\sin\phi \\ 0 \end{bmatrix}; \quad \vec{B} = B\begin{bmatrix} \cos\beta\cos\alpha \\ \sin\beta \\ \cos\beta\sin\alpha \end{bmatrix}; \quad \vec{C} = \vec{A} + \vec{B}; \quad \vec{D} = \vec{A}' - \vec{B}$$

By vector geometry:

$$\vec{A} \cdot \vec{B} = AB\cos\theta \tag{A1}$$

$$AB\cos\phi\cos\beta\cos\alpha + AB\sin\phi\sin\beta = AB\cos\theta$$

$$\vec{A}' \cdot \vec{B} = AB\cos\theta \tag{A2}$$

$$AB\cos\phi\cos\beta\cos\alpha - AB\sin\phi\sin\beta = AB\cos\theta$$

Subtracting:

$$2AB\sin\phi\sin\beta = 0 \tag{A3}$$

$\sin\phi \neq 0$, generally

$\therefore \sin\beta = 0$

$\therefore \beta = n\pi$ (let integer $n = 0$)

$\therefore \beta = 0$

$\therefore \vec{B}$ is parallel to the xz plane

Substituting and simplifying:

$$\cos\phi\cos\alpha = \cos\theta \tag{A4}$$

$$\therefore \alpha = \arccos\left(\frac{\cos\theta}{\cos\phi}\right)$$

Constraint:

$$\left(\frac{\cos\theta}{\cos\phi}\right) \leq 1 \tag{A5}$$

$$\therefore \cos\theta \leq \cos\phi$$

$$\therefore \phi_{max} = \theta$$

$$\vec{B}(\phi) = B\begin{bmatrix} \left(\frac{\cos\theta}{\cos\phi}\right) \\ 0 \\ \sqrt{1 - \left(\frac{\cos\theta}{\cos\phi}\right)^2} \end{bmatrix} \tag{A6}$$

$$where\ 0 \leq \phi \leq \theta$$

APPENDIX B: N DOF SPATIAL CHAIN MATLAB CODE

Output

```
DOF = 1                                    DOF = 5
R                                          RR-RRR
                                           R-R-RRR
DOF = 2                                    R-RR-RR
RR                                         R-RRR-R
R-R                                        RR-R-RR

DOF = 3                                    DOF = 6
RRR                                        RRR-RRR
R-RR                                       R-RR-RRR
R-R-R                                      R-RRR-RR
                                           RR-R-RRR
DOF = 4                                    RR-RR-RR
R-RRR
RR-RR
R-R-RR
R-RR-R
```

Source Code

```matlab
% N DOF Spatial Chain
% Marc Wiener
clc; close all;

global L1 L2 L3 L4 L5 L6

L1 = []; L2 = []; L3 = [];
L4 = []; L5 = []; L6 = [];
mech = zeros(3,1);

for size = 1:6

    minNodes = ceil(size/3);
    maxNodes = min(size,3);

    for nodes = minNodes:maxNodes
        if nodes == 1
            for R1 = 1:3
                if R1 == size
                    mech = [R1; 0; 0];
                    addToList(mech);
                end
            end
        elseif nodes == 2
            for R1 = 1:3
                for R2 = 1:3
                    if R1+R2 == size
                        mech = [R1; R2; 0];
                        addToList(mech);
                    end
                end
            end
        elseif nodes == 3
            for R1 = 1:3
                for R2 = 1:3
                    for R3 = 1:3
                        if R1+R2+R3 == size
```

147

```matlab
                                    mech = [R1; R2; R3];
                                    addToList(mech);
                                end
                            end
                        end
                    end
                end
            end
        end
end

fprintf('\nDOF = 1\n')
printList(L1)
fprintf('\nDOF = 2\n')
printList(L2)
fprintf('\nDOF = 3\n')
printList(L3)
fprintf('\nDOF = 4\n')
printList(L4)
fprintf('\nDOF = 5\n')
printList(L5)
fprintf('\nDOF = 6\n')
printList(L6)
fprintf('\n')
```

```matlab
function [] = addToList(mech)

    global L1 L2 L3 L4 L5 L6
    n = sum(mech);

    if n == 1
        if ~isDup(L1, mech)
            L1 = [L1 mech];
        end
    elseif n == 2
        if ~isDup(L2, mech)
            L2 = [L2 mech];
        end
    elseif n == 3
        if ~isDup(L3, mech)
            L3 = [L3 mech];
        end
    elseif n == 4
        if ~isDup(L4, mech)
            L4 = [L4 mech];
        end
    elseif n == 5
        if ~isDup(L5, mech)
            L5 = [L5 mech];
        end
    elseif n == 6
        if ~isDup(L6, mech)
            L6 = [L6 mech];
        end
    end
end
```

```matlab
function dup = isDup(list, mech)

    dup = 0;

    for i=1:size(list,2)
        if mech(2)==0 && mech(3)==0

            % Compare 1 to 1
            if list(1,i)==mech(1)
                dup = 1;
```

```matlab
            end
        elseif mech(3)==0

            % Compare 1,2 to 2,1
            if list(1,i)==mech(2) && list(2,i)==mech(1)
                dup = 1;
            end
        else

            % Compare 1,2,3 to 3,2,1
            if list(1,i)==mech(3) && list(2,i)==mech(2) && list(3,i)==mech(1)
                dup = 1;
            end
        end
    end
end


function [] = printList(list)

    for i=1:size(list,2)
        printMech(list(:,i));
    end
end


function [] = printMech(mech)

    for i=1:mech(1)
        fprintf('R');
    end

    if mech(2) > 0

        fprintf('-');

        for i=1:mech(2)
            fprintf('R');
        end

        if mech(3) > 0

            fprintf('-');

            for i=1:mech(3)
                fprintf('R');
            end
        end
    end

    fprintf('\n');
end
```

VITA

Marc R. Wiener was born in New Jersey on July 25, 1993 to Rosemarie and Richard Wiener. He received a B.S. in Mechanical Engineering with Highest Honors and a minor in computer science from Lehigh University in May, 2015. He is receiving an M.S. in Mechanical Engineering from Lehigh University in May, 2016 as a Presidential Scholar. Marc enjoyed making origami as a child.